

Design of a 4-Seat, General Aviation, Electric Aircraft

a project presented to
The Faculty of the Department of Aerospace Engineering
San José State University

in partial fulfillment of the requirements for the degree
Master of Science in Aerospace Engineering

by

Viralkumar Rathod

May 2018

approved by

Dr. Nikos J. Mourtos
Faculty Advisor



ABSTRACT

The proposed electric aircraft was designed to address the major challenges facing by electric aviation. The aircraft was designed to meet the flight parameters like 4 passenger capacities (including pilot), a range of 400 nm, a payload of 800 lbs, and a cruise speed of 130 knots. Current battery technology cannot make this type of aircraft feasible so, the proposed aircraft was designed based on future prediction of technologies. The feasibility of an electric propulsion system was examined along with aerodynamic and structural improvements aiming at reducing drag and structural weight. For an aircraft such as this, a large amount of research was done on experimental and current batteries that could possibly be sufficient. The chosen power source for proposed aircraft is combination of Lithium Ion and Aluminium Air cells with the rubber motor. The proposed aircraft was designed to meet the FAR-23 requirements. The methods were used throughout the design process was based on texts as Roskam, Sadraey, and Hepperle. The major design features include a tapered wing, a front mounted single propeller engine, fixed tricycle landing gear, and a T-tail empennage. By showing opportunities in the field of electrification of aircraft, further research can be better aimed at those topic that are of interest and that require the most progress.

Contents

CHAPTER 1.....	12
MISSION SPECIFICATIONS & COMPARATIVE STUDY.....	12
1.1) MISSION SPECIFICATIONS:	13
1.1.1) Mission Profile:.....	13
1.1.2) Market Analysis:.....	14
1.1.3) Technical and Economic Feasibility:.....	14
1.1.4) Critical Mission Requirements:	14
1.2) COMPARATIVE STUDY OF SIMILAR AIRPLANES:.....	15
1.2.1) Mission Capabilities and Configuration Selection:.....	15
a) Electro Light-2:.....	15
b) Pipistrel Taurus G4:	16
c) NASA Scuba Stingray:	17
d) Lange Aviation Antares 23E:.....	18
e) Yuneec International E430:	19
1.2.2) Comparison of Important Design Parameters:.....	20
1.3) DISCUSSION:.....	20
CHAPTER 2.....	21
CONFIGURATION DESIGN	21
2.1) COMPARATIVE STUDY OF SIMILAR AIRPLANES:.....	22
2.1.1) Comparison of Weights, Performance and Geometry of Similar Airplanes:.....	22
2.1.2) Configuration Comparison of Similar Airplanes:	22
a) Electro Light-2:.....	23
b) Pipistrel Taurus G4:	24
c) NASA Scuba Stingray:	24
d) Lange Aviation Antares 23E:.....	26
e) Yuneec International E430:	27
2.2) DISCUSSION:.....	28
2.3) CONFIGURATION SELECTION:.....	29
2.3.1) Overall Configuration:	29
2.3.2) Wing Configuration:	29
2.3.3) Empennage Configuration:	29
2.3.4) Integration of the Propulsion System:.....	30
2.3.5) Landing Gear Disposition:	30
2.3.6) Proposed Configuration:	31
CHAPTER 3.....	32
WEIGHT SIZING AND WEIGHT SENSITIVITIES.....	32

3.1)	MISSION WEIGHT ESTIMATES:	33
3.1.1)	Database for Take-off and Empty Weights of Similar Airplanes:	33
3.1.2)	Determination of Regression Coefficients A and B:	33
3.2)	DETERMINATION OF MISSION WEIGHTS:	35
3.2.1)	Manual Calculation of Mission Weights:	35
3.2.2)	Calculation of Mission Weights using the Advanced Aircraft Analysis (AAA) Program: 43	
3.3)	RANGE SENSITIVITIES:	45
3.3.1)	Manual Calculation of Range Sensitivities:	46
3.3.2)	Calculation of Take-off Weight Sensitivities using the AAA Program:	48
3.4)	TRADE STUDIES:	48
3.5)	DISCUSSION:	51
	CHAPTER 4	52
	PERFORMANCE CONSTRAINT ANALYSIS	52
4.1)	MANUAL CALCULATIONS OF PERFORMANCE CONSTRAINTS:	53
4.1.1)	Stall Speed:	53
4.1.2)	Take-off Distance:	54
4.1.3)	Landing Distance:	58
4.1.4)	Sizing To Climb Requirements:	61
4.1.4.1)	A Method for Estimating Drag Polar at Low Speed:	61
4.1.4.2)	FAR-23 Climb Requirements:	64
4.1.4.3)	Sizing to FAR-23 rate-of-climb requirements:	65
4.1.4.4)	Sizing to climb gradient requirements:	66
4.1.5)	Sizing to Maneuvering Requirements:	68
4.1.6)	Sizing to Cruise Speed Requirements:	69
4.1.7)	Matching Graph:	70
4.2)	CALCULATION OF PERFORMANCE CONSTRAINTS WITH THE AAA PROGRAM: ..	72
4.2.1)	Stall Speed:	72
4.2.2)	Take-off Distance:	72
4.2.3)	Landing Distance:	72
4.2.4)	Climb Constraints:	72
4.2.5)	Cruise Speed Constraints:	73
4.2.6)	Matching Graph:	73
4.3)	SELECTION OF PROPULSION SYSTEM:	75
4.3.1)	Selection of The Propulsion System Type:	75
4.3.2)	Selection of The Number of Engines:	77
4.3.3)	Propeller Sizing:	77
4.4)	DISCUSSION:	78

CHAPTER 5.....	80
FUSELAGE DESIGN.....	80
5.1) LAYOUT DESIGN OF COCKPIT:	81
5.1.1) Dimensions and Weights for Crew Member:.....	81
5.1.2) Layout of Cockpit Seating and Cockpit Controls:	82
5.1.3) Determination of Visibility from the Cockpit:.....	83
5.2) LAYOUT DESIGN OF THE FUSELAGE:	83
5.3) DISCUSSION:.....	85
CHAPTER 6.....	86
WING, HIGH-LIFT SYSTEM AND LATERAL CONTROL DESIGN.....	86
6.1) WING PLANFORM DESIGN:	87
6.1.1) Sweep Angle-Thickness Ratio Combination:	87
6.2) AIRFOIL SELECTION:.....	89
6.3) DESIGN OF HIGH-LIFT DEVICES:	93
6.4) DESIGN OF THE LATERAL CONTROL SURFACES:.....	97
6.5) DRAWINGS:.....	98
6.6) DISCUSSION:.....	100
CHAPTER 7.....	101
DESIGN OF THE EMPENNAGE AND THE LONGITUDINAL AND DIRECTIONAL CONTROLS.....	101
7.1) OVERALL EMPENNAGE DESIGN:.....	102
7.1.1) Empennage Disposition Calculations:	102
7.2) DESIGN OF THE HORIZONTAL STABILIZER:	103
7.3) DESIGN OF THE VERTICAL STABILIZER:	105
7.4) EMPENNAGE DESIGN EVALUATION:	107
7.5) DESIGN OF THE LONGITUDINAL AND DIRECTIONAL CONTROLS:	109
7.6) DRAWINGS:.....	111
7.7) DISCUSSION:.....	112
CHAPTER 8.....	113
LANDING GEAR DESIGN, WEIGHT AND BALANCE ANALYSIS.....	113
8.1) ESTIMATION OF THE CENTRE OF GRAVITY LOCATION FOR THE AIRPLANE: ...	114
8.2) LANDING GEAR DESIGN:.....	118
8.3) WEIGHT AND BALANCE ANALYSIS:	120
8.4) DISCUSSION:.....	122
CHAPTER 9.....	123
STABILITY AND CONTROL ANALYSIS / WEIGHT AND BALANCE- STABILITY AND CONTROL CHECK.....	123
9.1) STATIC LONGITUDINAL STABILITY:.....	124

9.2)	STATIC DIRECTIONAL STABILITY:	125
9.3)	EMPENNAGE DESIGN-WEIGHT AND BALANCE-LANDING GEAR DESIGN- LONGITUDINAL STATIC STABILITY AND CONTROL CHECK:.....	126
9.4)	DISCUSSION:.....	126
	CHAPTER 10.....	127
	DRAG POLAR ESTIMATION.....	127
10.1)	AIRPLANE ZERO-LIFT DRAG:	127
10.2)	LOW SPEED DRAG INCREMENTS:	129
10.2.1)	Flap Drag Increment for Take-off and Landing:.....	129
10.2.2)	Landing Gear Drag Increment for Take-off and Landing:.....	129
10.3)	COMPRESSIBILITY DRAG:	129
10.4)	AIRPLANE DRAG POLARS:	129
10.5)	DISCUSSION AND CONCLUSION:.....	132
	CHAPTER 11.....	133
	CONCLUSIONS AND RECOMMENDATIONS.....	133
11.1)	DRAWING & SUMMARY OF MOST IMPORTANT DESIGN PARAMETERS:	133
11.2)	RECOMMENDATIONS:.....	136
11.3)	ENVIRONMENTAL / ECONOMIC TRADE-OFFS:	136
11.4)	SAFETY / ECONOMIC TRADE-OFFS:.....	138
	CHAPTER 12.....	139
	CLASS II: LANDING GEAR DESIGN.....	139
12.1)	INTRODUCTION	139
12.2)	DETERMINATION OF ALLOWABLE WHEEL LOADS:	139
12.3)	TIRES: TYPES, PERFORMANCE, SIZING AND DATA:.....	141
12.4)	STRUT WHEEL INTERFACE, STRUTS AND SHOCK ABSORBERS:.....	143
	CHAPTER 13.....	147
	CLASS I: AIRPLANE INERTIAS.....	147
13.1)	INTRODUCTION:	147
13.2)	ESTIMATING MOMENT OF INERTIA WITH RADII OF GYRATION:.....	147
	CHAPTER 14.....	148
	V-n DIAGRAMS.....	148
14.1)	INTRODUCTION:	148
14.2)	V-n DIAGRAM: PROPOSED AIRPLANE	148
	CHAPTER 15.....	151
	CLASS II: WEIGHT ESTIMATES.....	151
15.1)	STRUCTURE WEIGHT ESTIMATION:	151
15.2)	POWERPLANT WEIGHT ESTIMATION:.....	151
15.3)	FIXED EQUIPMENT WEIGHT ESTIMATION:.....	152

15.4)	SUMMARY:.....	152
CHAPTER 16.....		153
BATTERY: ENERGY DENSITY OPTIMIZATION		153
16.1)	INTRODUCTION:	153
16.2)	TRADE STUDIES:.....	153
16.2.1)	Range vs Payload:.....	153
16.2.2)	Range vs L/D:	154
16.2.3)	Range vs Take-off Weight:.....	154
References.....		156

LIST OF TABLES

<i>Table 1: Mission Specifications: Proposed Aircraft</i> -----	13
Table 2: Electro Light -2 aircraft weights -----	15
Table 3: Pipistrel Taurus G4 Weights -----	16
Table 4: NASA Scuba Stingray Aircraft Weights -----	17
Table 5: Antares 23E Weights -----	18
Table 6 Yuneec E430 Weights-----	19
Table 7 Aircraft Models with notable Electric Battery and Motor Power -----	22
Table 8 Comparison of several types of batteries-----	30
Table 9 Aircraft Models with notable Take-off and Empty Weights -----	33
Table 10 Assumed Structure Weight using Class II Estimates -----	39
Table 11 Assumed Power Plant Weight using Class II Estimates -----	40
Table 12 Assumed Fixed Equipment Weights using Class II Estimates -----	41
Table 13 Comparison of Experimental Battery Properties -----	43
Table 14 Required value for (W/P) -----	57
Table 15 Drag polars for Proposed Aircraft-----	64
Table 16 The range of W/S and W/P for which the FAR 23.65 is satisfied-----	66
Table 17 Range of wing loading and power loading for which the FAR-23.65 climb gradient requirement is satisfied-----	67
Table 18 Range of take-off wing loading and power loading for which FAR-23.77 climb gradient requirement is satisfied-----	68
Table 19 Motor Trade Study-----	76
Table 20 Battery Configuration Comparison -----	76
Table 21 Fuselage Dimensions-----	84
Table 22 Wing Parameters -----	98
Table 23 The Weight Fractions for Similar Airplanes-----	114
Table 24 The Major Component Weight Summary for Proposed Electric Aircraft-----	115
Table 25 Component Weight Breakdown and Coordinate Data: Proposed Aircraft -----	115
Table 26 Revised Moment Arm: Proposed Aircraft -----	120
Table 27 New C.G. Location for Different Configuration: Proposed Aircraft -----	121
Table 28 Flap Drag Increment -----	129
Table 29 Landing Gear Drag Increment -----	129
Table 30 Zero Lift Drag Coefficient: Proposed Airplane-----	130
Table 31 Drag Polars: Proposed Aircraft -----	130
Table 32 The New L/D Values: Proposed Aircraft-----	130
Table 33 Geometric Parameters: Proposed Aircraft -----	135
Table 34 Tire Data for Nose & Main Gear-----	143
Table 35 Class II Structure Weight Estimates: Proposed Aircraft-----	151
Table 36 Class II Powerplant Weight Estimates: Proposed Aircraft-----	152
Table 37 Class II Fixed Equipment Weight: Proposed Aircraft-----	152

LIST OF FIGURES

Figure 1: Mission profile using preliminary estimates -----	13
Figure 2: Global electric market trends -----	14
Figure 3: Electro light – 2 -----	15
Figure 4: Pipistrel Taurus G4-----	16
Figure 5 NASA Scuba Stingray Proposed Model -----	17
Figure 6 Electro light-2 3-D Drawings -----	23
Figure 7 Pipistrel Taurus G4 3-D Drawings -----	24
Figure 8 NASA Scuba Stingray 3-D Drawings -----	25
Figure 9 Lange Aviation Antares 23E 3-D Drawings -----	26
Figure 10 Yuneec International E430 3-D Drawings -----	27
Figure 11 Low wing configuration-----	29
Figure 12 T-tail configuration-----	30
Figure 13 Top view of proposed configuration -----	31
Figure 14 Side view of proposed configuration-----	31
Figure 15 Take-off Weight versus Empty Weight-----	34
Figure 16 Comparison of Similar Gasoline Aircraft from Roskam vs Electric Aircraft -----	35
Figure 17 Lift-to-drag ratio for different aircraft -----	37
Figure 18 Efficiencies of Different Propulsion Systems-----	37
Figure 19 Class II Estimates from 'Airplane Design Part V' -----	39
Figure 20 Power plant Weight - Class II Estimates from 'Airplane Design Part V' -----	40
Figure 21 Fixed Equipment Weight - Class II Estimates from 'Airplane Design Part V' -----	41
Figure 22 Current Battery Technology and Expected Future Battery Specific Energy-----	43
Figure 23 Allowable Design Point for Proposed Aircraft -----	44
Figure 24 The Regression Point Calculation Result -----	44
Figure 25 The Take-off Weight Calculation Result-----	45
Figure 26 The Take-off Weight Sensitivities Result-----	48
Figure 27 Range vs Total Propulsive Efficiency Graph-----	49
Figure 28 Range vs Battery Energy Density Graph-----	49
Figure 29 Range vs Lift-to-drag ratio Graph -----	50
Figure 30 Payload vs Range Graph -----	50
Figure 31 Lift-to-drag ratio from Jan Roskam -----	53
Figure 32 Definition of FAR-23 Take-off Distances -----	54
Figure 33 Effect of take-off parameter on take-off distance -----	55
Figure 34 Relation between total take-off vs take-off ground-----	56
Figure 35 Effect of take-off wing loading and maximum take-off lift co-efficient on take-off power loading -----	57
Figure 36 Definition of FAR-23 Landing Distances-----	58
Figure 37 Effect of square of stall speed on landing ground run-----	59
Figure 38 Relation between ground run and landing distance-----	59
Figure 39 Allowable wing loading to meet a landing distance requirement -----	60
Figure 40 Equivalent parasite area vs Wetted area-----	62
Figure 41 a and b values based on skin friction co-efficient -----	62
Figure 42 Relation between wetted area vs take-off weight -----	63
Figure 43 Values for c and d for several types of aircraft -----	63
Figure 44 First Estimates for zero-lift drag co-efficient-----	64
Figure 45 Range of W/S and W/P values for which the FAR 23.65 climb requirement is satisfied ---	66

Figure 46 Range of W/S and W/P values for which the FAR 23.65 climb gradient requirement is satisfied	67
Figure 47 Range of W/S and W/P for which FAR-23.77 climb gradient requirement is satisfied	68
Figure 48 Airplane speed vs Power index	69
Figure 49 Allowable W/S and W/P to meet a given cruise speed	70
Figure 50 Matching Results for Sizing of a Proposed Aircraft	71
Figure 51 Calculation of take-off wing loading from stall speed	72
Figure 52 Take-off distance parameters	72
Figure 53 The value of take-off wing loading from landing distance parameters	72
Figure 54 The climb constraint parameters	73
Figure 55 The cruise speed value from AAA	73
Figure 56 The matching graph from AAA	74
Figure 57 Rubber Motor Parametric Study	77
Figure 58 Dimensions of Sitting Male Crew Member in Cockpit	81
Figure 59 Dimensions and Weights for Male Crew Members as Shown in Figure 1	82
Figure 60 Recommended Seat Arrangement for Civil Airplanes	82
Figure 61 Dimensions for Civil Cockpit Controls	83
Figure 62 Isometric View of Fuselage	84
Figure 63 Side View of Fuselage	84
Figure 64 Top View of Fuselage	85
Figure 65 Wing Parameters	86
Figure 66 Wing Geometric Data for Single Engine Propeller Driven Airplane	88
Figure 67 Thickness Ratio Values for Single Engine Propeller Driven Airplane	89
Figure 68 Airfoil Geometry	90
Figure 69 NACA 63412 Airfoil	90
Figure 70 NACA 63412 Plot Using XFLR5	91
Figure 71 Reynolds Number for NACA 63412	91
Figure 72 Co-efficient of lift versus angle of attack for NACA 63412	91
Figure 73 Co-efficient of lift versus co-efficient of drag for NACA 63412	92
Figure 74 Co-efficient of lift/Co-efficient of drag versus alpha for NACA 63412	92
Figure 75 Pitching Moment Co-efficient versus angle of attack for NACA 63412	93
Figure 76 Types of High-Lift Devices	93
Figure 77 Flap Geometry	95
Figure 78 Value of K based on flap chord ratio	95
Figure 79 Effect of Thickness Ratio and Flap Chord Ratio on $CL\delta f$	96
Figure 80 Effect of Flap Chord Ratio and Flap Deflection on K'	96
Figure 81 Aileron Data for Single Engine Propeller Driven Airplane	97
Figure 82 Wing Planform using AAA Program	98
Figure 83 3-D View of Wing using XFLR5	99
Figure 84 Front View of Wing using XFLR5	99
Figure 85 Side View of Wing using XFLR5	100
Figure 86 Top View of Wing using XFLR5	100
Figure 87 Tail Configurations	101
Figure 88 Empennage Moment Arms	102
Figure 89 Single Engine Propeller Driven Airplanes: Horizontal Tail Volume Data	103
Figure 90 Planform Design Parameters for Horizontal Tail	104
Figure 91 Single Engine Propeller Driven Airplanes: Vertical Tail Volume Data	105
Figure 92 Planform Design Parameters for Vertical Tail	106

Figure 93 The AAA Input Parameters for Horizontal Tail: Proposed Aircraft-----	107
Figure 94 The Horizontal Tail: Proposed Aircraft-----	107
Figure 95 The AAA Input Parameters for Vertical Tail: Proposed Aircraft -----	108
Figure 96 The Vertical Tail: Proposed Aircraft -----	108
Figure 97 NACA-0012 Airfoil -----	108
Figure 98 The AAA Input Parameters for Elevator: Proposed Aircraft-----	109
Figure 99 The Elevator Design: Proposed Aircraft -----	109
Figure 100 The AAA Input Parameters for Rudder: Proposed Aircraft-----	110
Figure 101 The Rudder Design: Proposed Aircraft -----	110
Figure 102 Empennage Configuration for Proposed Aircraft-----	111
Figure 103 Landing Gear Parameters-----	113
Figure 104 The C.G. Location for Major Component-----	116
Figure 105 General Arrangement for Proposed Aircraft-----	117
Figure 106 Proposed Aircraft: Weight-C.G. Excursion Diagram-----	117
Figure 107 Tip-over Criteria for Landing Gear Placement-----	118
Figure 108 Ground Clearance Criteria for Gear Placement-----	119
Figure 109 Proposed Aircraft: Landing Gear Arrangement-----	119
Figure 110 Geometry for Static Load Calculation-----	120
Figure 111 Proposed Aircraft: Weight-C.G. Excursion Diagram-----	122
Figure 112 The Longitudinal X-Plot: Proposed Aircraft-----	124
Figure 113 The Directional X-Plot: Proposed Aircraft-----	125
Figure 114 The Equivalent C_f Value -----	128
Figure 115 Compressibility Drag Behaviour -----	129
Figure 116 Clean Configuration Drag Polar -----	130
Figure 117 Take-off Flaps with Landing Gear Down Drag Polar -----	131
Figure 118 Landing Flaps with Landing Gear Down Drag Polar-----	131
Figure 119 All Drag Polar Conditions-----	132
Figure 120 Front View: Proposed Aircraft-----	133
Figure 121 Top View: Proposed Aircraft-----	133
Figure 122 Side View: Proposed Aircraft -----	134
Figure 123 Isometric View: Proposed Aircraft-----	134
Figure 124 Global Electric Aircraft Market Trends-----	137
Figure 125 The Current and Future Battery Trends-----	138
Figure 126 Recommended Tire Pressures for Various Surfaces -----	140
Figure 127 Effect of Tire Pressure and Tire Load on LCN -----	140
Figure 128 Types of Airplane Tyres-----	141
Figure 129 Definition of Rake and Trail -----	143
Figure 130 Nose gear Strut: Proposed Aircraft-----	144
Figure 131 Main Gear Strut: Propose Aircraft -----	144
Figure 132 Shock Absorption Device: Proposed Aircraft -----	145
Figure 133 V-n Diagram According to FAR-23 -----	148
Figure 134 V-n Diagram: Proposed Airplane -----	150
Figure 135 Range vs Payload: Proposed Aircraft -----	153
Figure 136 Range vs L/D: Proposed Aircraft-----	154
Figure 137 Range vs Take-off Weight (Practical $E^*=1.5$ kWh/kg): Proposed Aircraft-----	154
Figure 138 Range vs Take-off Weight (Theoretical $E^*=1.8$ kWh/kg): Proposed Aircraft -----	155

CHAPTER 1

MISSION SPECIFICATIONS & COMPARATIVE STUDY

Conventional aircraft have been serving the current aviation needs both for cargo and passenger travel. Depletion of the fossil fuel reserves, increasing levels of carbon emissions is urging us to search for an alternative means to power the aircraft engines or to change the entire aircraft design. There are many proposed solutions like hydrogen, electricity and bio-fuels to replace the conventional JetA-1 fuels. The main motto of aircraft design is to develop a geometrical conceptual description. In the past few decades, airlines have poured lump sum into research, but the innovations are still limited, winglets.

According to EPA (United States Environmental Protection Agency), 27 percent of U.S. greenhouse gas (GHG) emissions is from transportation and it is also the second leading source of GHG emissions in the United States [1]. From that, aircraft account for 12 percent of all U.S. transportation GHG emissions and 3 percent of total U.S. GHG emissions [2]. The emissions from aviation is contribute about 1 percent of the total air pollution, as states in GAO Repot 2008. Even though this contribution seems small, the air traffic is anticipated to increase at a rate of 60 percent by 2030 [3]. This GHG emissions from aircraft can be controlled by introducing zero-emission propulsion systems in accordance with appropriate airplane design. This can be achieved by designing of an electric airplane by using innovative technologies and noise reduction is also by-product of an electric aircraft.

Aerodynamic efficiency and propulsion system are the two factors that affect the sustainability of the aircraft design. But for the conventional aircraft, there has still been a compromise in one of these factors. An electric aircraft offers great improvements in the propulsion and as well as aerodynamic efficiency. Due to this, electric motors are preferred over the internal combustion engines for model aircraft back in 1970's which were not fully scaled because of low specific energy of the batteries. However, there is no reason why a fully scalable electric aircraft has not been developed with greatly improved battery efficiencies, especially in this era of rapid electric car development.

Electric batteries pose a design challenge in terms of weight. To meet the mission requirements, an aircraft must be equipped with sufficient power. Since the battery weight is directly proportional to the power output. It requires a motor that produces greater horsepower while keeping the weight minimum. Efficiency of a battery is a major design challenge which current technology limits their full-scale integration. However, in the upcoming design chapters all the limitations are carefully addressed, and all the possible design solutions will be documented. In this design report, mission specifications of the proposed aircraft configuration will be analysed.

1.1) MISSION SPECIFICATIONS:

Table 1: Mission Specifications: Proposed Aircraft

Power Supply	Take-off: Batteries Cruise: Batteries Landing: Batteries
Payload	3 Passengers
Crew	1 Pilot
Range	400 nm
Cruise Speed	130 kts
Mach	0.4
	General Aviation, FAR 23 Certifiable

1.1.1) Mission Profile:

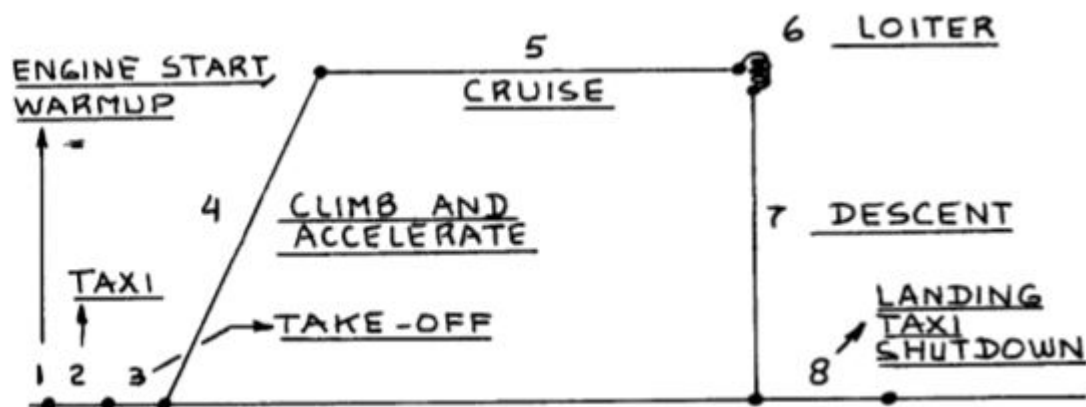


Figure 1: Mission profile using preliminary estimates

The above figure gives a detailed description about the proposed aircraft configuration.

- During **ground run; taxi; take-off**, the **batteries** generate the necessary energy for the aircraft.
- While **Cruising**, electricity is generated using batteries. This is an ideal time for the **batteries to be recharged** which is possible through the Ram Air Turbine (RAM)!!
- During the **Landing Sequence**, the batteries generate the necessary energy for the aircraft.

1.1.2) Market Analysis:

The main concern for aviation industries is the price of fuel, which is basically impelling them to look for alternatives to conventional fuel sources. Therefore, the electrical energy, as an alternative to conventional fuel, may boost the global electric aircraft market demand over the forecast period. It can also reduce the noise generation and ground pollution. This results in reducing the global warming, which is also one of the major reason to drive the global electric aircraft [4].

Below is a graphical representation of the electric aircraft market trends and this clearly portrays a projected market increase up to 4.33% globally.

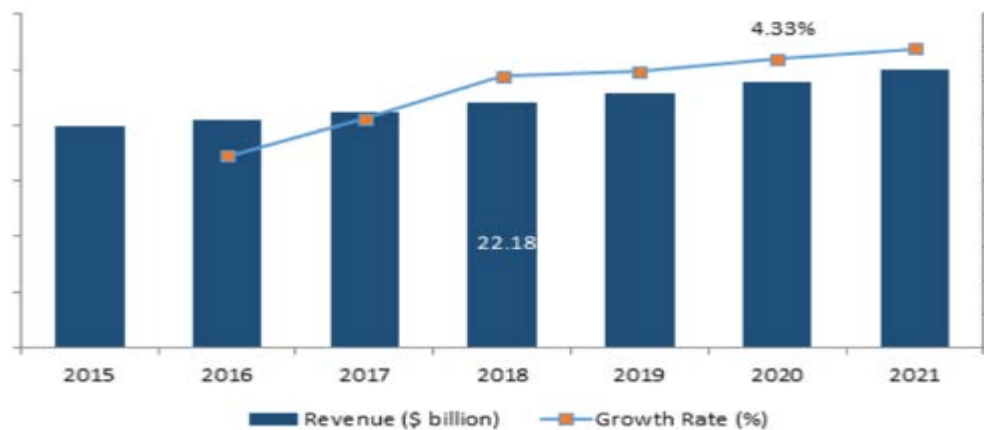


Figure 2: Global electric market trends

1.1.3) Technical and Economic Feasibility:

The technical and economic feasibility of this project is to push the limits of the current technology. Current battery technology is not efficient for long range more capacity airplane. Due to their limited efficiencies, they cannot generate the required power during take-off. Batteries should be carried on-board to power the aircraft during take-off and this results an additional weight. The electric motor developed by DARPA, just weigh 1.4 lbs and can deliver power output of 7 hp. The design of the battery should have the capabilities to fully utilize the motor power.

1.1.4) Critical Mission Requirements:

These are the critical mission requirements that make the electric aircraft the most exciting. Their success could be an asset for the entire aircraft industry.

- Range
- Brushless Motors
- Cruise Speed – 130 kts
- 4 occupants including Pilot

1.2) COMPARATIVE STUDY OF SIMILAR AIRPLANES:

1.2.1) Mission Capabilities and Configuration Selection:

a) Electro Light-2:



Figure 3: Electro light – 2

Table 2: Electro Light -2 aircraft weights

Take-off Weight (lbs)	6805.6
Empty Weight (lbs)	4062
Battery Weight (lbs)	736
Weight of Motor (lbs)	151
Motor Power (kW)	20
Power	Electric

b) Pipistrel Taurus G4:



Figure 4: Pipistrel Taurus G4

Table 3: Pipistrel Taurus G4 Weights

Take-off Weight (lbs)	992
Empty Weight (lbs)	628
Battery Weight (lbs)	287
Power	Electric

c) NASA Scuba Stingray:



Figure 5 NASA Scuba Stingray Proposed Model

Table 4: NASA Scuba Stingray Aircraft Weights

Take-off Weight (lbs)	3195
Empty Weight (lbs)	1438
Battery Weight (lbs)	957
Weight of Motor (lbs)	130
Power	Electric

d) Lange Aviation Antares 23E:



Figure 6: Antares 23E

Table 5: Antares 23E Weights

Take-off Weight (lbs)	11883
Empty Weight (lbs)	10717
Battery Weight (lbs)	1665
Weight of Motor (lbs)	629
Motor Power (kW)	42
Power	Electric

e) Yuneec International E430:



Figure 7: Yuneec E430

Table 6 Yuneec E430 Weights

Take-off Weight (lbs)	10155
Empty Weight (lbs)	3393
Battery Weight (lbs)	1600
Weight of Motor (lbs)	410
Motor Power (kW)	40
Power	Electric

1.2.2) Comparison of Important Design Parameters:

Table 7: Aircraft Models with notable Electric Battery and Motor Power

Aircraft Model	Take-off(lbs)	Empty Weight(lbs)	Battery Weight (lbs)	Weight of Motor (lbs)	Motor Power (kW)
ElectroLight2	6805.67	4062	735	151	19
Pipistrel Taurus G4	992	628	287	N/A	145
NASA Scuba Stingray	3195	1438	957	130	273
Lange Aviation Antares 23E	18365	10717	1665	629	42
Yuneec International E430	10155	3393	1600	411	40

1.3) DISCUSSION:

In the previous section a comparative analysis is provided for different aircraft that are powered by batteries. It is evident that the tabulated aircraft have different power efficiencies and seating capabilities which are almost limited to four passengers including Pilot. The gap is clearly between the requirements for environmentally clean aircraft, clean energy transport and technology limitations. The mission specifications listed in table 1 would be able to bridge the gap and can even revolutionise recreation, exercise flights with the most energy efficient generation techniques.

CHAPTER 2

CONFIGURATION DESIGN

Configuration design for this aircraft is based on the current and previous designs which include gasoline aircraft. Almost every aircraft today has an integrated gasoline engine with traditional configuration. The very fact that current aircraft follow certain traditions in terms of wing, engine, tail and fuselage placements. For commercial aviation; low/high wing configuration, engines dangling down the wings and sometimes integrated into the vertical tail can be vividly seen where these types of configurations are aerodynamically efficient which the aircraft have both the current/past technologies integrated into them.

The proposed aircraft is typically made to be efficient, stable and easily controllable. The mission specifications of documented similar aircraft will be compared again to check whether the integration of a lightweight motor made any difference while proving a point.

A comprehensive list of similar aircraft design with similar mission specifications will be discussed in the later sections where the key configuration parameters are tabulate. This is important as it helps in understanding a key aspect i.e. a relation between available technology versus integration of advanced technologies. For example, like gasoline aircraft; the availability of electric motors data leaves us with more options rather than assumptions. Propulsion system location is integrated based on the safety, reliability and efficiency. Though the mission requirements cannot be met due to certain limitations; the configuration design helps us to accomplish them.

The aircraft configuration is designed as per the trade-offs based on the aircraft data presented. Overall aircraft configuration will be made as simple and predictable that which matches the behaviour and performance of regular aircraft. These predictions which help us to evaluate the critical mission requirements at the end are viable because they save time and money which is crucial in aviation industry.

The main purpose of this report is to study the current aircraft configuration and to provide an analysis of your proposed aircraft. An overall configuration, wing configuration, empennage configuration, landing gear disposition with preliminary CAD drawing is presented in this report.

2.1) COMPARATIVE STUDY OF SIMILAR AIRPLANES:

2.1.1) Comparison of Weights, Performance and Geometry of Similar Airplanes:

Table 7 Aircraft Models with notable Electric Battery and Motor Power

Aircraft Model	ElectroLight 2	Pipistrel Taurus G4	NASA Scuba Stingray	Lange Aviation Antares 23E	Yuneec International E430
Take-off (lbs)	6805.67	992	3195	18365	10155
Empty Weight (lbs)	4062	628	1438	10717	3393
Weight of Motor (lbs)	151	N/A	130	629	411
Motor Power (kW)	19	145	273	42	40
Battery Weight (lbs)	735	287	957	1665	1600
Range (nm)	108	N/A	836	N/A	121
Wing Configuration	High Wing	Mid Wing	Low Wing	Mid Wing	High Wing
Tail Configuration	V-Tail only with Rudder	T-Tail	T-Tail	T-Tail	V-Tail
Wing Span (ft.)	34.4	75	37	75.46	45

2.1.2) Configuration Comparison of Similar Airplanes:

a) Electro Light-2:

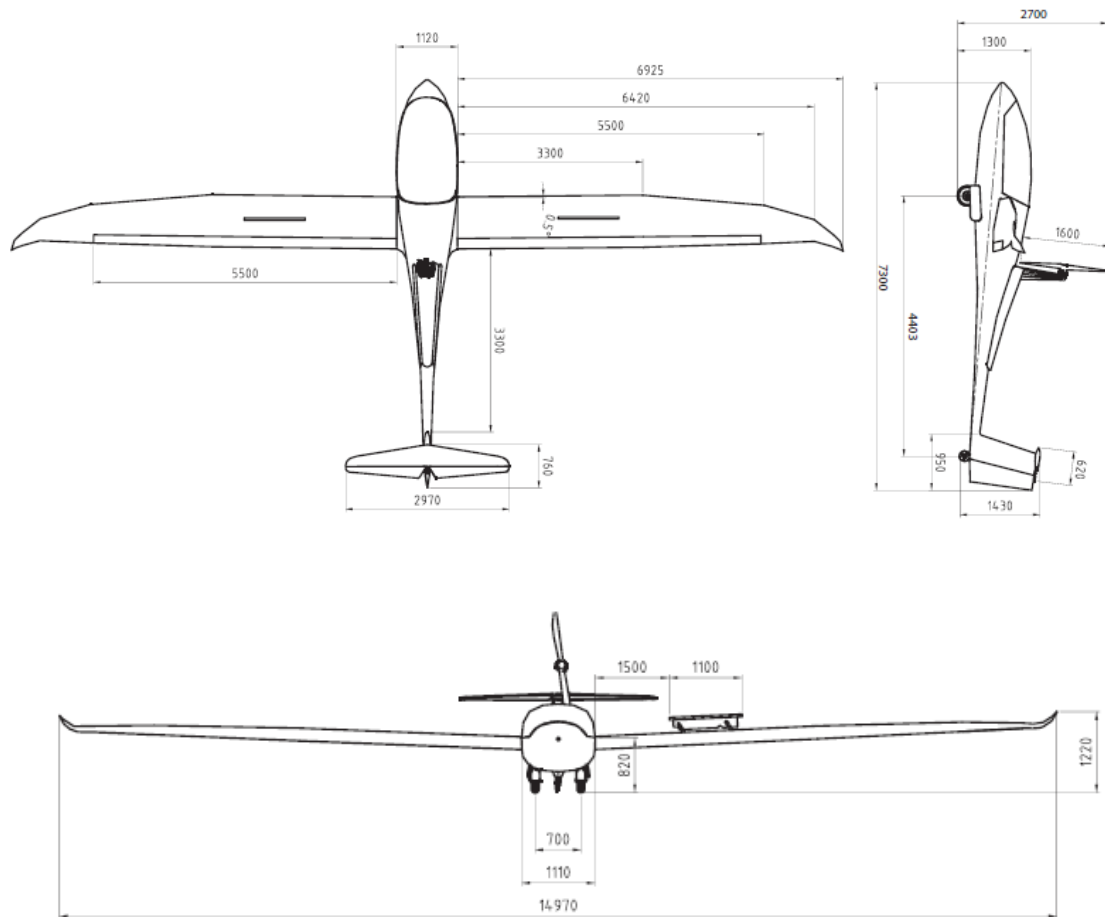


Figure 6 Electro light-2 3-D Drawings

b) Pipistrel Taurus G4:

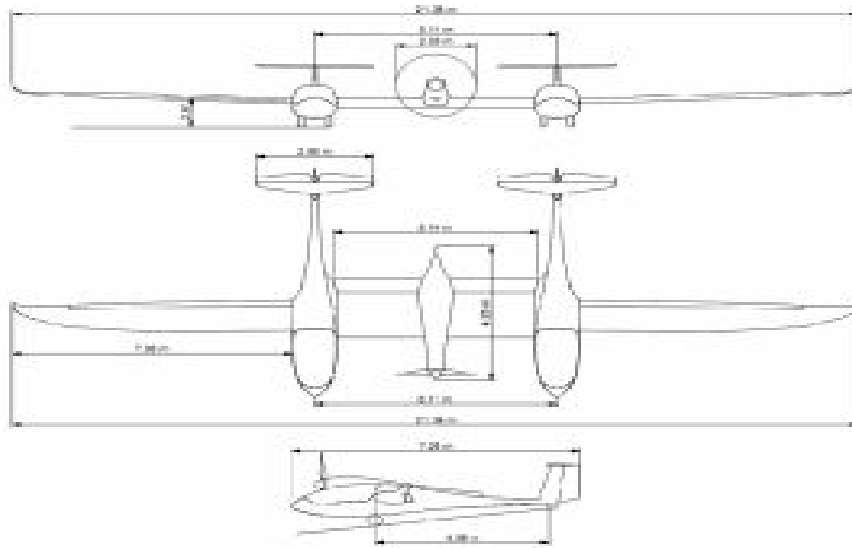


Figure 7 Pipistrel Taurus G4 3-D Drawings

c) NASA Scuba Stingray:

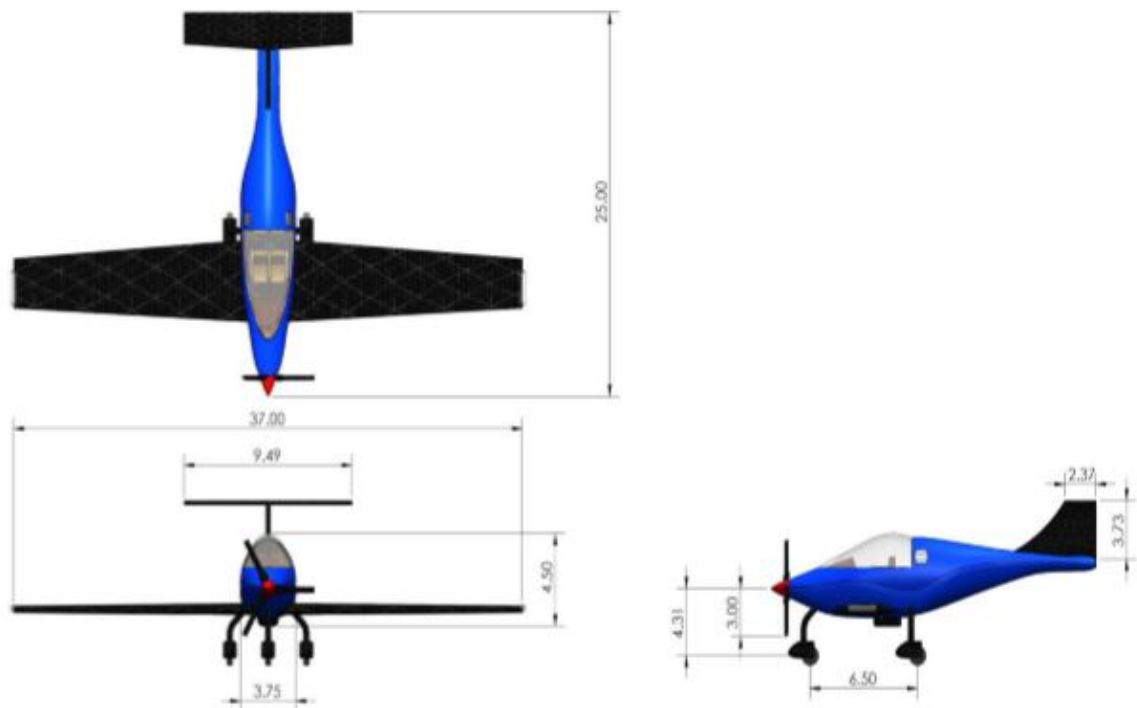


Figure 8 NASA Scuba Stingray 3-D Drawings

d) Lange Aviation Antares 23E:

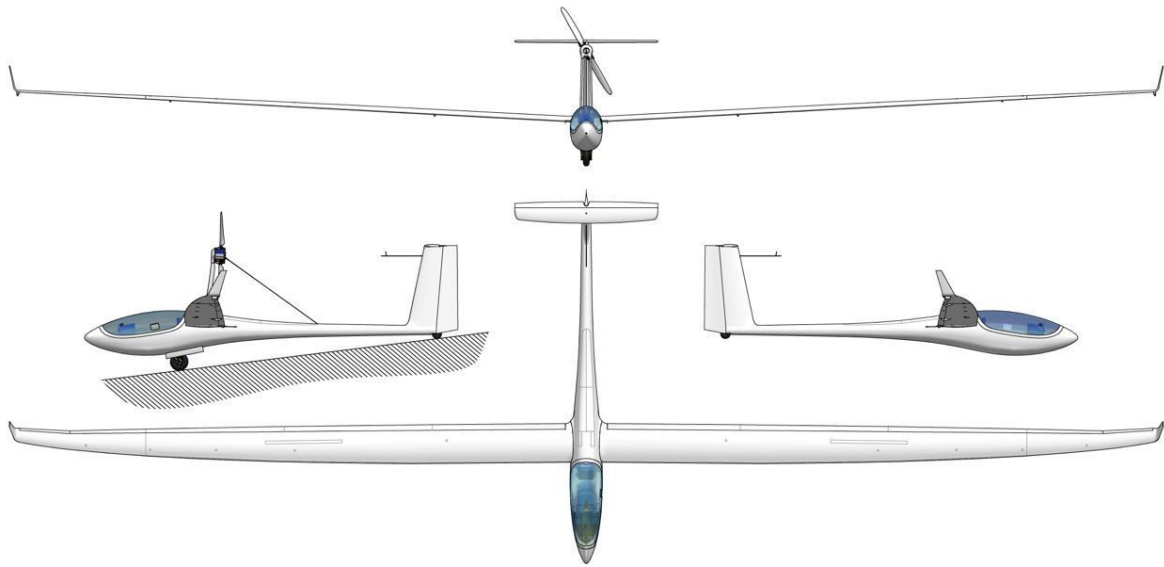


Figure 9 Lange Aviation Antares 23E 3-D Drawings

e) Yuneec International E430:



Figure 10 Yuneec International E430 3-D Drawings

2.2) DISCUSSION:

In the previous section, 3-D drawings are provided for different aircraft that are powered by batteries. It is evident that the tabulated aircraft have different power efficiencies and seating capabilities which are almost limited to four passengers including Pilot. The gap is clearly between the requirements for environmentally clean aircraft, clean energy transport and technology limitations. The propulsion system for the aircraft listed above differ in their locations. Almost all the aircraft of general aviation have propeller blades at the nose, indeed it has some advantages. Nose propellers are simple in design and much more aerodynamically stable. It also makes the aircraft much easier to control. It is safer and easier to fly with small propeller aircraft.

The second key design parameter is wing configuration. The tabulated aircraft data in the previous sections gives us a glimpse of their respective wing configurations. We can see that two out of five have high wing configuration, two of them have mid wing configuration and one have low wing configuration. Low wing aircraft are attached at the bottom of fuselage, so it is easy to refuel aircraft. Low wing aircraft causes better ground effect which increases lift and reduces drag of aircraft when it is nearer to the earth's surface. High wing aircraft offers longitudinal stability while in low wing, it is achieved/compensated by giving 'dihedral' to the wings. The landing gear can be retracted into the low wing configuration. For small aircraft like this there would be an adverse impact on its performance if the landing gear sticks outside as it increases the drag and making it less efficient.

The next design parameter is tail configuration. As we can see, two out of five aircraft have V-tail and three have T-tail configurations. The main advantage of T-tail is a reduction of interference that would result from the placement of the horizontal tail directly behind the main wing. This T-tail configuration may give more predictable design characteristics and better pitch control. The main disadvantage of using T-tail is aircraft may suffer from flutter and deep stall problems.

2.3) CONFIGURATION SELECTION:

2.3.1) Overall Configuration:

A land based conventional configuration is used for the proposed aircraft. The conventional configuration is mainly used as it is the widespread practice which results in aerodynamically efficiency. Bearing in mind the mission that this aircraft should achieve; it is important to take advantage of the previous geometries, design practices to ensure mission success. Also, the use of smaller engines, future technologies and batteries in conjunction with these geometries can be an added advantage.

2.3.2) Wing Configuration:

Wing configuration play a significant role in the overall lift for the aircraft. This is the section where the key aspect of the wing will be thoroughly analysed. Conventional aircraft has three wing placement options i.e. high, low and mid wing. Each has its own advantages and disadvantages. Since, the proposed aircraft is used for passenger travel the low wing configuration will keep the aircraft afloat during an event of 'ditching'. Low wing configuration does not require the use of struts for structural support. Also, the aircraft is not designed for supersonic applications, the drag reduction through swept wings is not necessary.

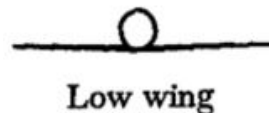


Figure 11 Low wing configuration

2.3.3) Empennage Configuration:

The T-tail configuration is chosen for the proposed aircraft. It offers excellent weight reductions and better tail efficiencies. As mentioned above, it is simple in design and requires a strong rudder due to the movement of the lift forces to the top of the empennage and a lower take-off roll. It also reduces the interference that would result from the placement of the horizontal tail directly behind the main wing and the propeller slipstream.

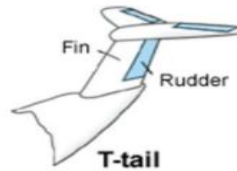


Figure 12 T-tail configuration

2.3.4) Integration of the Propulsion System:

This proposed aircraft will integrate propulsion into the fuselage. The motors are placed in fuselage which enhanced the diameter of propeller. The power source is batteries only. In comparison, power generated from batteries are differ in terms of specific energy, power output and weight. Some remarkable battery configuration are as follows:

Table 8 Comparison of several types of batteries

Experimental Batteries	Specific Energy (kWh/kg)	Environmental Impact	Rechargeable
Lithium Air	~11.4	Zero Emission	YES
Lithium Sulphur	~2.4	Zero Emission	YES
Aluminium Air + Lithium Ion	~1.8	Zero Emission	NO
Aluminium Air + Lithium Sulphur	~4.2	Zero Emission	NO

2.3.5) Landing Gear Disposition:

The landing gear will be stowed into the fuselage and not into the wings because of the joined wing configuration. Also, it is non-retractable and conventional or tricycle configuration. Some of the advantages of tricycle configuration are:

- Good Visibility
- Directionally stable on ground and during taxi
- Large crab angle during cross wind landing
- Increased number of wheels will increase the aircraft performance
- Better protection for propellers

2.3.6) Proposed Configuration:

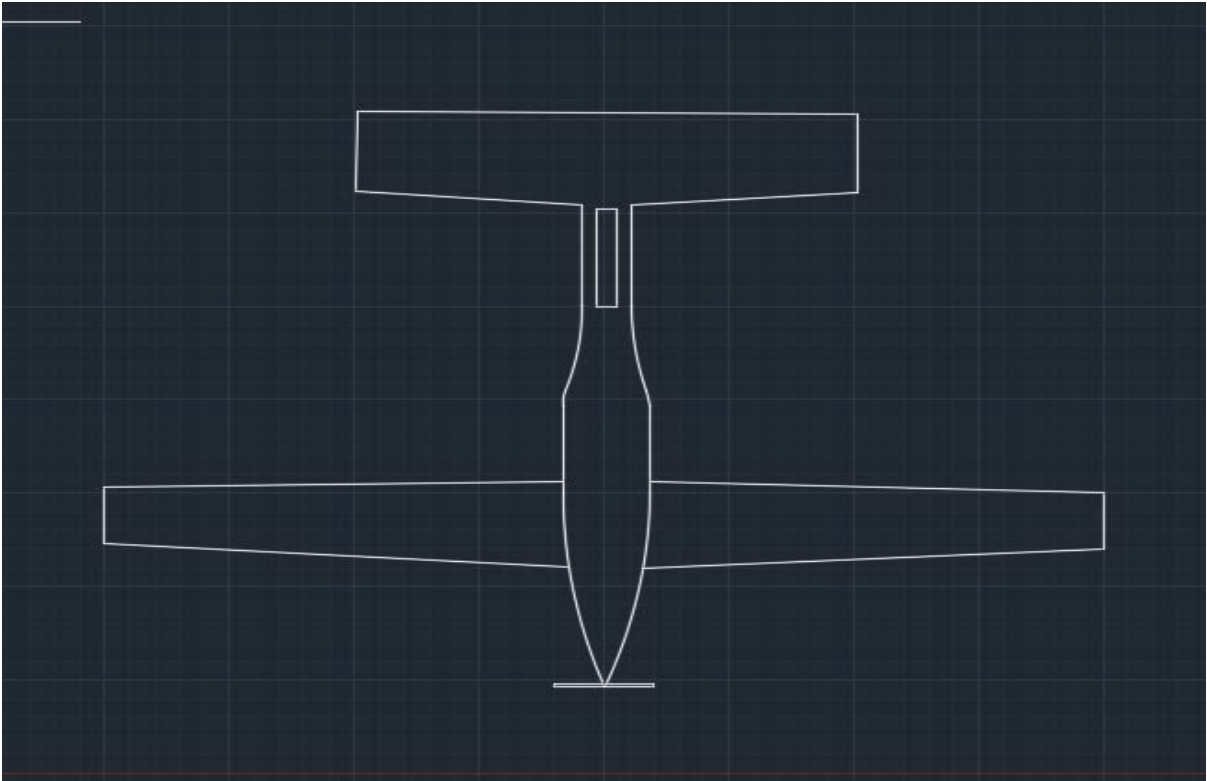


Figure 13 Top view of proposed configuration

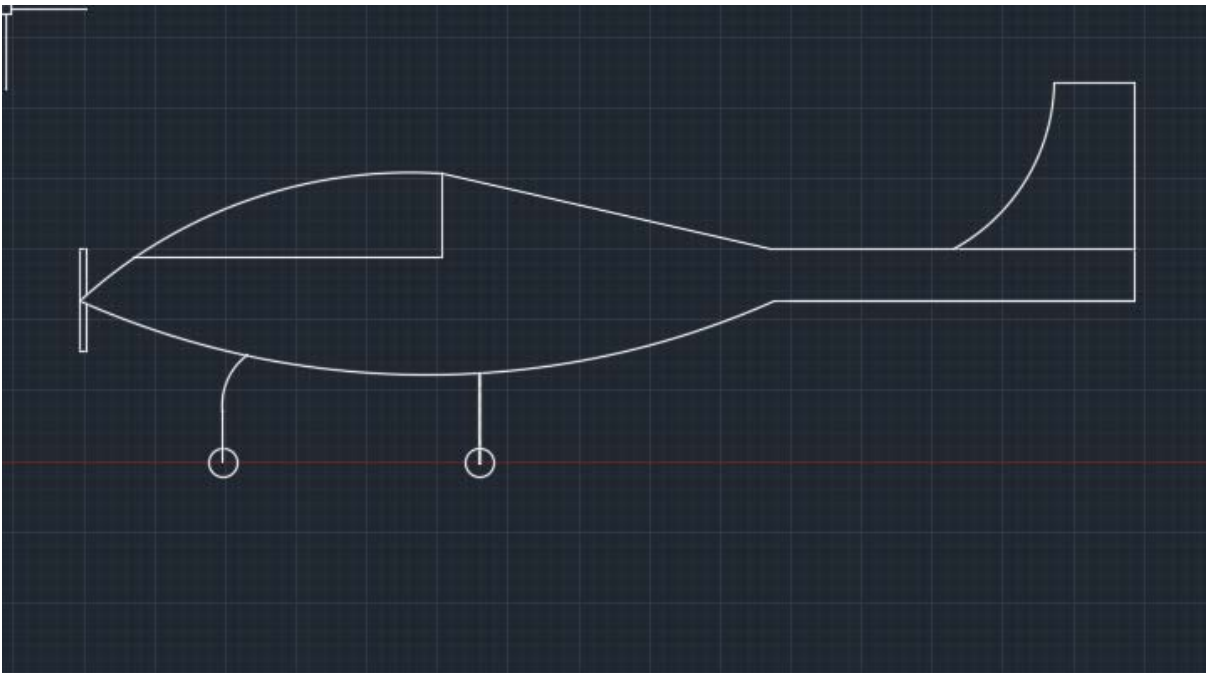


Figure 14 Side view of proposed configuration

CHAPTER 3

WEIGHT SIZING AND WEIGHT SENSITIVITIES

Weight estimation is one of the key areas in the aircraft design. A conventional gasoline weight sizing is a standard process with many different approaches. But for an electric aircraft, the procedures have not been put in place which requires a standard as the conventional aircraft. Growing concerns over environment is one of the sole requirements for the increased demand of non-polluting environment friendly aircraft. For carrying a given payload, aircraft must meet its objectives like cruise speed, range and endurance.

Previously, the urge for developing gasoline aircraft became the basis for standard procedures and how it is important to have robust design practices for an unconventionally propelled aircraft (i.e. by means of batteries, fuel-cells, bio-fuels). Since these design practices are for developing full-scale future aircraft; the weight estimations process also includes few suppositions which may reduce the overall reliability on this process. One of the key developments includes the range equation of the electric aircraft. The range equation is a powerful estimation tool for the preliminary analysis which gives us a clear estimate as to how much the calculated aircraft range matches the proposed value.

There are four categories that contribute to the overall take-off weight.

- Empty weight – Includes structural and fixed-equipment weights
- Battery weight
- Motor weight
- Payload – Weight of passengers and baggage

The main purpose of this report is to study the current aircraft weights and to provide an analysis of your proposed aircraft. Firstly, regression coefficients are calculated based on the similar aircraft take-off and empty weight database. The next step is weight estimation using range equation followed by take-off weight sensitivities, trade studies.

3.1) MISSION WEIGHT ESTIMATES:

3.1.1) Database for Take-off and Empty Weights of Similar Airplanes:

Table 9 Aircraft Models with notable Take-off and Empty Weights

Aircraft	Take-off Weight (lbs)	Empty Weight (lbs)	Battery Weight (lbs)	Motor Weight (lbs)
Electrolight-2	6805	4062	735	151
Pipistrel Taurus G4	992	628	287	N/A
NASA Scuba Stingray	3195	1438	957	130
Lange Aviation Antares 23E	18365	10717	1665	629
Yuneec International E430	10155	3393	1600	411
Lak-17B FES	11883	5315	691	158
Lange Aviation Antares 20E	14260	9506	1664	629
Pipistrel Taurus Electro G2	11883	5466	907	238
UAV Factory Penguin BE	465	212	95	14
Silent 2	6482	4321	778	184

3.1.2) Determination of Regression Coefficients A and B:

The regression coefficients determined in this section are based on the take-off and empty weights of the similar aircraft database presented above. Regression coefficients allows us to determine the relation between the take-off and empty weight. An allowable weight for any aircraft would be determined from above determined relation.

The following figure is the log-log plot of take-off versus empty weight:

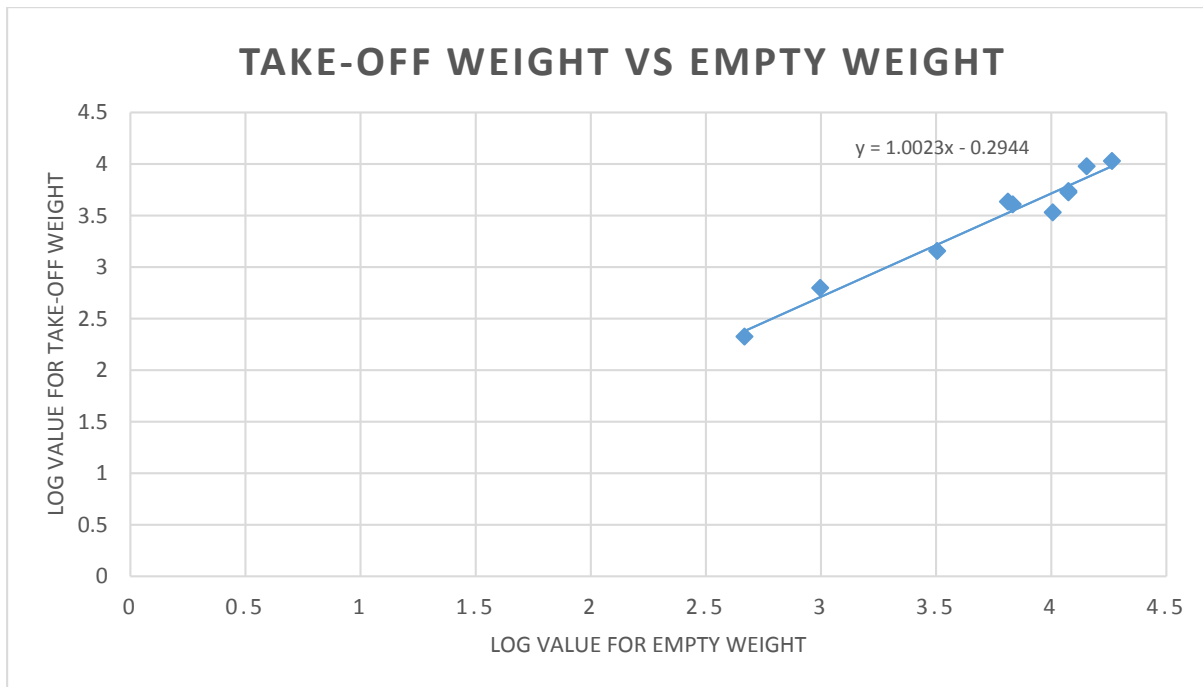


Figure 15 Take-off Weight versus Empty Weight

The regression coefficients are calculated from the trend line equation:

$$y = 1.0023x - 0.2944 \quad (3.1)$$

The relationship equation between take-off weight and empty weight for aircraft in the considered weight category is given by:

$$\log W_{TO} = A + B \log W_E \quad (3.2)$$

$$\log W_E = (\log W_{TO} - A) / B \quad (3.3)$$

By comparing the equation (3.1) & (3.3),

$$y = \log W_E$$

$$x = \log W_{TO}$$

$$\gg 1/B = 1.0023$$

$$\gg \mathbf{B = 0.9977} \quad (3.4)$$

$$\gg \mathbf{A = 0.2933} \quad (3.5)$$

When sizing a gasoline aircraft, there are many resources available to get a clear understanding of where the proposed aircraft configuration stands in the current trend. On the other hand, an electric aircraft, since it includes futuristic technology, there are not many scaled models to predict the stand of proposed aircraft configuration with respect to other available models. For comparative analysis and for pristine idea, a graphical representation is provided below by comparing gasoline aircraft from Roskam and Electric aircraft.

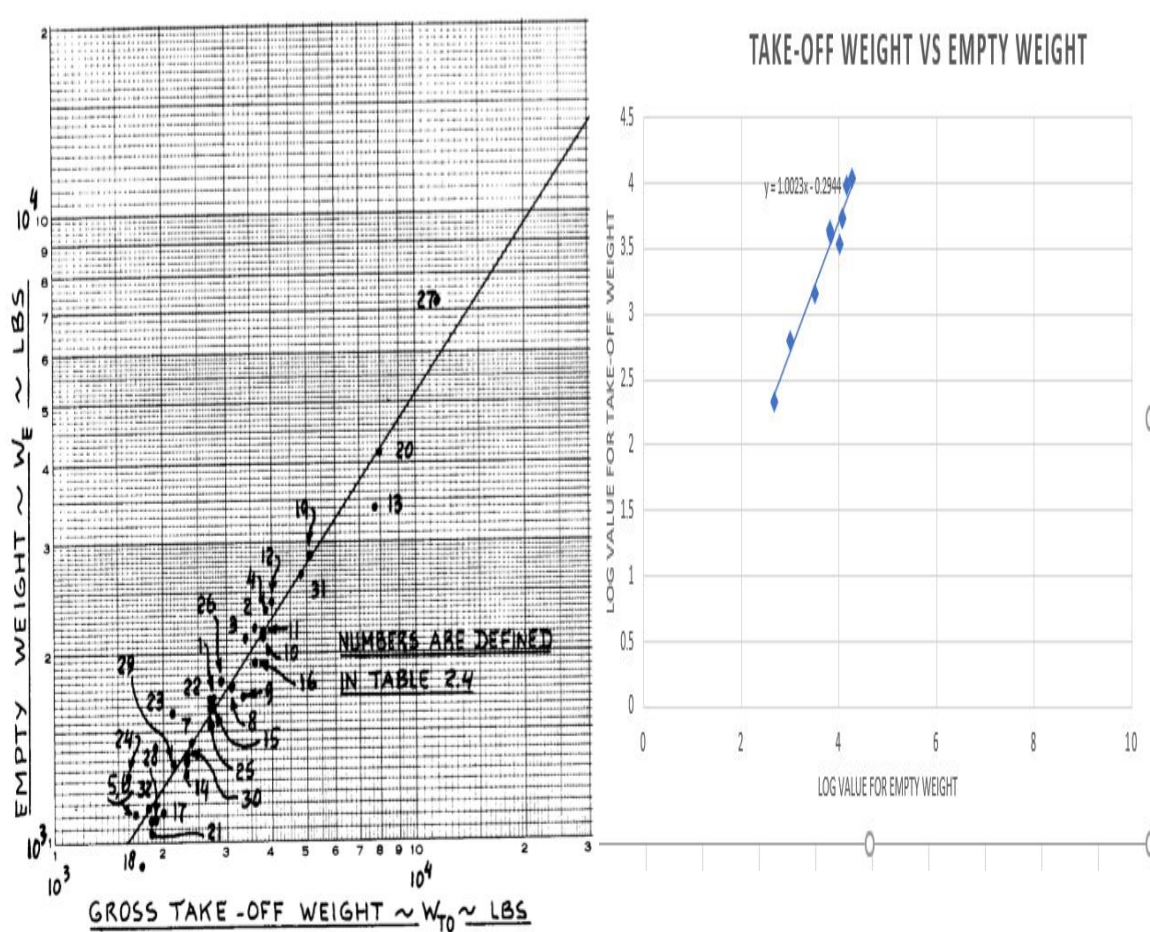


Figure 16 Comparison of Similar Gasoline Aircraft from Roskam vs Electric Aircraft

From the graphical comparison between gasoline aircraft from Roskam and electric aircraft, it is clear that results are almost similar. The only difference is that, Roskam used around 21 aircraft, which are based on old technologies, while we used only 9 aircraft. But, these 9 aircraft are developed using modern technologies (i.e. Composite materials) and it is more current. This new graphical representation will be used in next sections to determine aircraft characteristics.

3.2) DETERMINATION OF MISSION WEIGHTS:

In this section, the mission weights are calculated using two methods, which allows us to understand both methods and gives us a chance to compare the results. The first method is a manual calculation of mission weights, which is basically done by using the range equation of electric aircraft. The second method of calculating the mission weights is by using AAA (Advanced Aircraft Analysis) software.

3.2.1) Manual Calculation of Mission Weights:

The range of the electric aircraft is highly depending on the available energy, the propulsion system, the mass of the aircraft and the aerodynamic properties of the aircraft. The range equation for all the electric aircraft is given by:

$$R = \frac{W_{Battery}}{W} * \frac{L}{D} * \frac{1}{g} * E^* * \eta_{total} \quad (3.6)$$

Where,

R = Range of the aircraft (kms)

$\frac{W_{Battery}}{W} = \text{Battery fraction}$

$\frac{L}{D} = \text{Lift to drag ratio}$

$E^* = \text{Specific Energy Density of the battery or power source}$

$\eta_{total} = \text{Aircraft total efficiency}$

It is clear from the above equation that range is not dependent on the flight speed and to achieve maximum range, the following parameters should be maximized:

- The ratio of battery fraction
- The lift to drag ratio
- The specific energy of the battery
- The total aircraft efficiency

Lift to drag ratio is an aerodynamic parameter that determine the aircraft capabilities of generating lift for the overall aerodynamic drag. Every designers aim is to develop an aircraft which has a maximum L/D through which fuel efficiency can be greatly improved. From the below table (From Roskam), the reasonable and an attainable L/D value for single propeller engine aircraft is 10. This value is used for rest of the calculations.

Mission Phase No. (See Fig. 2.1)	Cruise			Loiter				
	L/D	c_j lbs/lbs/hr	c_p lbs/hp/hr	η_p	L/D	c_j lbs/lbs/hr	c_p lbs/hp/hr	η_p
Airplane Type								
1. Homebuilt	8-10*		0.6-0.8	0.7	10-12		0.5-0.7	0.6
2. Single Engine	8-10		0.5-0.7	0.8	10-12		0.5-0.7	0.7
3. Twin Engine	8-10		0.5-0.7	0.82	9-11		0.5-0.7	0.72
4. Agricultural	5-7		0.5-0.7	0.82	8-10		0.5-0.7	0.72
5. Business Jets	10-12	0.5-0.9			12-14	0.4-0.6		
6. Regional TBP's	11-13		0.4-0.6	0.85	14-16		0.5-0.7	0.77
7. Transport Jets	13-15	0.5-0.9			14-18	0.4-0.6		
8. Military Trainers	8-10	0.5-1.0	0.4-0.6	0.82	10-14	0.4-0.6	0.5-0.7	0.77
9. Fighters	4-7	0.6-1.4	0.5-0.7	0.82	6-9	0.6-0.8	0.5-0.7	0.77
10. Mil. Patrol, Bomb, Transport	13-15	0.5-0.9	0.4-0.7	0.82	14-18	0.4-0.6	0.5-0.7	0.77
11. Flying Boats, Amphibious, Float Airplanes	10-12	0.5-0.9	0.5-0.7	0.82	13-15	0.4-0.6	0.5-0.7	0.77
12. Supersonic Cruise	4-6	0.7-1.5			7-9	0.6-0.8		

Notes: 1. The numbers in this table represent ranges based on existing engines.
 2. There is no substitute for common sense! If and when actual data are available, these should be used.
 3. A good estimate for L/D can be made with the drag polar method of Sub-section 3.4.1.
 * Homebuilts with smooth exteriors and/or high wing loadings can have L/D values which are considerably higher.

Figure 17 Lift-to-drag ratio for different aircraft

The proposed range for electric aircraft is 400 nmi. Ten years from now, if the battery densities have been increased to maximum then the chances for attaining a L/D of 10 are fair. The efficiencies of different propulsion systems are shown in below figure:

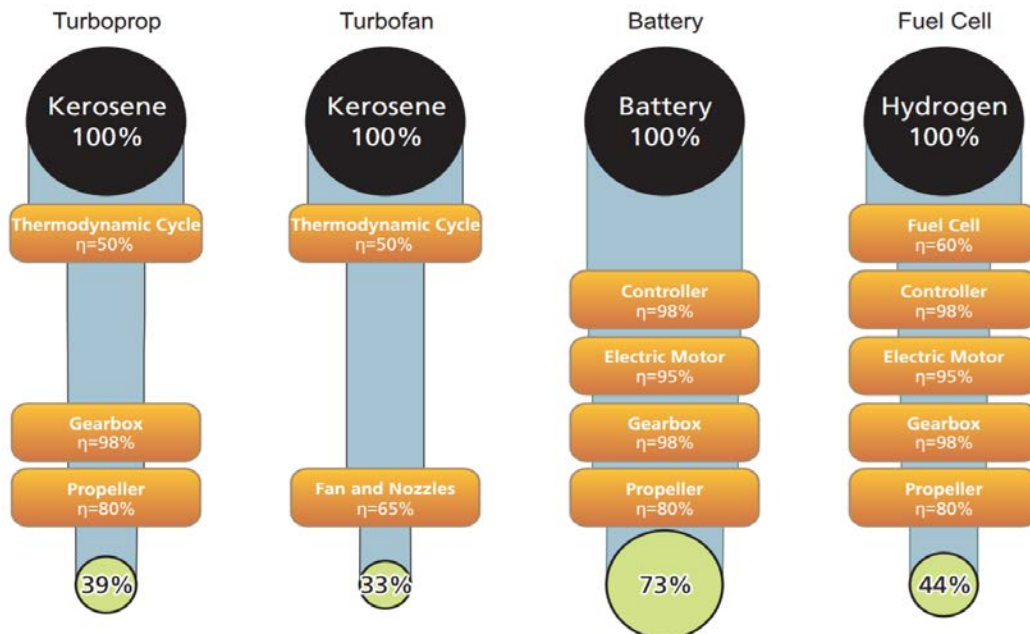


Figure 18 Efficiencies of Different Propulsion Systems

The batteries are being used to generate electricity, when compared with other fuels, battery has an overall propulsive efficiency of 73%. If the battery efficiency has been improved over years, an estimate of 90% efficiency is a reasonable value. The efficiencies of controller, electric motor, gear box and propeller are 98%, 95%, 98%, 80% respectively.

Weight fraction of the batteries can be calculated using the inputs.

$$\Rightarrow 400 \text{ nmi} = \frac{W_{\text{Battery}}}{W} * \frac{L}{D} * \frac{1}{g} * E^* * \eta_{\text{total}} \quad (3.7)$$

$$\Rightarrow 400 = \frac{W_{\text{Battery}}}{W} * 10 * \frac{1}{9.8} * E^* * 0.90$$

$$\Rightarrow \frac{400 \times 9.8}{10 \times 0.90} = \frac{W_{\text{Battery}}}{W} * E^*$$

$$\Rightarrow \frac{W_{\text{Battery}}}{W} * E^* = 435 \text{ nmi}$$

$$\Rightarrow \frac{W_{\text{Battery}}}{W} = \frac{435}{E^*} \quad (3.8)$$

To use equation (3.8), it is important that we have broad range of battery weight fractions available. One of the three crucial factors that affect the range of an electric aircraft is battery weight. Payload and empty weight are other two factors. The payload of any aircraft includes the weight of passengers, crew and baggage. The payload and empty weight vary inversely i.e. if the empty weight is minimum then we can maximize the payload capacity. The payload weight is calculated using following below equation:

$$W_{\text{PL}} = \text{number of passengers} * (\text{weight of each passenger} + \text{each bag weight}) + \text{number of weight} * (\text{weight of each crew} + \text{each bag weight})$$

$$W_{\text{PL}} = 3 * (175 + 30) + 1 * (175+30) \quad (\text{lbs})$$

$$W_{\text{PL}} = 820 \text{ (lbs)} \quad (3.9)$$

Jan Roskam provides a good estimate of the class II sizing of the aircraft components to compute the weight fractions made up of empty weights. The proposed aircraft is electric so the aircraft part of the weights are dropped down to those proposed by Jan Roskam in 'Airplane Design Part V'. Shown below is the breakdown of the weights from 'Airplane Design Part V'.

Component	Methods: Class I Page 9	USAF	Torenbeek	Use as Class II Estimate
=====				
Structure weight, W_{struct} :				
=====				
Wing	738	580	410	576
Adjustment for Fowler flaps, 2 percent:				12
Empennage	179	149	155	161
Fuselage	621	830	1,130	860
Nacelles	249	N.A.	272	261
Landing gear	380	196	313	296
=====				
<u>W_{struct}</u>	2,167	1,755	2,280	2,166
=====				
		excl.nac.		
=====				

Figure 19 Class II Estimates from 'Airplane Design Part V'

Table 10 Assumed Structure Weight using Class II Estimates

Component	Weight (lbs)	Percent of Structure (%)	Assumed Weight / Weight Benefits (lbs)	New Percentages (%)
Wing	590	27	230 / -360*	22
Empennage	170	8	170 / 0*	16
Fuselage	880	40	400 / -480*	38
Nacelles	261	12	0 / -261*	0
Landing Gear	300	14	240 / -60*	23
Total	2201		1040	

Structure weight is one of the three computing factors of empty weight. The above component estimates are based on the gasoline aircraft. Assumptions have been made in the component weights because weights / weight benefits in the above table are based on gasoline aircraft structure weight. For e.g. a weight bonus of 261 lbs can be attained through the nacelles because of the weight reductions being offered by the motors. Also, the other component weight is decreased for proposed electric aircraft because of the development of new composite materials.

Component	Methods: Class I Page 9	USAF	Torenbeek	Use as Class II Estimate
=====				
Powerplant weight, W_{pwr}:				
=====				
Engines	1,400	1,400	1,400	1,400
Air induction	in pwrplt		88	88
Propellers	200	250	250	233
Fuel system	in pwrplt	157	135	146
$W_{pwr} - W_{fs}$		2,162*	2,165**	
Powerplant inst.	108			108
=====				
W_{pwr}	1,708	2,319	2,300	1,975

Figure 20 Power plant Weight - Class II Estimates from 'Airplane Design Part V'

Table 11 Assumed Power Plant Weight using Class II Estimates

Component	Weight (lbs)	Percent of Structure (%)	Assumed Weight / Weight Benefits (lbs)	New Percentage (%)
Engines	1400	75	150*	14
Battery	N/A	N/A	800	76
Air Induction	88	5	50	4
Propeller (with spinner)	233	12	50	4
Fuel System	146	8	N/A	N/A
	1867		1050	

(* = Engine weight includes the weight of motor & drive train assembly)

Power to weight ratio in an electric aircraft is the weight saving factor that these technologies provide compared to gasoline aircraft. Siemens, developed an electric motor with 260kW power output, 110 lbs weight and a power to weight ratio of 5 kW/kg. With this technology, an all-electric aircraft can maximize on the range and could also result in long haul travel with further advancements in the motor and battery efficiencies. 'Emrax' electric motors claim that they have developed a EM348 motor which can deliver a power to weight ratio of 8-10 kW/kg, power output of 350kW, weight of 93 lbs. Even 'Launchpoint' electric motors have developed a halbach array architecture motor which has power to weight ratio of 6.5 kW/kg. It is clear from the above facts that a power to weight ratio of 10 kW/kg can be attained in the plausible future with a power output of 600 kW. Electrical wiring is only needed to connect the batteries to the motors.

Component	Methods: Class I Page 9	Cessna	USAF	T'beek	Use as Class II Estimate
=====					
Fixed equipment weight, W_{feq} :					
=====					
W_{fc}		133	294	91	173
W_{hps} : this is included in W_{fc}					
W_{els}		212	210	209	210
W_{iae}				103	103
W_{api}				88	88
W_{ox}			GD: 25		25
W_{fur}		258		410	334
W_{pt}				Table A3.2a:	48
=====					
W_{feq}		1,025	not complete		981
=====					

Figure 21 Fixed Equipment Weight - Class II Estimates from 'Airplane Design Part V'

Table 12 Assumed Fixed Equipment Weights using Class II Estimates

Component	Weight (lbs)	Percent of Structure (%)	Assumed Weight / Weight Benefits (lbs)	New Percentage (%)
Flight Controls/Hydraulics/Pneumatic	173	20	0	0
Electrical	210	25	180	42
Avionics/Instrumentation	103	12	80	19
Oxygen	25	2	25	5
Furnishings	334	40	140	33
Total	845		425	

The fixed equipment weight fraction estimates provided in table 13 gives us weight benefits with respect to 5 components. Oxygen tanks will be carried since the aircraft cruises at 10,000 ft. There is a requirement for cabin pressurization system. It is mentioned in the

previous sections that this empty weight approximation is made using gasoline aircraft, the furnishings weight for proposed electric aircraft are estimated to 140 lbs.

Now, this brings us to an overall weight savings being offered by the electric aircraft. For a single engine aircraft, from Jan Roskam, Airplane Design Part V, Appendix – A; the empty weights constitute 60% of the aircraft gross weight. This value is before assuming the weight bonus and is a combination of structure, power plant and fixed equipment weight. Table 2, 3 and 4 gives us the final weight fractions of proposed electric aircraft. Any other weight savings could accommodate more payload which would change the weight fractions.

The empty weight is calculated as below:

$$W_{Empty} = W_{Structure} + W_{PowerPlant} + W_{FixedEquipment} \quad (3.10)$$

Since, all the preliminary weights have been determined, take-off weight can be estimated as follows:

$$\begin{aligned} W_{TO} &= W_{PL} + W_{Battery} + W_{Empty} \\ W_{TO} &= 820 + 800 + (1040 + 250 + 425) \quad (lbs) \\ \mathbf{W_{TO} = 3335 lbs} \quad &\mathbf{(3.11)} \end{aligned}$$

Now, to find the required specific battery energy value for the mission, we need to put all values in equation (3.8).

$$\begin{aligned} \Rightarrow \frac{W_{Battery}}{W} &= \frac{435}{E^*} \\ \Rightarrow E^* &= \frac{435}{0.24} \\ \therefore E^* &= \mathbf{1812 \frac{Wh}{kg}} \quad (12) \end{aligned}$$

The lithium batteries have been widely used in aircraft for powering electronics and key flight instrumentation. Lithium ion batteries are cheap, and their manufacturing costs are relatively low. They can produce specific energy of 200 Wh/kg and further developments could scale up this value to 250 Wh/kg.

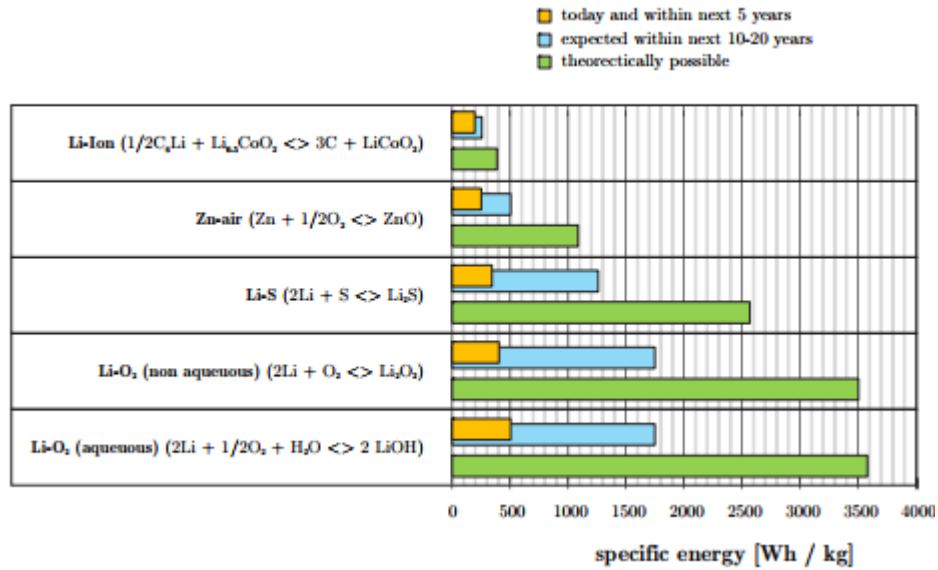


Figure 22 Current Battery Technology and Expected Future Battery Specific Energy

Currently, large amount of experimental concepts research has been going on and it gives the most promise in terms of specific energy. While these all batteries are in the research phase, it is assumed that they would be produced by 2020. The Aluminium Air and Lithium Ion is chosen as the power source because of its effectiveness, promising future, and ease of implementation. The bellow table is provided the detail information about different experimental batteries.

Table 13 Comparison of Experimental Battery Properties

Battery Name	Specific Energy (kWh/kg)	Environmental Impact	Rechargeable	Expected Production Date
Lithium Air	~ 11.4	Zero Emission	YES	N/A
Lithium Sulphur	~ 2.4	Zero Emission	YES	~ 2020
Aluminium Air + Lithium Ion	~ 1.8	Zero Emission	NO (Replace Al & H ₂ O)	2017-2019
Aluminium Air + Lithium Sulphur	~ 4.2	Zero Emission	YES (Replace Al & H ₂ O)	N/A

3.2.2) Calculation of Mission Weights using the Advanced Aircraft Analysis (AAA) Program:

The following below graph represents the allowable weight for proposed electric airplane:

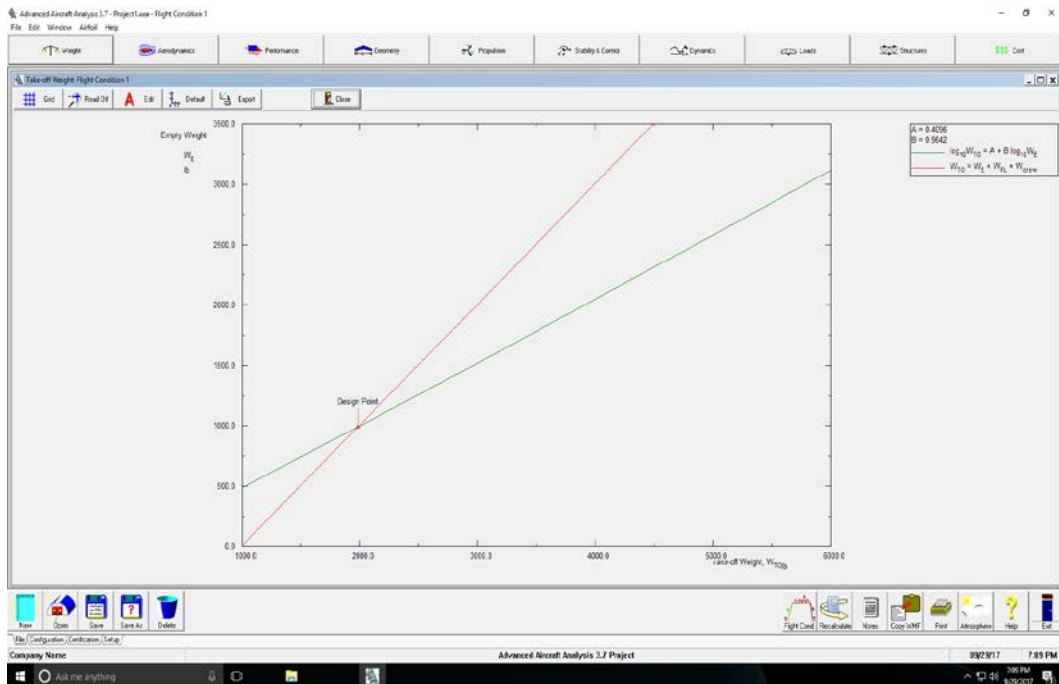


Figure 23 Allowable Design Point for Proposed Aircraft

The Regression Point Calculation from AAA are as follows:

Empty Weight - Take-off Weight Table			
#	Airplane Name	W _{TO} lb	W _E lb
1	NASA Scuba Stingray	3195.0	1438.0
2	Silent 2	6482.0	4321.0
3	Electrolight 2	6805.0	4062.0
4	Pipistrel Taurus G4	992.0	628.0
5	Lange Aviation Antares 23E	18365.0	10717.0
6	Yuneec International E430	10155.0	3393.0
7	Lak-17B FES	11883.0	5315.0
8	Lange Aviation Antares 20E	14260.0	9506.0
9	Pipistrel Taurus G2	11883.0	5466.0
10	UAV Factory Penguin BE	465.0	212.0

Output Parameters			
A	<input type="text" value="0.4096"/>	B	<input type="text" value="0.9642"/>

Figure 24 The Regression Point Calculation Result

The Take-off Weight Calculation from AAA are as follows:

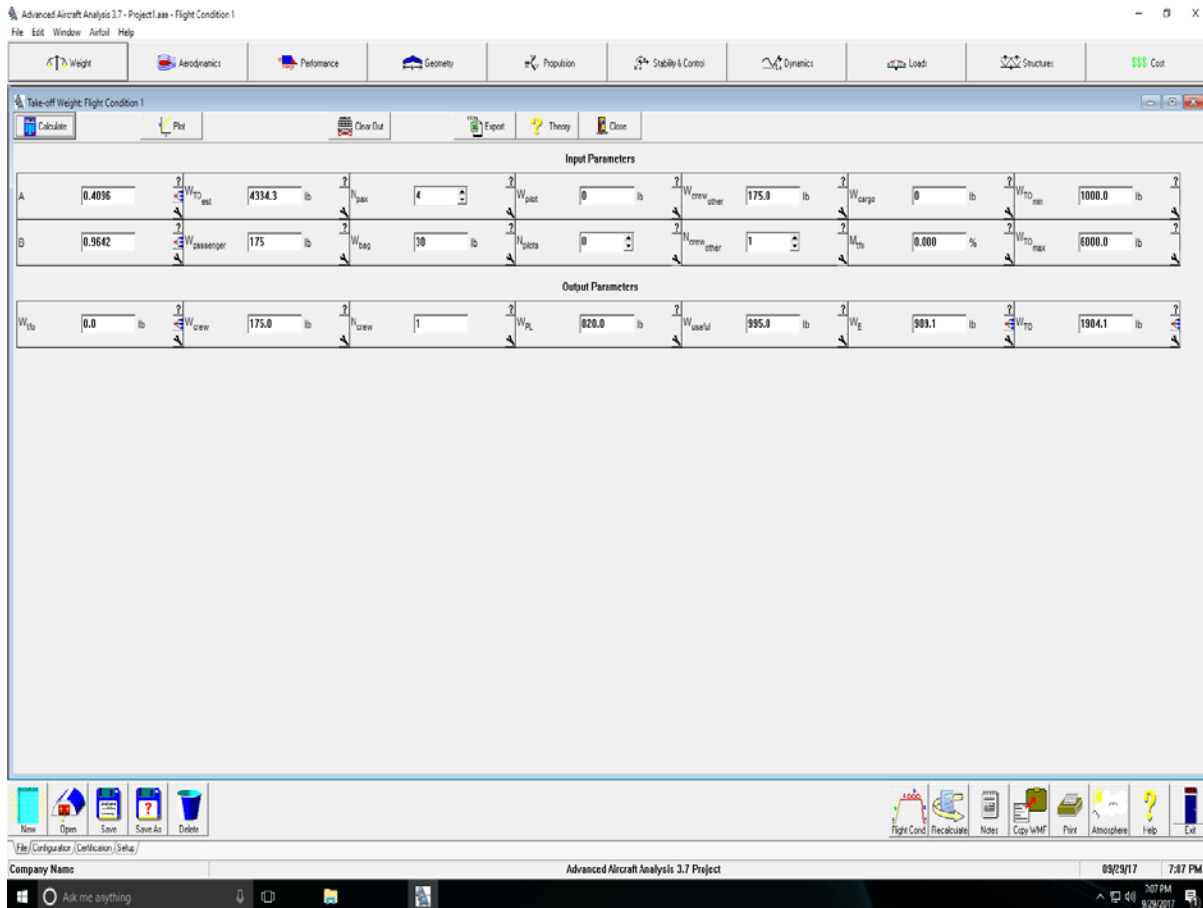


Figure 25 The Take-off Weight Calculation Result

From the AAA software results, it is clear that there is a difference between the manual calculation and the software calculated results. The AAA software calculated take-off weight is less than the manual calculated take-off weight. The reason for that is simple. The AAA software is not fully developed to determine the battery efficiencies, battery weights and the required motor power. In the future design reports, only the manual calculation results will be used and compared with the existing electric aircraft data to maintain coherence.

3.3) RANGE SENSITIVITIES:

It is obvious from the way the results in section (3.2) were obtained, that their outcome depends on the values selected for the various parameters in the range equation. Once the preliminary sizing has been done, it is required to conduct sensitivity studies on some critical parameters. The reasons behind the sensitivity studies are:

- To find out which parameters 'drive' the design
- To determine which areas of technological change must be pursued, if some new mission capability must be achieved
- If parameters like Lift-to-drag ratio, Specific fuel consumption, and Propeller efficiency were selected optimistically (or pessimistically), the sensitivity

studies provide a quick estimate of the impact of such optimism (or pessimism) on the design

In case of the battery powered electric aircraft, the mass of the aircraft stays constant and hence the range equation is simplified. The range sensitivities are calculated in following section.

3.3.1) Manual Calculation of Range Sensitivities:

In this section, the sensitivities of the proposed aircraft with respect to range, empty weight, Lift-to-drag ratio, and battery specific energy will be addressed.

A more complete analysis of existing and prospective electric aircraft showed that the acceptable mass growth depends on aircraft mass: for heavier aircraft, a higher limit can be accepted. Based on the numerical results, the following empirical relation has been developed:

$$\begin{aligned} \left(\frac{\partial m}{\partial R}\right)^* &= \frac{1}{4200} * m^{1.27} \left[\frac{kg}{km} \right] \quad (3.13) \\ \Rightarrow \left(\frac{\partial m}{\partial R}\right)^* &= \frac{1}{4200} * 1513^{1.27} \left[\frac{kg}{km} \right] \\ \therefore \left(\frac{\partial m}{\partial R}\right)^* &= 2.60 \left[\frac{kg}{km} \right] \end{aligned}$$

Empty and Payload Mass fractions

To obtain maximum range, it is important that the empty mass, payload mass fractions are minimum. This relation can be clearly understood from the equation (3.14). The Ultimate Range of the aircraft can be determined by equating the payload mass to zero.

$$R = E^* * \eta_{total} * \frac{1}{g} * \frac{L}{D} * \left(1 - \frac{m_{empty}}{m} - \frac{m_{payload}}{m}\right) \quad (3.14)$$

Note: The determined practical range of the aircraft must be lower than the ultimate range of the aircraft.

The range sensitivity of empty, payload mass fraction is dependent on the L/D, total efficiency and E*. The empty mass and payload mass fraction sensitivities with respect to range will be determined using equation (3.15).

$$\begin{aligned} \frac{\partial R}{\partial f_e} = \frac{\partial R}{\partial f_p} &= -\frac{1}{g} \eta_{total} * E^* * \frac{L}{D} \quad (3.15) \\ \Rightarrow \frac{\partial R}{\partial f_e} = \frac{\partial R}{\partial f_p} &= -\frac{1}{10} * 0.90 * 1812 * 10 \\ \therefore \frac{\partial R}{\partial f_e} = \frac{\partial R}{\partial f_p} &= -1631 km \end{aligned}$$

The obtained range value with respect to payload and empty mass fractions is -1631 km. This value is unclear and does not actually convey the total empty, payload mass required for a kilometre increase in the range. For a clear idea, an inverse of the obtained value is taken, and this gives us $\frac{-0.0006}{km}$. Hence, this value needed to be added for extra addition of range.

Range Sensitivity with respect to Total Mass

Now, the range sensitivity with respect to total mass will be determined. Equation (3.16) clearly illustrates that the range sensitivity is affected by the inverse mass, which in the case of heavier aircraft it does not make sense to change the mass unlike a light weight aircraft.

$$\begin{aligned}\frac{\partial R}{\partial m} &= -\frac{1}{g} * \eta_{total} * E^* * m_{battery} * \frac{L}{D} * \frac{1}{m^2} \quad (3.16) \\ \Rightarrow \frac{\partial R}{\partial m} &= -\frac{1}{10} * 0.90 * 1812 * 800 * 10 * \frac{1}{3335^2} \\ \therefore \frac{\partial R}{\partial m} &= -0.117 \frac{km}{kg}\end{aligned}$$

The total range to mass sensitivity value for proposed aircraft is $-0.117 \frac{km}{kg}$. This value clearly shows that the total mass of the aircraft should decrease to attain greater range while keeping the E^* constant.

Range Sensitivity with respect to L/D

The lift-to-drag ratio is an important aerodynamic property and play's a crucial role in case of light weight aircraft. To obtain greater range; the empty, payload mass fractions should be minimum while maximizing the battery efficiency and density. Typically, for proposed aircraft a L/D value of 10 is initially assumed which is like a Cessna 172.

$$\begin{aligned}\frac{\partial R}{\partial \left(\frac{L}{D}\right)} &= (1 - f_e - f_p) * \frac{1}{g} * E^* * \eta_{total} \quad (3.17) \\ \Rightarrow \frac{\partial R}{\partial \left(\frac{L}{D}\right)} &= (1 - 0.51 - 0.25) * \frac{1}{9.81} * 1812 * 0.90 \\ \therefore \frac{\partial R}{\partial \left(\frac{L}{D}\right)} &= 40km\end{aligned}$$

Range Sensitivity with respect to Energy Density of the Battery

This is the final parameter of concern and the sensitivity of range with respect to energy density of the battery is determined using equation (18).

$$\frac{\partial R}{\partial E^*} = (1 - f_e - f_p) * \frac{1}{g} * \eta_{total} * \frac{L}{D} \quad (3.18)$$

$$\Rightarrow \frac{\partial R}{\partial E^*} = (1 - 0.51 - 0.25) * \frac{1}{9.81} * 0.90 * 10$$

$$\therefore \frac{\partial R}{\partial E^*} = 0.220 \text{ km/Wh/kg}$$

3.3.2) Calculation of Take-off Weight Sensitivities using the AAA Program:

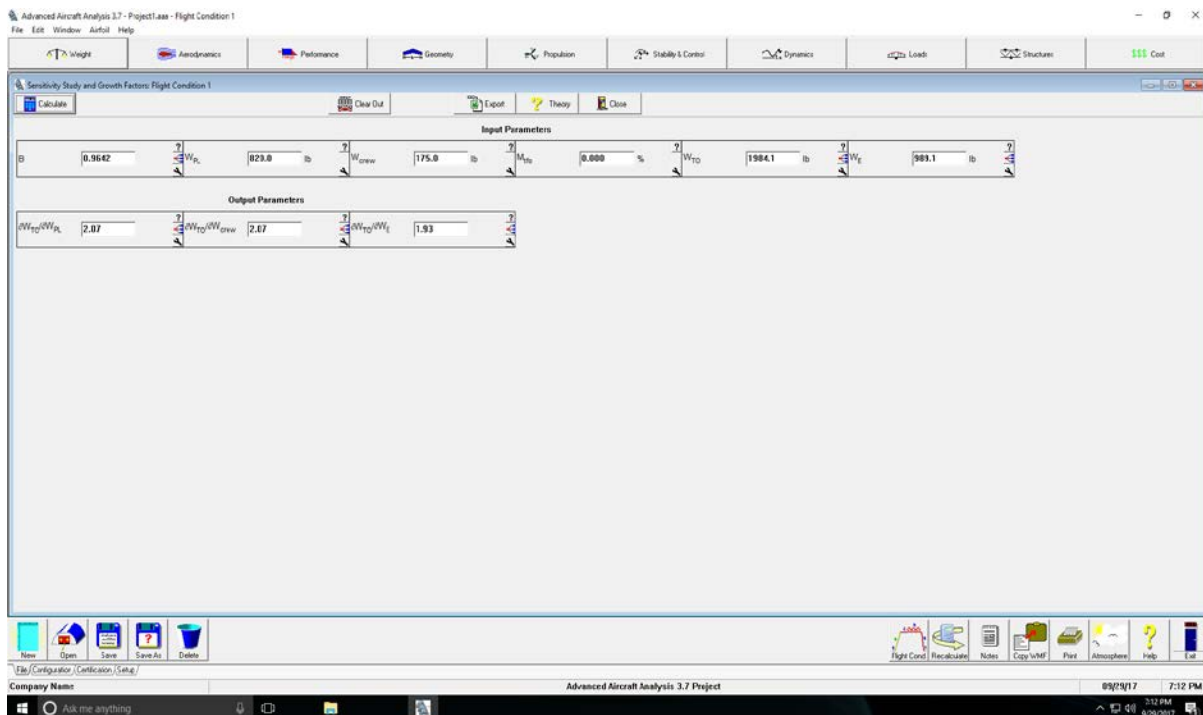


Figure 26 The Take-off Weight Sensitivities Result

The AAA software is not fully developed to determine the range sensitivities of an electric aircraft. In the future design reports, only the manual calculation will be used and compared with the existing electric aircraft data to maintain coherence.

3.4) TRADE STUDIES:

The trade studies are based on equation (3.6).

$$R = \frac{W_{Battery}}{W} * \frac{L}{D} * \frac{1}{g} * E^* * \eta_{total}$$

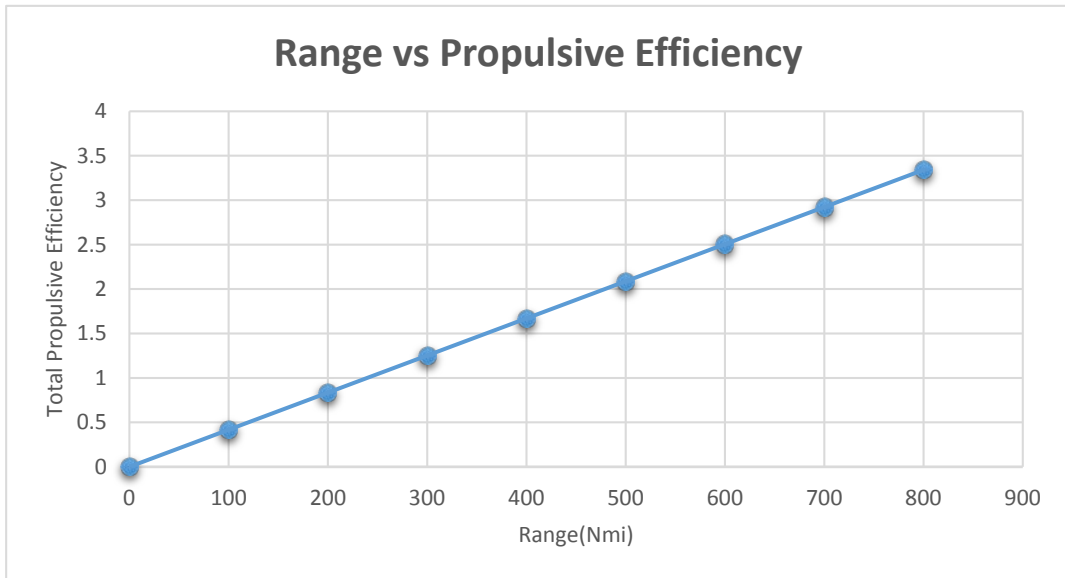


Figure 27 Range vs Total Propulsive Efficiency Graph

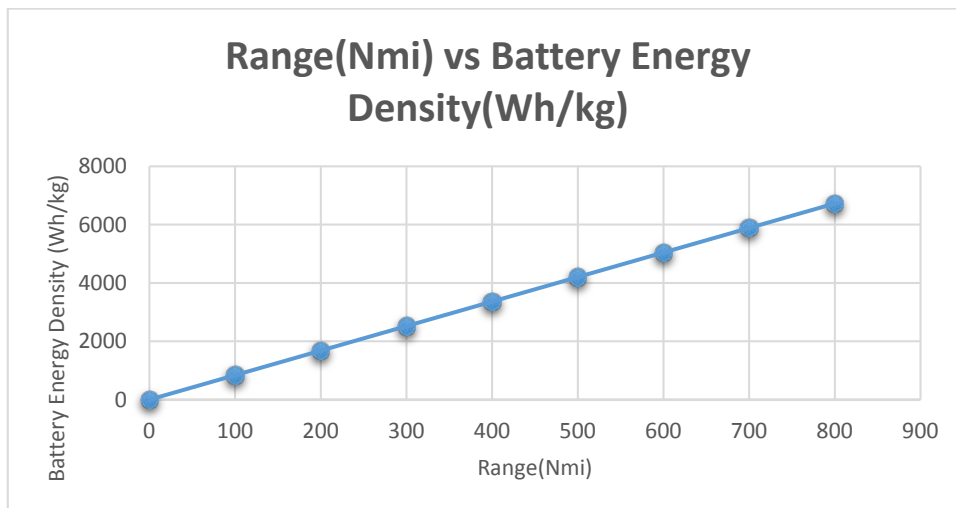


Figure 28 Range vs Battery Energy Density Graph

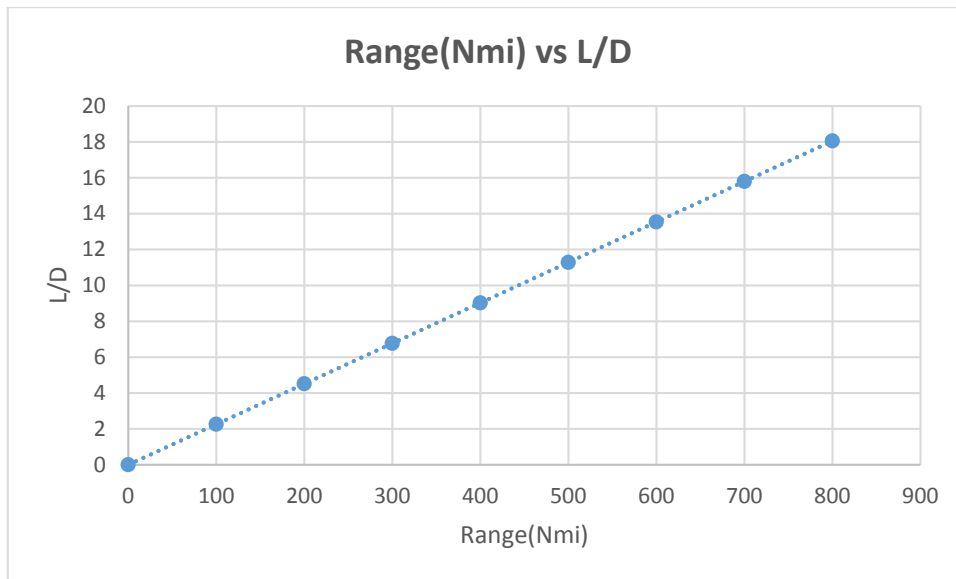


Figure 29 Range vs Lift-to-drag ratio Graph

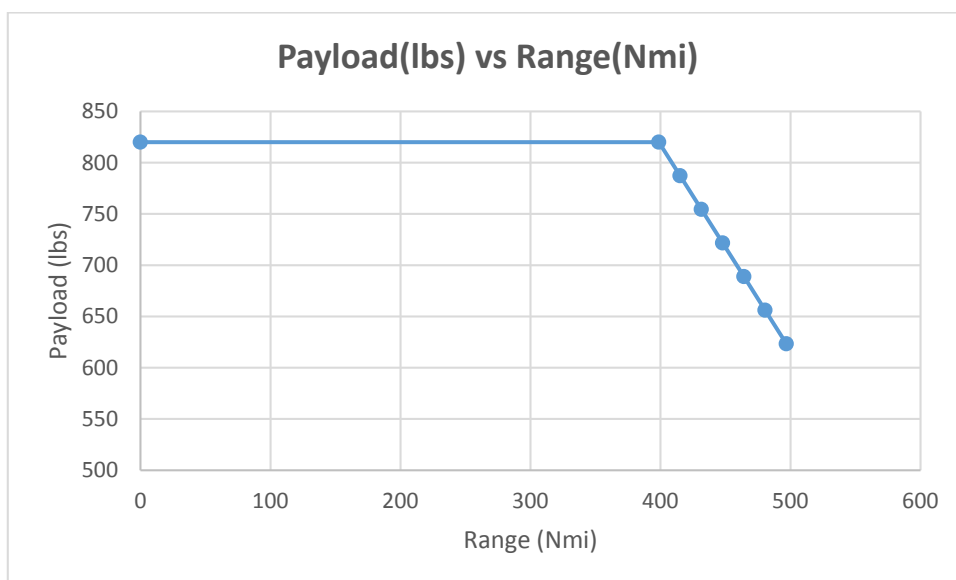


Figure 30 Payload vs Range Graph

3.5) DISCUSSION:

This part of the design report covered the class I preliminary weight estimation which includes all electric aircraft. The regression coefficient plays a vital role in calculation of aircraft allowable weight. In the earlier section of the report, the structural, powerplant and fixed equipment weights have been determined and discussed thoroughly, through which the weight estimates for proposed electric aircraft are locked at this point.

Assumptions have been made in the range equation especially on the total propulsive efficiency; which would directly affect the overall aircraft range as the proposed configuration is an electric and in the calculations, it is directly used. The battery energy efficiency per density is calculated based on the estimated weight fractions through which we obtained a value of 1812 Wh/kg. As per the current battery efficiency trends, attaining this value in the next 5 years is not that much challenging task especially with an efficiency growth rate of 100 Wh/kg. Recent innovations in battery reckons that the electric air travel would soon be a reality. The payload weight (820 lbs) is pre-determined.

The sensitivity studies govern the key parameters with respect to the range which basically gives an idea about proposed aircraft sensitivities regarding L/D ratio, empty and payload mass fraction, total mass, and energy density of batteries. The limitations of AAA program especially with the electrical aircraft does not allow to calculate the exact sensitivities and even weight estimation.

CHAPTER 4

PERFORMANCE CONSTRAINT ANALYSIS

The airborne performance of the airplane suddenly became of primary importance after the rapid development of aviation during the pre-World War I era. In previous reports, the mission specification, configuration selection and weight sizing of proposed aircraft were introduced. In the present chapter, we begin a new phase of study. The airplane will be treated as a rigid body on which four forces are exerted: lift, drag, thrust and weight.

The airplane performance is an important part of aircraft design. In addition to meeting the range, endurance and cruise speed objectives, airplanes are usually designed to meet performance objectives in the following categories:

- Stall Speed
- Take-off distance
- Landing distance
- Cruise speed
- Climb rate
- Manoeuvring

The main purpose of this report is to provide methods which allow the rapid estimation of proposed aircraft design parameters which have a major impact on the above listed performance categories. Since, the proposed aircraft is an electric powered general aviation aircraft and with a take-off weight of less than 6000 lbs, this proposed aircraft falls into FAR-23 certification category. Thus, all the performance constraint calculation will be determined based on the FAR-23 guidelines.

The proposed methods will result in the determination of a range of values of wing loading, thrust or power loading, and maximum lift co-efficient. A matching plot will be presented and the combination of the highest possible wing loading and the lowest possible thrust loading which still meets all performance requirements results in an aircraft with the lowest weight and the lowest cost.

4.1) MANUAL CALCULATIONS OF PERFORMANCE CONSTRAINTS:

4.1.1) Stall Speed:

A stall is a condition where lift coefficient generated by a foil starts reducing as angle of attack increases. As per the guidelines for FAR-23 certification, a single engine airplane may not have a stall speed greater than 61 knots at Take-off weight less than 6000 lbs. Since, proposed aircraft is below 6000 lbs and is an electric general aviation aircraft, the stall speed should be under 61 knots.

The power-off stall speed for proposed aircraft can be derived from:

$$V_{stall} = \left(\frac{2 * \frac{W}{S}}{\rho * C_{Lmax}} \right)^{\frac{1}{2}} \quad (4.1)$$

Where, V_{stall} = Stall speed at power – off

$\frac{W}{S}$ = maximum allowable wing loading

ρ = density at sea – level

C_{Lmax} = maximum co – efficient of lift

The lift co-efficient is influenced by such factors as:

- Wing and airfoil design
- Flap type and size
- Centre of gravity location

The lift co-efficient is represented in following figure which is from Roskam book:

Airplane Type	C_{Lmax}	$C_{Lmax_{TO}}$	C_{Lmax_L}
1. Homebuilts	1.2 – 1.8	1.2 – 1.8	1.2 – 2.0
2. Single Engine Propeller Driven	1.3 – 1.9	1.3 – 1.9	1.6 – 2.3
3. Twin Engine Propeller Driven	1.2 – 1.8	1.4 – 2.0	1.6 – 2.5
4. Agricultural	1.3 – 1.9	1.3 – 1.9	1.3 – 1.9
5. Business Jets	1.4 – 1.8	1.6 – 2.2	1.6 – 2.6
6. Regional TBP	1.5 – 1.9	1.7 – 2.1	1.9 – 3.3
7. Transport Jets	1.2 – 1.8	1.6 – 2.2	1.8 – 2.8
8. Military Trainers	1.2 – 1.8	1.4 – 2.0	1.6 – 2.2
9. Fighters	1.2 – 1.8	1.4 – 2.0	1.6 – 2.6
10. Mil. Patrol, Bomb and Transports	1.2 – 1.8	1.6 – 2.2	1.8 – 3.0
11. Flying Boats, Amphibious and Float Airplanes	1.2 – 1.8	1.6 – 2.2	1.8 – 3.4
12. Supersonic Cruise Airplanes	1.2 – 1.8	1.6 – 2.0	1.8 – 2.2

Figure 31 Lift-to-drag ratio from Jan Roskam

From figure (32) it is seen that the maximum lift co-efficient values for single engine propeller driven aircraft are within the ‘state-of-the-art’:

$$C_{L_{max_{TO}}} = 1.90 \text{ and } C_{L_{max_L}} = 2.00$$

The density at altitude of 3000 m is approximately 0.05 lb/ft³. Now we can determine the wing loading value by using equation (1) as follows:

$$\frac{60^2 * 0.05 * 1.9}{2} > \left(\frac{W}{S}\right)_{take-off}$$

$$\left(\frac{W}{S}\right)_{take-off} < \mathbf{171 \text{ psf}} \quad (4.2)$$

$$\frac{60^2 * 0.05 * 2.0}{2} > \left(\frac{W}{S}\right)_{landing}$$

$$\left(\frac{W}{S}\right)_{landing} < \mathbf{180 \text{ psf}} \quad (4.3)$$

From equation (4.2) & (4.3), the wing loading value must be less than 171 psf.

4.1.2) Take-off Distance:

According to Jan Roskam, the take-off distance of aircraft is determined by following factors:

- Take-off weight, W_{TO}
- Take-off speed, V_{TO}
- Thrust-to-weight ratio, $(T/W)_{TO}$ (or Weight-to-power ratio, $(W/P)_{TO}$)
- Aerodynamic drag co-efficient
- Ground friction co-efficient
- Pilot technique

For proposed aircraft, it is assumed that take-offs take place from hardened surface. The following below figure (33) represents a definition of FAR-23 Take-off distances used in the process of sizing a proposed airplane.

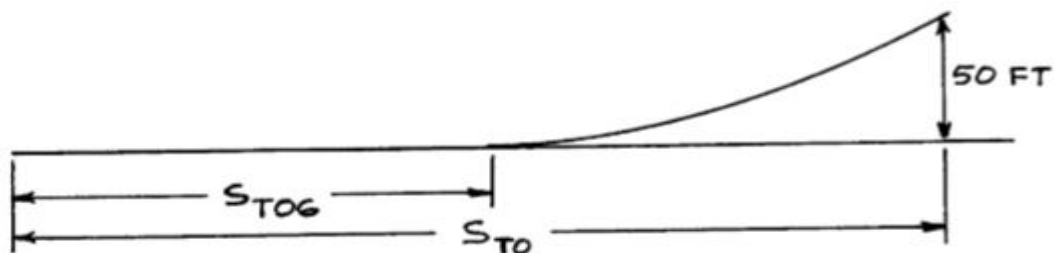


Figure 32 Definition of FAR-23 Take-off Distances

The take-off ground run, S_{TOG} is proportional to take-off wind loading $(W/S)_{TO}$, take-off power loading $(W/P)_{TO}$, and to the maximum take-off lift-co-efficient, C_{LmaxTO} :

$$S_{TOG} \propto \left[\frac{\left(\frac{W}{S}\right)_{TO} * \left(\frac{W}{P}\right)_{TO}}{\sigma * C_{LmaxTO}} \right] = TOP_{23} \quad (4.4)$$

Where, TOP_{23} is called take-off parameter for FAR-23 aircraft and its unit is $\text{lbs}^2/\text{ft}^2\text{hp}$. The lift co-efficient at lift-off, C_{LTO} is defined as follows:

$$C_{LTO} = \frac{C_{LmaxTO}}{1.21} \quad (4.5)$$

While calculating the total take-off distance, it should be kept in mind that it is not too short because aircraft would need higher co-efficient of lift max at take-off which will complicated the flap design. The following figure (34) from Jan Roskam gives the relation between take-off ground run and take-off parameter.

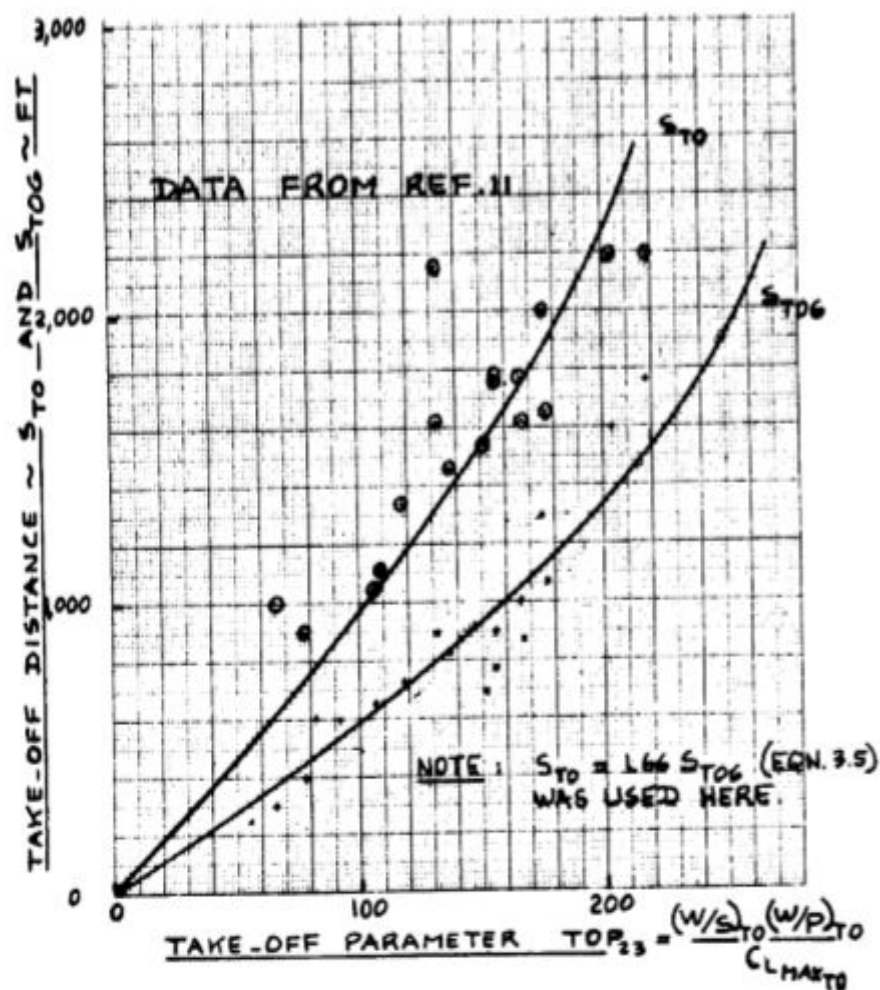


Figure 33 Effect of take-off parameter on take-off distance

From above figure (34), the following relation can be suggested:

$$S_{TOG} = 4.9TOP_{23} + 0.009TOP_{23}^2 \quad (4.6)$$

The following below figure (35) gives the relationship between take-off ground run and total take-off run.

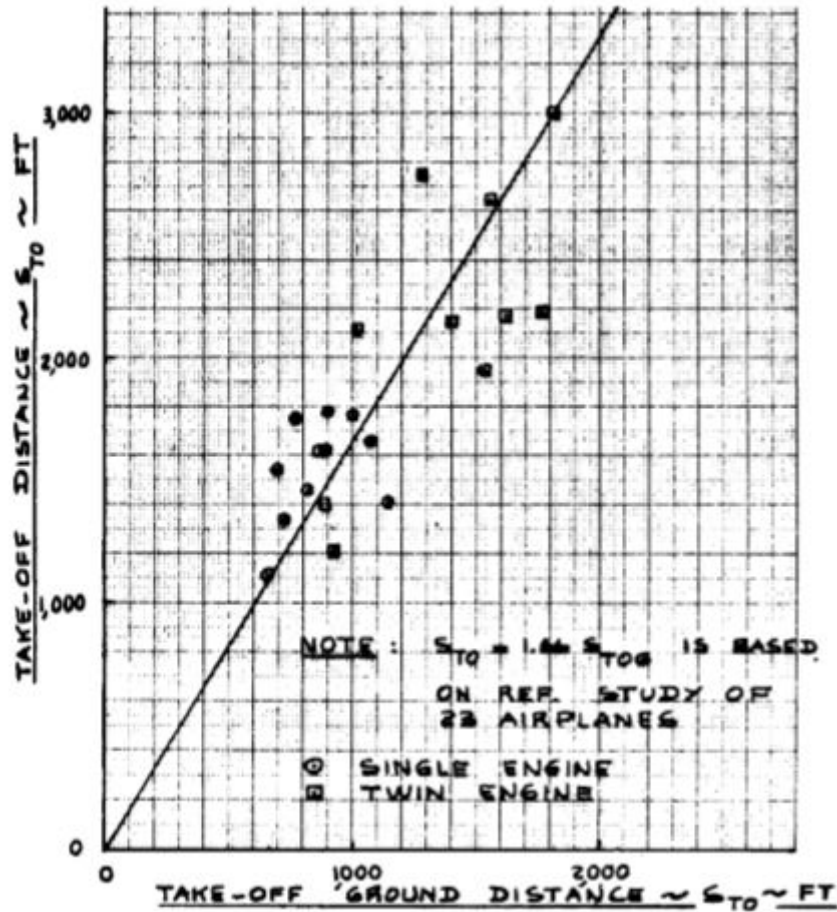


Figure 34 Relation between total take-off vs take-off ground

The correlation suggests the following relationships:

$$S_{TO} = 1.66S_{TOG} \quad (4.7)$$

From equation (4.6) & (4.7),

$$S_{TO} = 8.134TOP_{23} + 0.0149TOP_{23}^2 \quad (4.8)$$

Now, assume that the total take-off distance is 2500 feet which is under FAR-23 requirements. So, from equation (4.8),

$$2500 = 8.134TOP_{23} + 0.0149TOP_{23}^2 \quad (4.9)$$

$$TOP_{23} = 219.277 \frac{lbs^2}{ft^2 * hp} \quad (4.10)$$

Since $\sigma = 0.7142$ at 3000 m, from equation (4.4)

$$\left[\frac{\left(\frac{W}{S}\right)_{TO} * \left(\frac{W}{P}\right)_{TO}}{C_{LmaxTO}} \right] = TOP_{23} * \sigma$$

$$\left[\frac{\left(\frac{W}{S}\right)_{TO} * \left(\frac{W}{P}\right)_{TO}}{C_{LmaxTO}} \right] < 219.277 * 0.7142 = 156.6 \frac{lbs^2}{ft^2 * hp} \quad (4.11)$$

From the equation (4.11), we can calculate the take-off power loading which tabulated below:

Table 14 Required value for (W/P)

W/S (psf)	Clmax	1.2	1.6	1.9	2	2.4
10	W/P	18.792	25.056	29.754	31.32	37.584
20		9.396	12.528	14.877	15.66	18.792
30		6.264	8.352	9.918	10.44	12.528
40		4.698	6.264	7.4385	7.83	9.396
50		3.7584	5.0112	5.9508	6.264	7.5168
60		3.132	4.176	4.959	5.22	6.264
70		2.684571	3.579429	4.250571	4.474286	5.369143
80		2.349	3.132	3.71925	3.915	4.698

Figure (36) translates this tabulation into regions of $(W/S)_{TO}$ and $(W/P)_{TO}$ for given values of C_{LmaxTO} so that the take-off distance requirement is satisfied. The design point should be below the C_L line for optimum design.

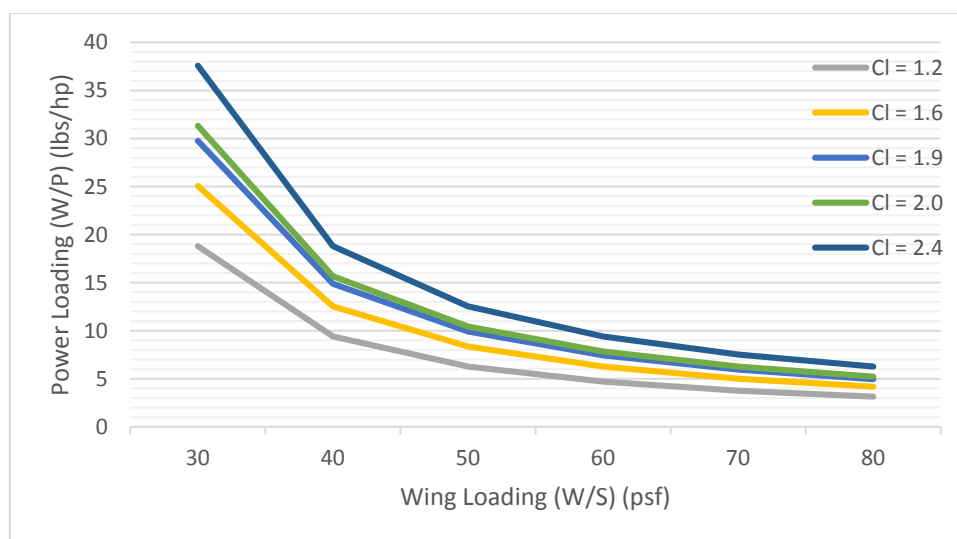


Figure 35 Effect of take-off wing loading and maximum take-off lift co-efficient on take-off power loading

4.1.3) Landing Distance:

According to Jan Roskam, the landing distance is determined by following factors:

- Landing Weight
- Approach Speed
- Deceleration method used
- Flying quantities of the airplane
- Pilot technique

The following below figure (37) represents a definition of FAR-23 landing distances used in the process of sizing a proposed airplane.

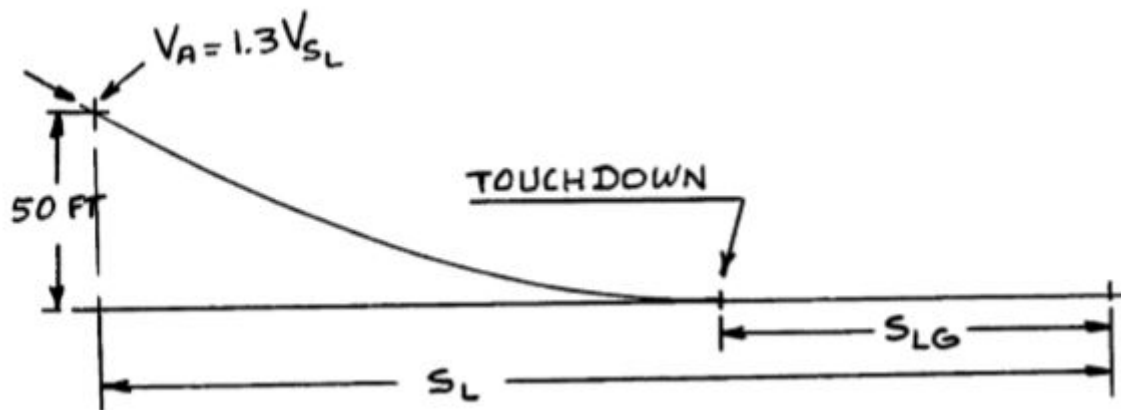


Figure 36 Definition of FAR-23 Landing Distances

The approach speed is calculated as:

$$V_A = 1.3 * V_{S_L} \quad (4.12)$$

The proposed aircraft is an electric thus the landing weight will be heavier than the conventional general aviation aircraft. The battery weight is basically dry weight. Therefore, it will not change during the flight envelope and due to that, the weight ratio of maximum landing weight to take-off weight will be constant.

For calculation of landing distance, following assumptions will be made:

- Standard conditions
- Applied brakes to stop the aircraft
- Take-off weight is 3335 lbs

The following below figure (38) shows the relation between the landing ground run, S_{LG} to the square of the stall speed, V_{S_L} .

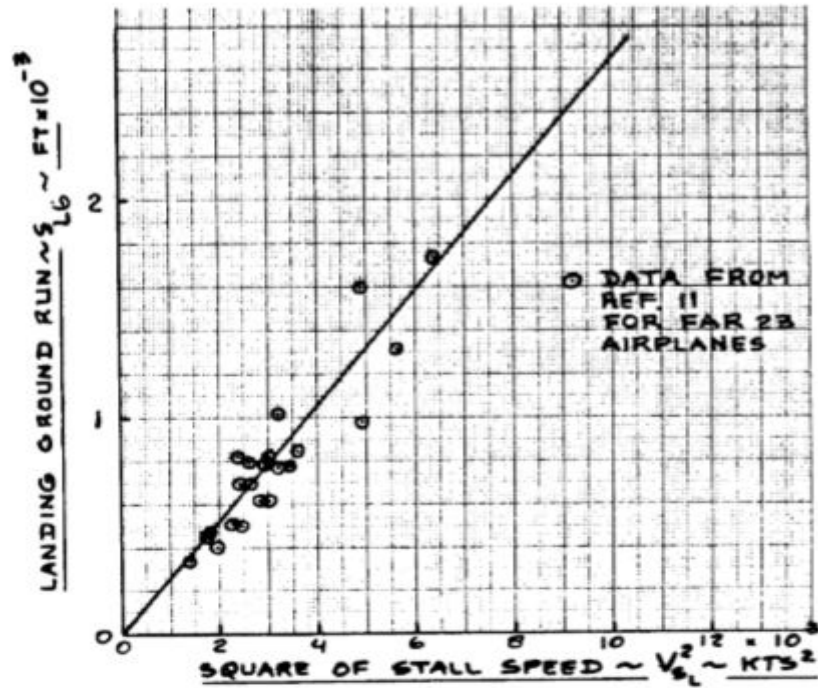


Figure 37 Effect of square of stall speed on landing ground run

The above figure (38) suggests the following relation:

$$S_{LG} = 0.265 * V_{S_L}^2 \quad (4.13)$$

Note: The stall speed is in knots and the distance is in feet.

The following below figure (39) shows the relation between total landing distance to the landing ground run.

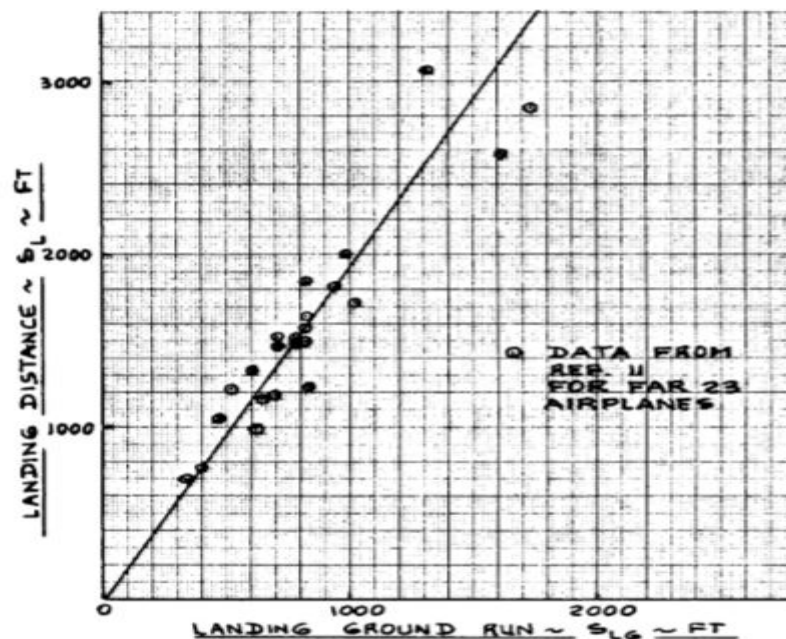


Figure 38 Relation between ground run and landing distance

The above figure suggests the following relationship:

$$S_L = 1.938 * S_{LG} \quad (4.14)$$

Combining equation (4.13) & (4.14):

$$S_L = 0.5136 * V_{S_L}^2 \quad (4.15)$$

Assuming the landing field length of 1700 feet at 0 feet altitude. The design landing weight to take-off weight ratio is 1.

From equation (4.15) it follows that:

$$V_{S_L} = \left(\frac{1700}{0.5136} \right)^{\frac{1}{2}}$$

$$V_{S_L} = 57.53 \text{ knots}$$

With the help of equation (4.1) this translates into the following requirement:

$$\frac{2 * \left(\frac{W}{S} \right)_L}{0.002049 * C_{L_{maxL}}} = (57.53 * 1.688)^2$$

$$\frac{2 * \left(\frac{W}{S} \right)_L}{0.002049 * C_{L_{maxL}}} = 9430.47 \frac{ft^2}{sec^2}$$

$$\left(\frac{W}{S} \right)_L = 9.66 * C_{L_{maxL}} \quad (4.16)$$

Now, the landing weight to take-off weight ratio is 1, this yield:

$$\left(\frac{W}{S} \right)_{TO} = 9.66 * C_{L_{maxL}} \quad (4.17)$$

Figure (40) shows the range of values of $(W/S)_{TO}$ and $C_{L_{maxL}}$ which meet the landing distance requirement.

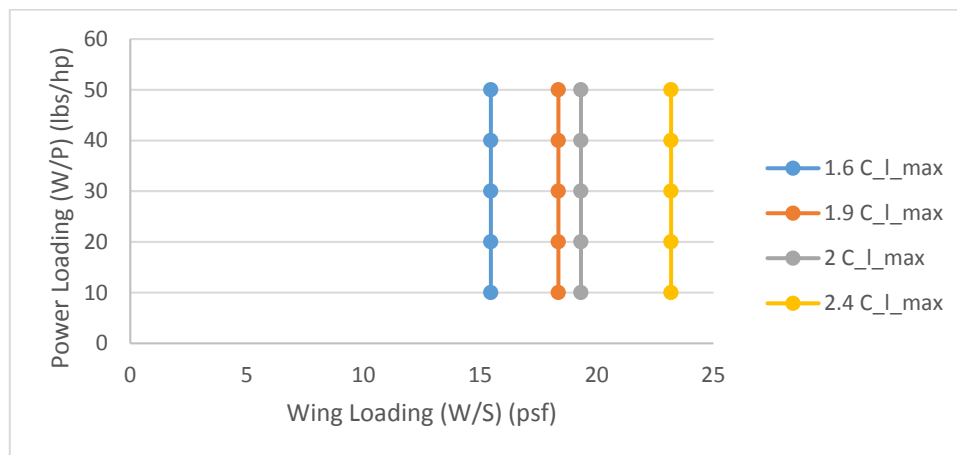


Figure 39 Allowable wing loading to meet a landing distance requirement

4.1.4) Sizing To Climb Requirements:

Mainly there are two primary reasons to evaluate climb performance:

- Aircraft must climb over obstacles to avoid hitting them
- Climbing to higher altitudes can provide better weather, fuel economy, and other benefits

The drag polar is necessary to size an airplane for climb requirements. The proposed aircraft comes under FAR-23 climb requirements.

4.1.4.1) A Method for Estimating Drag Polar at Low Speed:

The drag co-efficient is given by following equation:

$$C_D = C_{D_o} + \frac{C_L^2}{\pi A e} \quad (4.18)$$

Where,

$e = \text{Oswald's efficiency factor}$

$A = \text{Aspect ratio}$

$C_{D_o} = \text{Zero - lift drag co - efficient}$

The zero-lift drag co-efficient can be expressed as:

$$C_{D_o} = \frac{f}{S} \quad (4.19)$$

Where,

$f = \text{Equivalent parasite area}$

$S = \text{Wing area}$

Now, it is possible to relate equivalent parasite area to the wetted area from below figure (41). The relation between them is given by:

$$\log_{10} f = a + b * \log_{10} S_{wet} \quad (4.20)$$

The constants a and b are a function of the equivalent skin friction co-efficient of an airplane, c_f . The c_f value for proposed aircraft is around **0.090**.

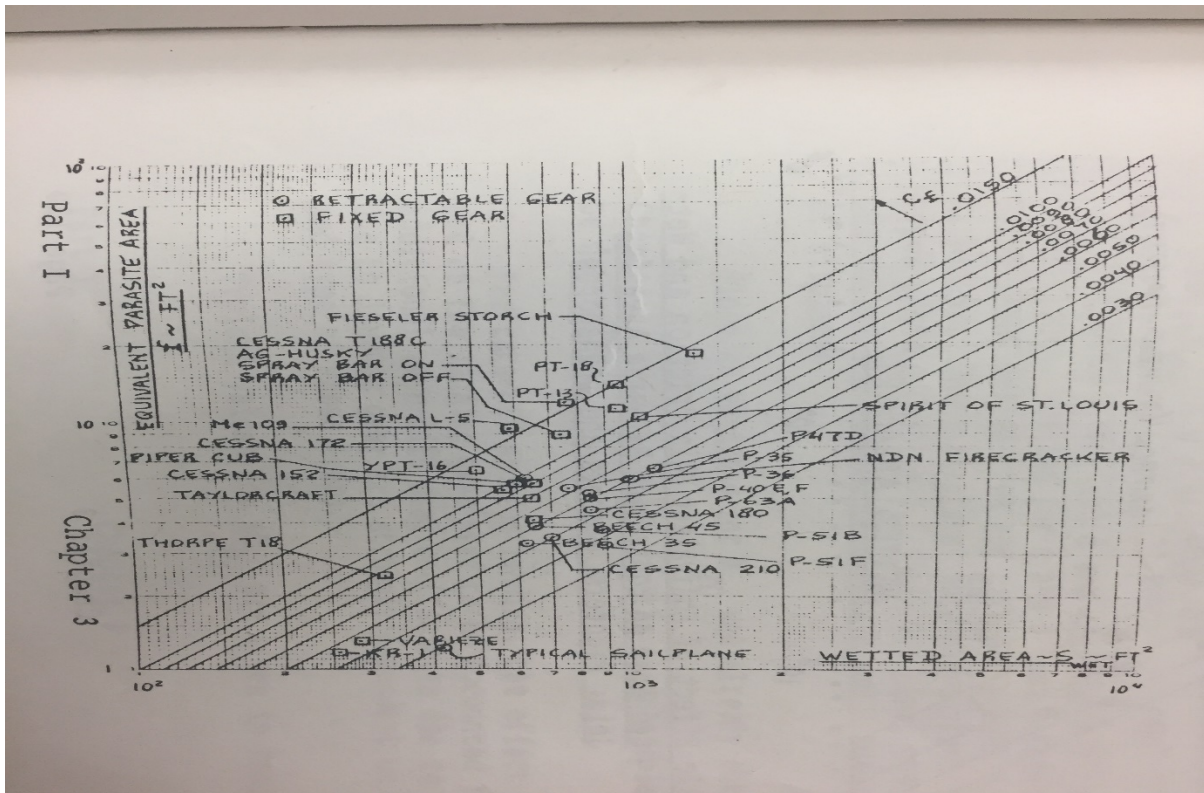


Figure 40 Equivalent parasite area vs Wetted area

The values a and b can be found (based on c_f values) from following figure (42):

Equivalent Skin Friction Coefficient, c_f	a	b
0.0090	-2.0458	1.0000
0.0080	-2.0969	1.0000
0.0070	-2.1549	1.0000
0.0060	-2.2218	1.0000
0.0050	-2.3010	1.0000
0.0040	-2.3979	1.0000
0.0030	-2.5229	1.0000
0.0020	-2.6990	1.0000

Figure 41 a and b values based on skin friction co-efficient

The values of a and b is as follows: **a = -2.0458 & b = 1.0000**. It is found that wetted area of airplane is correlates with take-off weight. Figure (43) shows this. Almost all aircraft falls in ten percent band due to differences in nacelle design and wing loading.

Figure (43) gives the following relation:

$$\log_{10} S_{wet} = c + d * \log_{10} W_{T0} \quad (4.21)$$

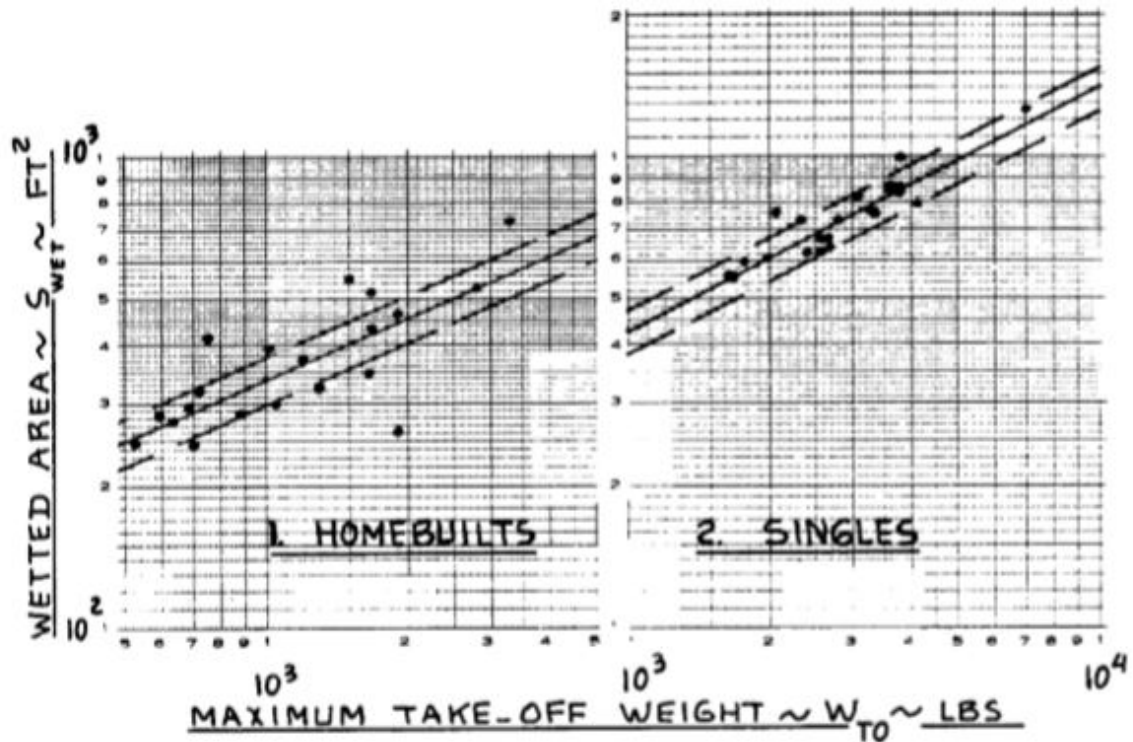


Figure 42 Relation between wetted area vs take-off weight

The values for c and d can be found from below figure (44):

Airplane Type	c	d
1. Homebuilts	1.2362	0.4319
2. Single Engine Propeller Driven	1.0892	0.5147
3. Twin Engine Propeller Driven	0.8635	0.5632
4. Agricultural	1.0447	0.5326
5. Business Jets	0.2263	0.6977
6. Regional Turboprops	-0.0866	0.8099
7. Transport Jets	0.0199	0.7531
8. Military Trainers*	0.8565	0.5423
9. Fighters*	-0.1289	0.7506
10. Mil. Patrol, Bomb and Transport	0.1628	0.7316
11. Flying Boats, Amph. and Float	0.6295	0.6708
12. Supersonic Cruise Airplanes	-1.1868	0.9609

* For these airplanes, wetted areas were correlated with 'clean', maximum take-off weights. No stores were accounted for.

Figure 43 Values for c and d for several types of aircraft

For, single engine propeller driven aircraft the c and d values are as follows:

$c = 1.0892$ & $d = 0.5147$ and the take-off weight is 3335 lbs.

From equation (4.21),

$$\begin{aligned}\log_{10} S_{wet} &= c + d * \log_{10} W_{TO} \\ \log_{10} S_{wet} &= 1.0892 + (0.5147) * \log_{10} 3335 \\ \log_{10} S_{wet} &= 2.9025 \\ S_{wet} &= 797.99 \text{ ft}^2\end{aligned}$$

From equation (4.20),

$$\begin{aligned}\log_{10} f &= a + b * \log_{10} S_{wet} \\ \log_{10} f &= -2.0458 + (1.0000) * \log_{10} 797.99 \\ \log_{10} f &= 0.8561 \\ f &= 7.1795 \text{ ft}^2\end{aligned}$$

Now, to find zero-lift drag co-efficient, Roskam gives some estimated values as:

Configuration	ΔC_{D_0}	e
Clean	0	0.80 - 0.85
Take-off flaps	0.010 - 0.020	0.75 - 0.80
Landing Flaps	0.055 - 0.075	0.70 - 0.75
Landing Gear	0.015 - 0.025	no effect

Figure 44 First Estimates for zero-lift drag co-efficient

Assuming the values of Aspect ratio (A) = 10 and $e = 0.85$, and $C_{D_0} = 0.0065$, then it is possible to find the 'clean' drag polar, from equation (4.18), at low speed as:

$$C_D = 0.0065 + 0.0374C_L^2 \quad (4.22)$$

For other configuration the values are as follows:

Table 15 Drag polars for Proposed Aircraft

Configuration	C_{D_0}	Aspect Ratio	e	Drag Polar
Take-off flaps	0.0165	10	0.80	$C_D = 0.0165 + 0.0398C_L^2$
Landing flaps	0.0615	10	0.75	$C_D = 0.0065 + 0.0424C_L^2$
Landing gear	0.0215	10	No effect	$C_D = 0.0215 + 0.0424C_L^2$

4.1.4.2) FAR-23 Climb Requirements:

The proposed aircraft comes under FAR-23 climb requirements which is as follows:

- a. *FAR 23.65 (All Engines Operating)*
The minimum climb rate at sea level is 300 fpm and a steady climb angle of 1:12 for landplanes. (@ Take-off)
- b. *FAR 23.67 (One Engine Inoperative)*
For multiengine airplane with take-off weight more than 6000 lbs, the steady climb rate must be at least $0.027V_{S_0}^2$ fpm, at 5000 ft. altitude.
- c. *FAR 23.77 (All Engines Operating)*
The steady climb angle shall be at least 1:30. (@Balked landing)

4.1.4.3) Sizing to FAR-23 rate-of-climb requirements:

The rate-of-climb is given by following equation:

$$RC = \text{Rate of climb} = \frac{dh}{dt} = 33,000 * RCP \quad (4.23)$$

Where:

$$RCP = \text{Rate of climb Parameter} = \left\{ \frac{\eta_p}{\frac{W}{P}} \right\} - \left[\frac{\frac{W^{\frac{1}{2}}}{S}}{19 * \left(\frac{C_L^{\frac{3}{2}}}{C_D} \right) * \sigma^{\frac{1}{2}}} \right] \quad (4.24)$$

For FAR 23.65: $RCP = 33000^{-1} * RC$

$$RCP = 33000^{-1} * 300$$

$$RCP = 0.0091 \frac{hp}{lbs}$$

For FAR 23.67: The proposed aircraft is single engine with take-off weight ≤ 6000 lbs so, it is not required to satisfy the constraints mention under FAR 23.67 requirement.

The drag polar for proposed aircraft is already found as:

$$C_D = 0.0065 + 0.0374C_L^2$$

With this drag polar the value of $\left(\frac{C_L^{\frac{3}{2}}}{C_D} \right)_{max} = 22.57$. The propeller efficiency is 0.80.

From equation (4.24) it now follows that:

$$\left\{ \frac{0.80}{\frac{W}{P}} \right\} - \left[\frac{\frac{W^{\frac{1}{2}}}{S}}{19 * 22.57 * 1.0} \right] = 0.0091$$

The above relationship will give following table:

Table 16 The range of W/S and W/P for which the FAR 23.65 is satisfied

$\frac{W}{S_{TO}}$ (psf)	$\frac{W}{P}$ cont. (lbs/hp)	$\frac{W}{P}$ take-off ($\frac{\text{lbs}}{\text{hp}}$) [*]
20	40.98	37.25
30	36.57	33.24
40	33.55	30.5
50	30.91	28.1

(“*” -- the ratio of $\frac{P_{to}}{P_{max.cont.}}$ was taken to be 1.1)

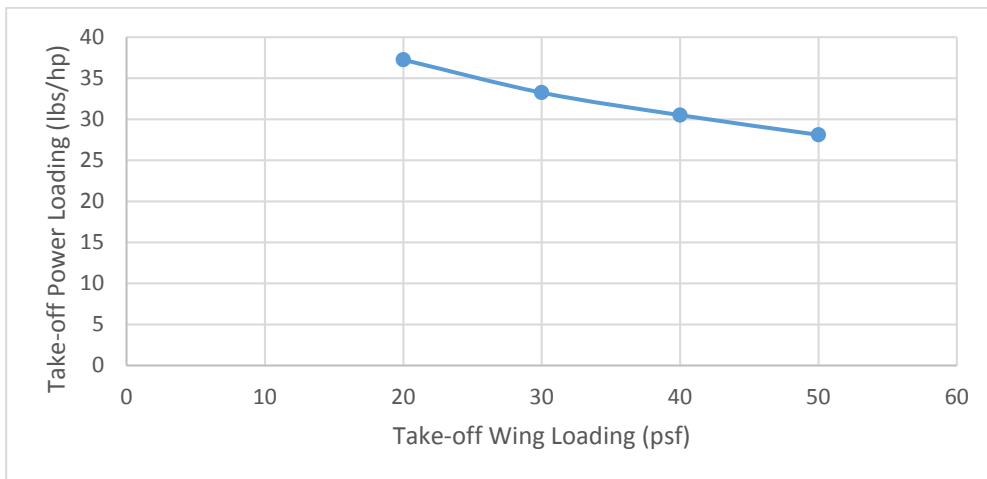


Figure 45 Range of W/S and W/P values for which the FAR 23.65 climb requirement is satisfied

The design point should be below the above plotted line.

4.1.4.4) Sizing to climb gradient requirements:

The design point should be below the figure (47) plotted line. Climb gradient requirements are calculated based on following equation:

$$CGRP = \frac{18.97 * \eta_p * \sigma^{\frac{1}{2}}}{\frac{W}{P} * \frac{W^{\frac{1}{2}}}{S}} = \frac{\{CGR + (\frac{L}{D})^{-1}\}}{C_L^{\frac{1}{2}}} \quad (4.25)$$

For FAR 23.65: CGR = 1/12 = 0.0833. The drag polar was already found as:

$$C_D = 0.0065 + 0.0374C_L^2$$

The value of $C_{L_{max}} = 1.9$ is already assumed. By taking a margin of 0.2:

$$C_{L_{climb}} = 1.7$$

This gives us: $\frac{L}{D_{climb}} = 14.84$

Therefore:

$$CGRP = \frac{\{0.0833 + (14.84)^{-1}\}}{1.7^{\frac{1}{2}}} = 0.1155$$

This requirement now yields:

$$\frac{W}{P} * \frac{W^{\frac{1}{2}}}{S} = \frac{18.97 * 0.80 * 1.0}{0.1155} = 131.39 \quad (4.26)$$

The above equation (4.26) will give following table:

Table 17 Range of wing loading and power loading for which the FAR-23.65 climb gradient requirement is satisfied

$\frac{W}{S_{TO}}$ (psf)	$\frac{W}{P}$ cont. (lbs/hp)	$\frac{W}{P}$ take-off ($\frac{lbs}{hp}$)*
20	29.37	26.7
30	23.98	21.8
40	20.77	18.88
50	18.58	16.89

(* -- the ratio of $\frac{P_{to}}{P_{max.cont.}}$ was taken to be 1.1)

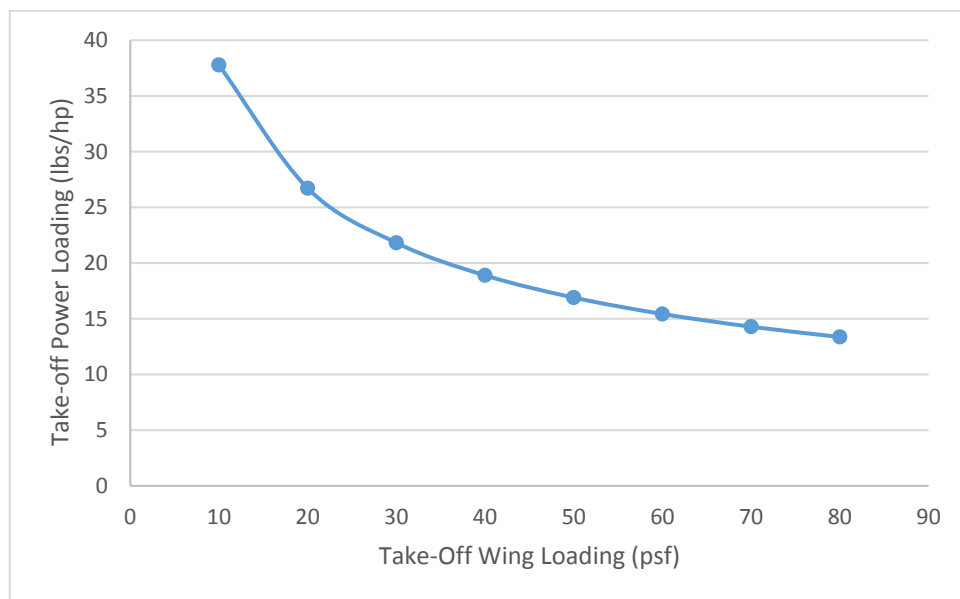


Figure 46 Range of W/S and W/P values for which the FAR 23.65 climb gradient requirement is satisfied

For FAR-23.77: $CGR = 1/30 = 0.0333$. It is already assumed that $C_{L_{maxLanding}} = 2.0$. And assuming that climb is carried out with the same margin as before:

$$C_{L_{climb}} = 1.8$$

The drag polar in this case is:

$$C_D = 0.0065 + 0.0424C_L^2$$

This gives us: $\frac{L}{D_{climb}} = 12.51$

Therefore:

$$CGRP = \frac{\{0.0333 + (12.51)^{-1}\}}{1.8^{\frac{1}{2}}} = 0.08437$$

This requirement now yields:

$$\frac{W}{P} * \frac{W^{\frac{1}{2}}}{S} = \frac{18.97 * 0.80 * 1.0}{0.08437} = 179.87 \quad (4.27)$$

The above equation (4.27) will give following table:

Table 18 Range of take-off wing loading and power loading for which FAR-23.77 climb gradient requirement is satisfied

$\frac{W}{S_{TO}}$ (psf)	$\frac{W}{P}$ take-off ($\frac{lbs}{hp}$)
20	40.22
30	32.83
40	28.44
50	25.43

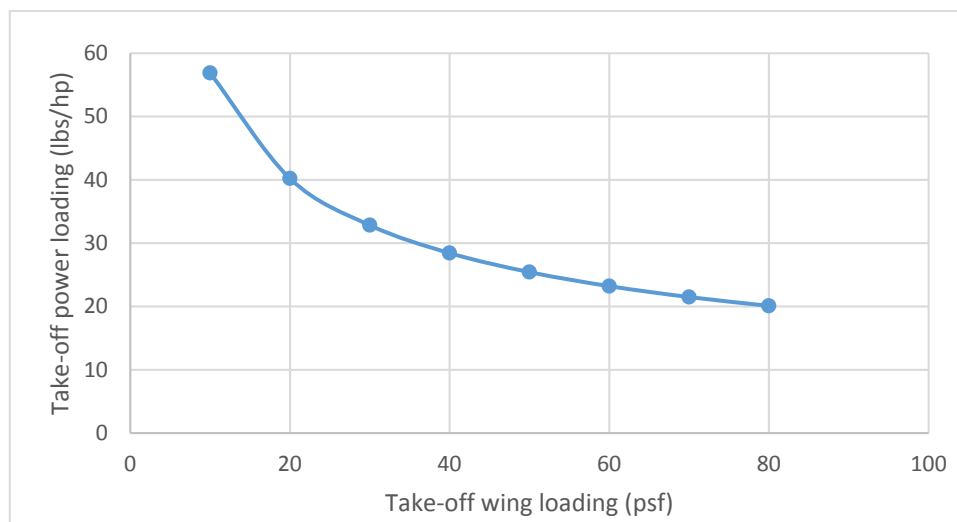


Figure 47 Range of W/S and W/P for which FAR-23.77 climb gradient requirement is satisfied

4.1.5) Sizing to Maneuvering Requirements:

Since, the proposed aircraft is general aviation aircraft and the maneuvering requirements specified in Roskam is only for utility, agricultural, aerobatic, and military airplane, the proposed aircraft do not include those capabilities. So, the aircraft will not be sized to meet these requirements.

4.1.6) Sizing to Cruise Speed Requirements:

The cruise speed for any propeller driven aircraft is calculated at 70 to 80 percent of total power. From which, it can be shown that the profile drag is higher than the induced drag. From the reference (Loftin), cruise speed is proportional to the factor called ‘the power index’.

$$V_{cr} \propto \frac{W^{\frac{1}{3}}}{\sigma * \frac{W}{S}} \quad (4.28)$$

Where,

$$\frac{W^{\frac{1}{3}}}{\sigma * \frac{W}{S}} = I_p \quad (4.29)$$

The following figure will give the relationship between power index and cruise speed:

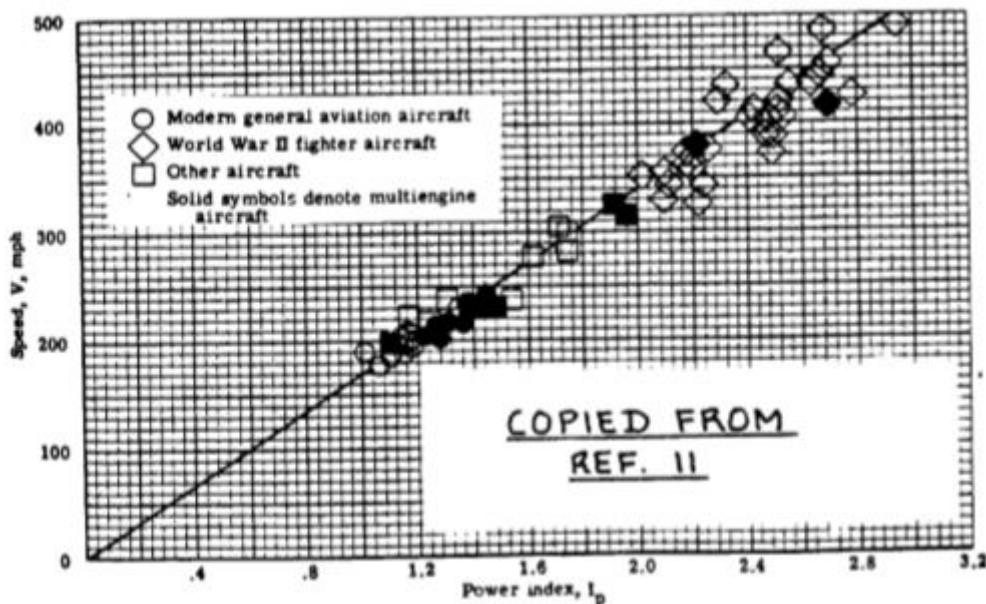


Figure 48 Airplane speed vs Power index

The cruise speed of propeller driven electric airplane is around 145 knots (166.86 mph) at 85 percent power at 10,000 feet and at take-off weight.

So, from figure (49), the power index = 1.0.

At 10,000 feet, $\sigma = 0.7368$. Therefore, from equation (4.29):

$$\frac{W}{S} = 0.7368 * \frac{W}{P} \quad (4.30)$$

Figure (50) shows the range of combinations of W/S and W/P for which the cruise speed requirement is met. The design point should be below the trendline.

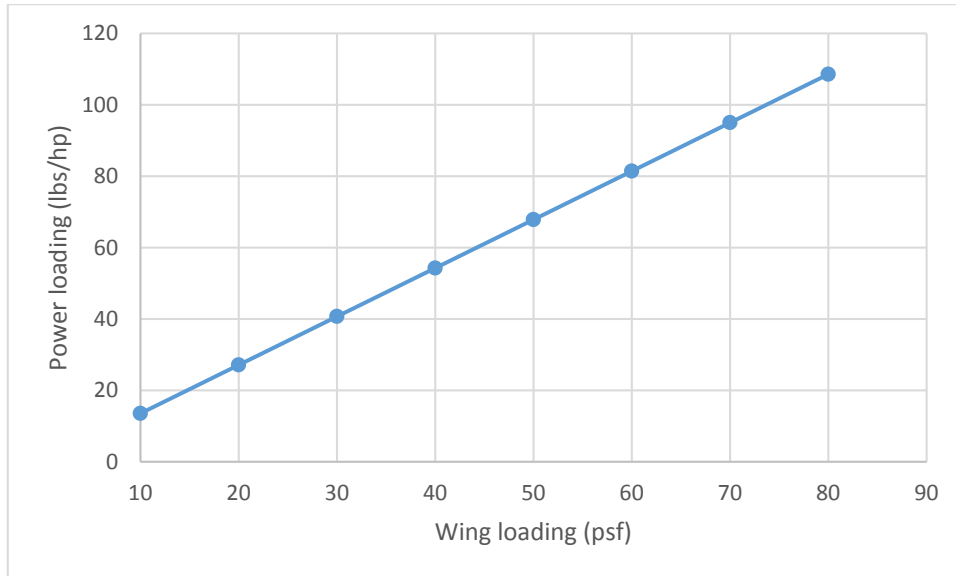


Figure 49 Allowable W/S and W/P to meet a given cruise speed

The zero-lift drag co-efficient can also be found using the power index.

$$C_{D_o} = 1.114 * 10^5 * \left(\frac{I_p}{V}\right)^3 \quad (4.31)$$

$$C_{D_o} = 1.114 * 10^5 * \left(\frac{0.68}{115.90}\right)^3$$

$$C_{D_o} = 0.02249$$

4.1.7) Matching Graph:

It is now possible to determine the best combination of wing loading, maximum required lift coefficients and aspect ratio from matching process. The star shows the design point for proposed aircraft. The matching graph for proposed aircraft is as follows:

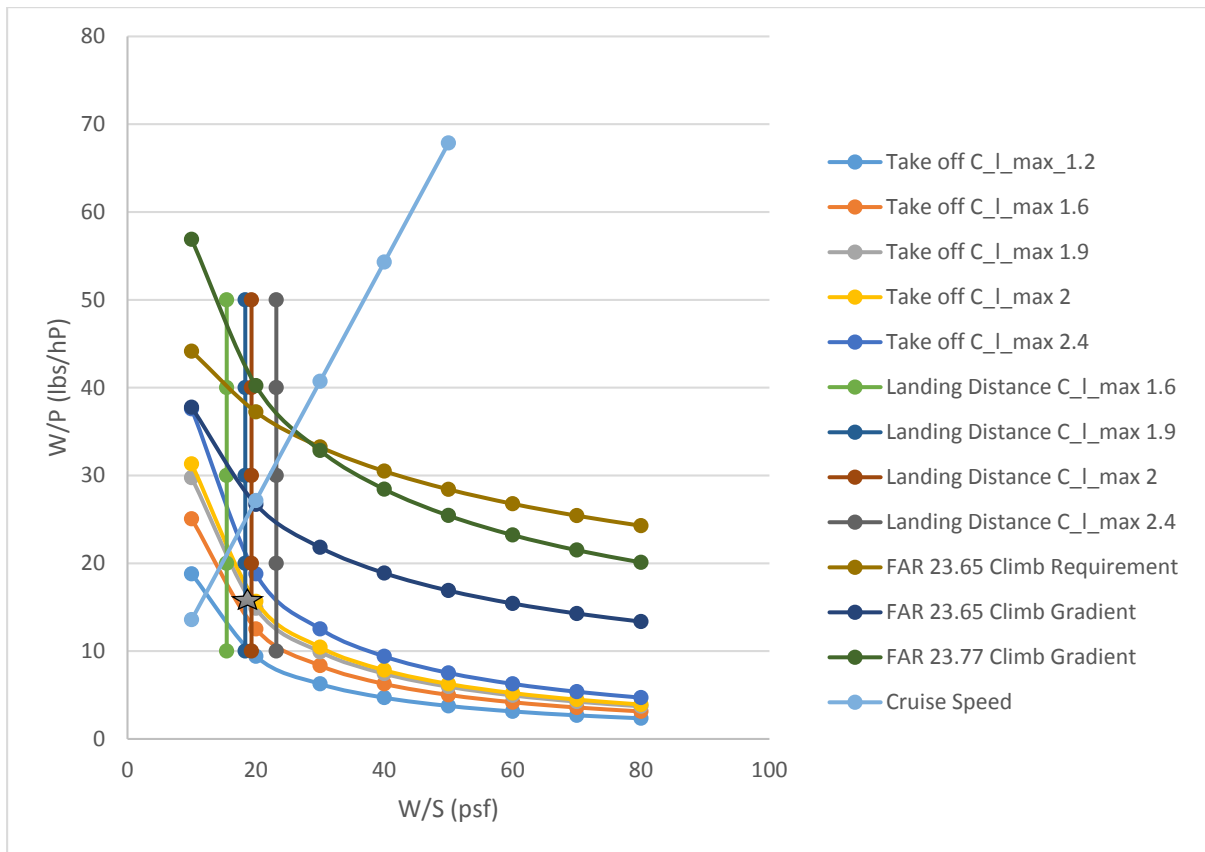


Figure 50 Matching Results for Sizing of a Proposed Aircraft

With this design point, the single propeller driven electric airplane is now characterized by the following design parameters:

Take-off weight: 3335 lbs

Empty weight: 1715 lbs

Battery weight: 800 lbs

These are already known from weight sizing.

Maximum lift coefficients:

Clean: $C_{L_{max}} = 1.7$

Take-off: $C_{L_{max_{TO}}} = 1.9$

Landing: $C_{L_{max_L}} = 2.0$

Aspect Ratio: 10

Take-off wing loading: 19 psf

Wing area: 175.52 ft^2

Power loading at take-off: 15 lbs/hp

Take-off power: 222.33 hp

4.2) CALCULATION OF PERFORMANCE CONSTRAINTS WITH THE AAA PROGRAM:

4.2.1) Stall Speed:

The value for take-off wing loading from stall speed is about 19.19 psf which is closed to the value calculated by manually (19 psf!!).

The screenshot shows the 'Input Parameters' section with the following values: $h_s = 9800$ ft, $\Delta T_s = -50.0$ deg F, $V_{s_{clean}} = 60.00$ kts, $V_s = 61.00$ kts, $W_s/W_{TO} = 1.000$, $C_{L_{max_{S_{ch}}}} = 1.700$, and $C_{L_{max_S}} = 1.900$. The 'Output Parameters' section shows $(W/S)_{TO_{S_{ch}}} = 16.61$ lb/ft² and $(W/S)_{TO_S} = 19.19$ lb/ft². A label 'Stall Speed or the Minimum Speed' is positioned above the output parameters.

Figure 51 Calculation of take-off wing loading from stall speed

4.2.2) Take-off Distance:

The take-off distance parameters for proposed aircraft is as follows:

The screenshot shows the input parameters for take-off distance: $h_{TO} = 0$ ft, $F_{TO} = 1.000$, $\Delta T_{TO} = 0.3$ deg F, $S_{TO} = 2500$ ft, $C_{L_{max_{TO}}} = 1.900$, $\text{Plot } \Delta C_{L_{max}} = 0.200$, and $S_{TOG} = 1506$ ft.

Figure 52 Take-off distance parameters

4.2.3) Landing Distance:

The value for take-off wing loading from landing distance parameters is 21.19 psf which is closed to the manually calculated value (19 psf!!).

The screenshot shows the input parameters for landing distance: $h_L = 0$ ft, $\Delta T_L = 30.0$ deg F, $W_L/W_{TO} = 1.000$, $C_{L_{max_L}} = 2.000$, $\text{Plot } \Delta C_{L_{max}} = 0.200$, and $S_L = 1700$ ft. The 'Output Parameter' section shows $(W/S)_L = 21.19$ lb/ft².

Figure 53 The value of take-off wing loading from landing distance parameters

4.2.4) Climb Constraints:

The climb constraints parameters are as follows:

$F_{MaxCont}$	0.800	$C_{L_{max_{clean}}}$	1.700	$C_{L_{max_L}}$	2.000	$C_{D_{0_down}}$	0.0065	η_{prop}	0.800	RC/V_S^2	0.027 $\frac{ft/min}{kts^2}$
F_{5000}	0.909	$C_{L_{max_{TO}}}$	1.900	W_{Cr}/W_{TO}	1.000	B_{DP_down}	0.0065	$\Delta C_{L_{Cl-Max}}$	0.200	$CGR_{23.77}$	0.033

Figure 54 The climb constraint parameters

4.2.5) Cruise Speed Constraints:

The cruise speed calculated from AAA is about 169 knots which is like manually calculated value (170 knots!!).

Input Parameters							
h_{cr}	10000 ft	$V_{Cr_{max}}$	170.00 kts	AR_w	10.00	e_{clean}	0.8500
F_{Cr}	0.800	W_{Cr}/W_{TO}	1.000	$C_{D_{0_clean,M}}$	0.0065	η_{prop}	0.800
Output Parameters							
$M_{Cr_{max}}$	0.266	$B_{DP_{clean}}$	0.0374				

Figure 55 The cruise speed value from AAA

4.2.6) Matching Graph:

The matching graph from AAA is as follows:

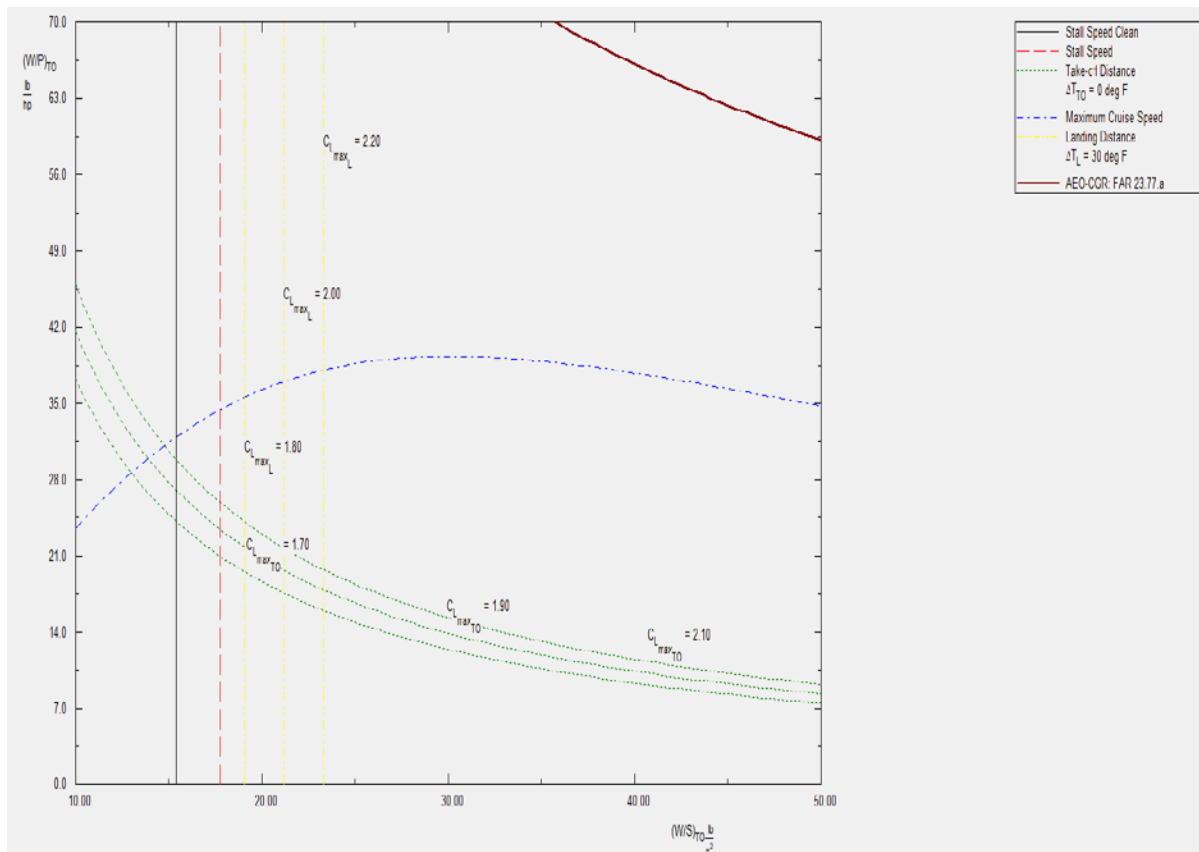


Figure 56 The matching graph from AAA

4.3) SELECTION OF PROPULSION SYSTEM:

The selection and to the integration of propulsion system is provided in this chapter. This involves the three decisions as follows:

1. Selection of the propulsion system type
2. Determination of the number of engines to be used
3. Integration of these engines into the configuration

4.3.1) Selection of The Propulsion System Type:

There are couple of factors which needs to consider while selecting the propulsion system for proposed aircraft. These factors are as follow:

1. Power density
2. Energy density
3. Safety
4. Cost
5. Reliability
6. Maintainability

An aircraft to be able to fly, the engine must produce enough thrust to accelerate the aircraft to lift-off speed. Compared to a jet engine the batteries have the advantage. Analogous way, compared to a piston engine the electric motor has advantage. All electric vehicles can be powered by two ways: fuel cells or batteries. Both produce electricity by eliminating pollution. Batteries obtained their energy from the electrical grid and fuel cells obtained from hydrogen.

Both have their own advantages and disadvantages. The extra weight to increase the range of the fuel cell vehicle is negligible compare to battery weight. Each extra kg of battery weight to increase range requires extra structural weight, heavier brakes, a larger traction motor. But the round-trip efficiency of a battery might be 80%, whereas fuel cell electric vehicles are less efficient and its only 52%. The high fuel economy for battery vehicle, coupled with a relatively low-cost fuel with stable pricing, results in a vehicle that is very inexpensive to fuel.

From above comparison, the most suitable option for proposed aircraft is battery mainly due to high efficiency and low-cost fuel and it can produce less Green House Gas for proposed range.

The next study for propulsion system is between motor and a piston engine. The motor is small, and it has no reciprocating but only rotating parts. Electric motors should be extremely effective in the air, since they work well at low-drag high altitudes, where the density is low enough to cause problems for combustion engines. For selection of motor, the parametric study was conducted by McDonald. The following table (20) shows the relationship between torque and power for a variety of configurations. The Launch-Point is also developed a high-efficiency, high power density motor which called 'Halbach Array Motor'. This new Halbach Array Motor utilize the same brushless, axial flux permanent magnet design with an ironless rotor and stator.

Table 19 Motor Trade Study

Company	UQM	Tesla	AC Propulsion	UQM	Rubber Motor	Halbach Array
Engine	Power Phase 220	Tesla Roadster	AC-150	Power Phase 250	Rubber Motor	Permanent magnet motor
Type	Brushless	3-Phase Induction	3-Phase Induction	Brushless	Brushless	Brushless
Max Power	220 kW	225 kW	150 kW	250 kW	273 kW	N/A
Max Torque	700 Nm	370 Nm	>225 Nm	900 Nm	1135 Nm	N/A
Max RPM	6000	14000	13000	5500	3123	N/A
Cont. Power	120 kW	N/A	40 kW	150 kW	205 kW	N/A

From the above trade study, it is clear that rubber motor is like UQM Power Phase 250 except the fact that rubber motor has more maximum and continuous power. So, for proposed aircraft the rubber motor is best suitable option to use. The rubber motor has also high power to weight ratio. Additionally, a gearbox is necessary to maintain the rpm of the propeller.

The last and the most important parameter is selection of battery system. In comparison, the power generated from batteries are differ in terms of specific energy, power output and weight. The trade study has been done to select best suitable battery technology for proposed aircraft. Some remarkable battery configuration (experimental + currently available) are as follows:

Table 20 Battery Configuration Comparison

Battery	Specific Energy (W-hr/kg)
Pb/acid	170
Ni/Cd	240
NiMH	470
Li-ion	700
Li-Po	735
LiS	2400
Lithium Air	11400
Aluminium Air + Lithium Ion	1800
Aluminium Air + Lithium Sulphur	4200

The batteries with most specific energy are Lithium Air, Lithium Sulphur and Aluminium Air + Lithium Ion hybrid system which are currently not available in market, but they would be available around 2020. The Aluminium Air has already been executed in some

forms of transportation. So, this hybrid combination is the ideal power source for proposed aircraft. The aluminium acts as an anode and oxygen acts as the cathode. When aluminium air is used with lithium ion, the aluminium air works as a range extender. The TESLA Gigafactory will be the major supplier of the Lithium Ion batteries by 2020. Eventually, the Aluminium Air and Lithium Ion is chosen for proposed aircraft because of its effectiveness, low environmental impact and its ease of implementation.

4.3.2) Selection of The Number of Engines:

The current electric motor technology cannot produce the required horsepower. Therefore, the parametric study was performed for proposed rubber motor and the parameters for an engine could be calculated. Following figure shows the relationship between torque and rate with efficiencies for a variety of torque/rate configurations. Form figure (58), it can be concluded that the required power for cruise is 206 kW and RPM at 94% efficiency is 2323 with torque approximately 847 Nm.

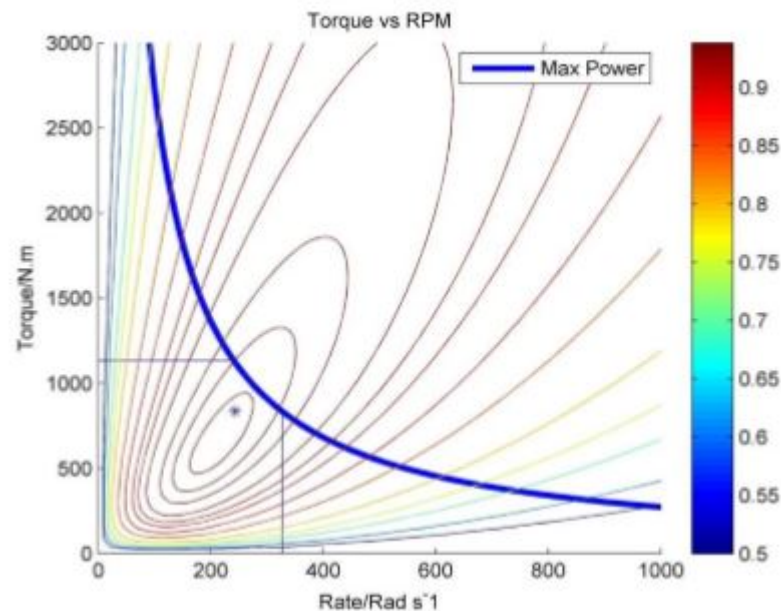


Figure 57 Rubber Motor Parametric Study

So, the number of engines for proposed aircraft is only one and it is propeller driven. The location of the proposed engines is at nose of the plane (on the fuselage) with single propeller. The propeller diameter and blade profile will be discussed in following section.

4.3.3) Propeller Sizing:

The airplane wings and propellers are both made up of airfoil sections designed to generate an aerodynamic force. The wing force provides lift to sustain the airplane in the air;

the propeller force provides thrust to push the airplane through the air. However, the propeller blades are twisted so that the chord line changes from almost parallel to free stream velocity.

All early airplanes before 1930 had fixed-pitch propellers. The maximum propeller efficiency could be obtained only at a specific value of the advance ratio. At other velocities, propeller always operated at less efficiencies. The next version is variable pitch propeller which is fixed to a hub. In this type, the pitch is varying continuously to maintain maximum efficiency at all flight velocities. In addition, the next development is the constant-speed propeller, which allowed the pitch angle to be varied continuously and automatically to maintain the proper torque.

The chosen characteristics of the propeller are as follows:

- Low weight
- Low noise level

By increasing the number of blades, noise can be reduced but it decreases the blade efficiency. On the other hand, by decreasing the number of blades, the propeller diameter increases which reduces the ground clearance. The Roskam provides a relation between maximum engine power, propeller diameter and number of propeller blades for single engine FAR-23 certified airplanes.

The diameter of propeller is obtained from following equation:

$$D_p = \left(\frac{4 * P_{max}}{\pi * n_p * P_{bl}} \right)^{0.5} \quad (4.32)$$

Where,

D_p = Propeller Diameter

P_{max} = Maximum engine power = 206 kW

P_{bl} = Power loading per blade, $\frac{hp}{ft^2} = 3.2$ (from Roskam)

n_p = number of blades = 3

$$D_p = \left(\frac{4 * 276.251}{\pi * 3 * 3.7} \right)^{0.5}$$

$$D_p = 5.63 \text{ feet}$$

4.4) DISCUSSION:

The performance constraint analysis for proposed aircraft gives some of the crucial parameters. The performance constraints calculated by manually and using AAA program is about to same values. The design parameters chosen for proposed aircraft is from manually calculated matching graph even though the values from AAA software are about the same. To select the design point, trade-off has been done between landing distance and take-off distance wing loading values.

The calculation of wing loading, and power loading are comparable with the Scuba Stingray aircraft. The Scuba Stingray has a wing loading of 21.3 lb/ft² and a power loading of 11.6 lb/hp. The manual calculated wing loading and power loading for proposed aircraft is 19 lb/ft² and 15 lb/hp respectively. The AAA calculated values for wing loading and power loading are 20.5 lb/ft² and 18 lb/hp respectively. Therefore, the values are almost similar.

The selected design point is based on the values of wing loading and power loading at take-off which also satisfies the all FAR-23 requirements with the smallest possible wing. The wing size increases by decreasing the wing loading and vice versa. Since, the maximum take-off weight of proposed aircraft is relatively low, a high-power loading was not necessary.

To satisfy the all FAR-23 requirement, the design point must be below the cruise speed curve. Furthermore, the point must be below the take-off distance curve with appropriate coefficient of lift. In an equivalent way, the design point must be on left side of the landing distance curve. Also, the design point should be below the all climb requirements.

The design point selected for proposed aircraft gives the wing loading of 19 lb/ft² and power loading of 15 lb/hp, where $C_{L_{max_{take-off}}} = 1.9$ and $C_{L_{max_L}} = 2.0$, *Wing area* = 175.52 ft². The critical design requirements for proposed aircraft are take-off distance and landing distance.

CHAPTER 5

FUSELAGE DESIGN

The proposed general aviation electric aircraft is now beginning to take shape. The preliminary estimate of take-off weight and take-off wing loading has been done in chapter 3 and 4 respectively. So, the next step is to size and design of the fuselage. The following points must be considered when designing a fuselage:

- The size of the payload and its location
- Landing gear
- Wing carry through
- Engine placement
- Avionics
- Fuel storage

The purpose of this report is to make realistic layouts for the cockpit (also called flight deck) and fuselage. The section (5.2) will provide a necessary design layout of cockpit by considering the guidelines for visibility, human factors in terms of control and instrument placement and crew seats. The section (5.3) will give the fuselage design with the effect of fuselage shape on drag. The passenger seating arrangements, seats, window and exit placement will be considered in designing of fuselage layout.

5.1) LAYOUT DESIGN OF COCKPIT:

Since, the proposed aircraft is general aviation electric aircraft and it comes under FAR-23 certification, there is no specific requirement for cockpit layout. It can be design together with the fuselage design. In terms of cockpit design, there is a requirement to monitor the battery management system (i.e. Battery health, Inverter condition, time of remaining flight) and additional interface units. In this portion, the civil airplane cockpit design procedure is mentioned just to give general idea. The weights and dimensions for crew members should be same for proposed aircraft. The following factors must consider while designing the cockpit:

- The pilot can reach all controls comfortably
- The pilot must be able to see all 'flight essential'
- Communication by voice or by touch must be possible without undue effort
- Visibility from the cockpit must adhere to certain minimum standards

5.1.1) Dimensions and Weights for Crew Member:

The cockpit will be designed for one pilot with standard height of 1830 mm and weight of 175 lbs (not wearing helmet!). It is initially sized to hold one male crew member, as female crew member is typically smaller in size. The dimensions of standing male crew member are as follows:

- Body width across shoulders: 533 mm
- Body width across elbows: 561 mm
- Body width across hips: 457 mm

The following figure (59) & (60) provides a baseline data for dimensions of sitting male crew member.

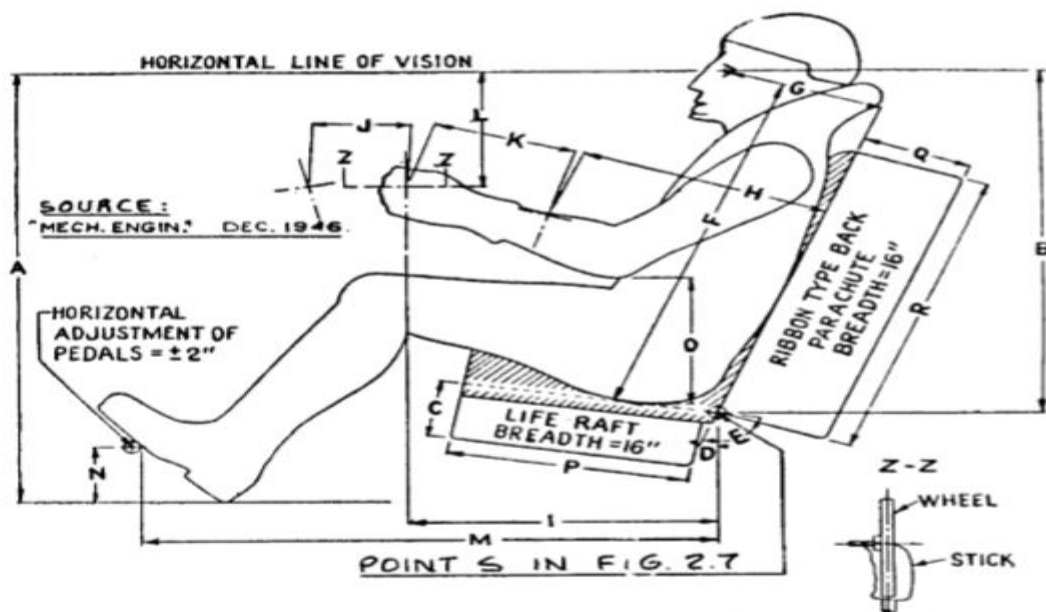


Figure 58 Dimensions of Sitting Male Crew Member in Cockpit

For Wheel Type Controllers:

A	B	C	D	E	F	G	H	I	J
37	30.25	5	21	101	29.75	10.00	16.63	19	6
39	30.75	5	19	101	30.25	9.75	15.75	19	6
41	31.50	5	16	101	31.00	9.75	15.13	19	6
43	31.75	5	16	101	31.25	10.00	15.13	19	6

A	L	M	N	O	P	Q	R
37	10.00	36.0	5	9.25	15	7	25
39	10.50	35.0	5	9.25	15	7	25
41	10.75	34.5	5	9.25	15	7	25
43	11.00	34.5	5	9.25	15	7	25

Figure 59 Dimensions and Weights for Male Crew Members as Shown in Figure 1

5.1.2) Layout of Cockpit Seating and Cockpit Controls:

The following figure (61) shows the typical arrangement of pilot seat and pilot controls for civil airplanes. The proposed airplane is designed to use a wheel control system.

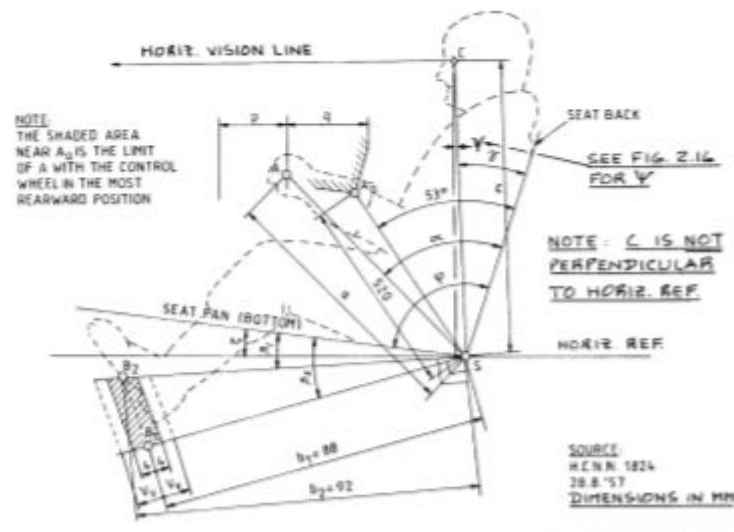


Figure 60 Recommended Seat Arrangement for Civil Airplanes

The geometric quantities in figure (61) are defined in figure (62) with some adjustments:

Symbol	Wheel Control
a	67 (+/- 4)
ξ	7° (+/- 2°)
p = Forward motion of point A:	18 (+/- 2)
q = Rearward motion of point A:	22 (+/- 2)
r = Sidewise motion of point A from center*:	-----
d = Distance between handgrips of wheel*:	38 (+/- 5)
e = Wheel rotation from center*:	85° (max.)
v = Distance between rudder pedal center lines*:	38 (+/- 12)
α	64° (+/- 3°)
β_1	22°
β_2	10°
c	77 (+/- 2)
γ	21° (+/- 1°)
φ	102° (+/- 2°)
V _v = Adjustment range of pedals from center position B:	7 (+/- 2)
U _v = Forward and aft pedal motion from center position B*:	10 (+/- 2)
S _h = Horizontal adjustment range of S from center position*:	< 10
S _v = Vertical adjustment range of S from center position*:	8 (+/- 1)
* Not shown in Figure 2.7.	

Figure 61 Dimensions for Civil Cockpit Controls

5.1.3) Determination of Visibility from the Cockpit:

The reasons why good visibility is essential are as follows:

- During take-off and landing pilot must have a good view of surroundings
- The pilot must be able to observe conflicting traffic

According to Jan Roskam, the visibility from the cockpit is defined as the angular area obtained by intersecting the airplane cockpit with radial vectors emanating from the eyes of the pilot.

5.2) LAYOUT DESIGN OF THE FUSELAGE:

The fuselage design of proposed airplane is based on the similar types of single propeller driven aircraft. For the FAR-23 airplanes, there is no fixed requirement of door and window placement, so it is assumed that the windows and doors are perpendicular to the seats. The following table and figures shows the detailed dimensions with various views of the proposed airplane fuselage design.

Table 21 Fuselage Dimensions

Fuselage Parameter	Dimension
Total Length	26 ft
Diameter	4.5 ft
Width	3.75 ft
Fineness Ratio	5.78
Tail Cone Length	13 ft
Cabin Length	9 ft
Nose Length	4 ft
Distance Between Two Seating Rows	2.7 ft
Distance Between Two Adjacent Seats	0.25 ft

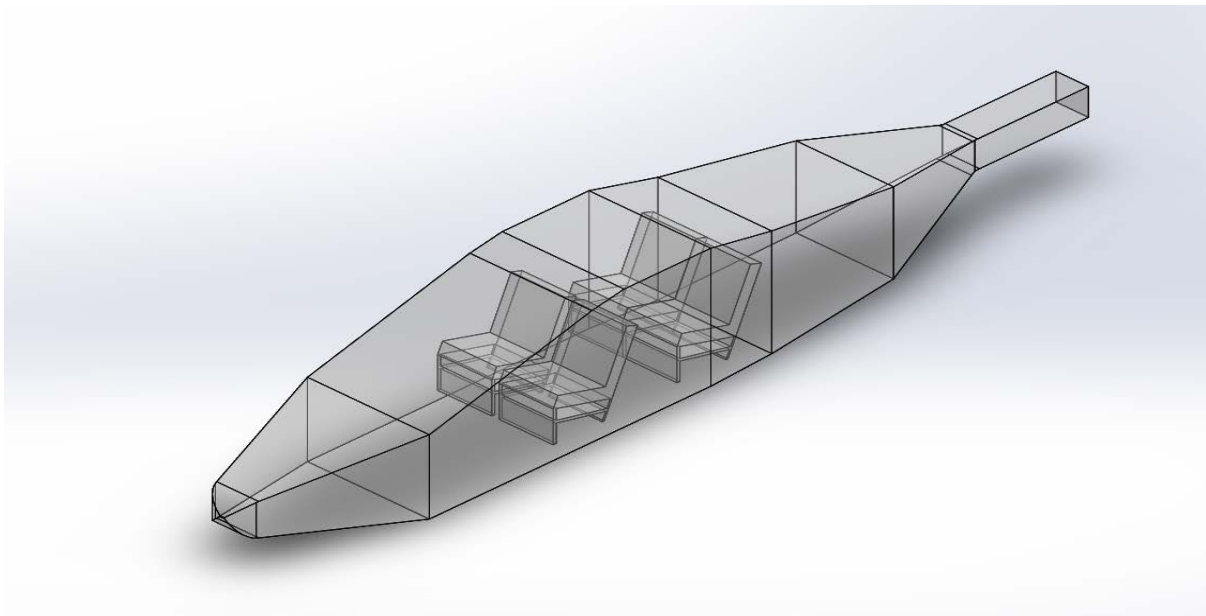


Figure 62 Isometric View of Fuselage

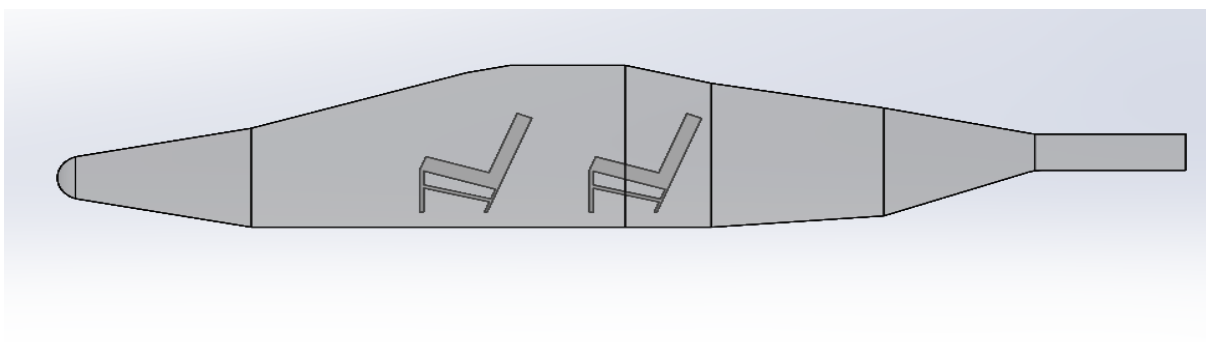


Figure 63 Side View of Fuselage

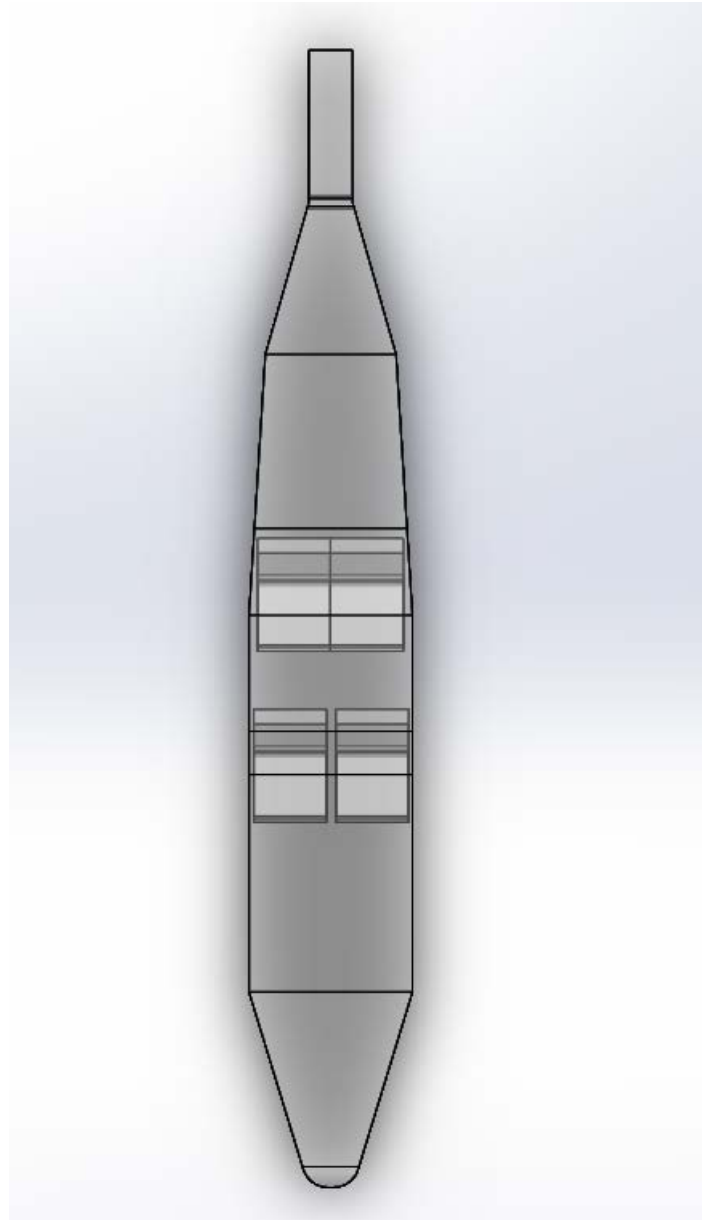


Figure 64 Top View of Fuselage

5.3) DISCUSSION:

As it is mentioned in above sections that the fuselage was designed based on similar types of airplanes; because fuselage design does not have many requirements. The fineness ratio (fuselage length to diameter ratio) was the main factor which drives the fuselage design and necessary for designing an empennage.

CHAPTER 6

WING, HIGH-LIFT SYSTEM AND LATERAL CONTROL DESIGN

The planform of a vehicle means collectively the sweep of the leading edge, aspect ratio, taper ratio, and the top view of the wing. The choice of the planform is especially significant as it influences the vehicle aerodynamics significantly and gives the aircraft its characteristic shape. These planform parameters are shown in figure (66).

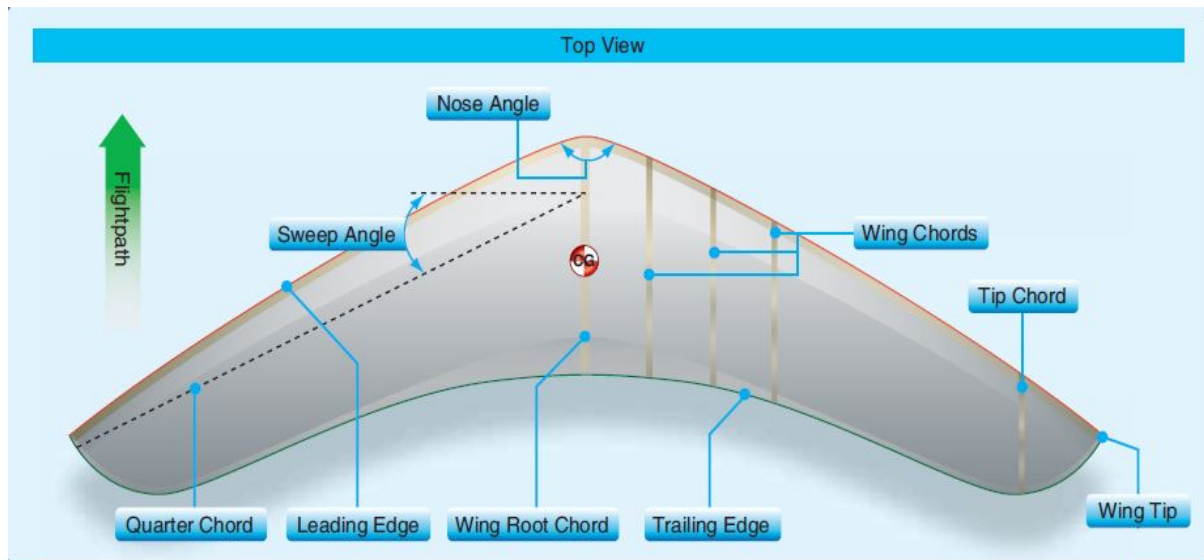


Figure 65 Wing Parameters

Generally, an airfoil section and planform are selected to give high lift co-efficient and high wing fuel volume with minimum zero-lift drag. The above requirements are impossible because of conflicting conditions. Thus, the selection of planform is a compromise with the priorities established by the mission requirement.

The wing area and aspect ratio are already known from preliminary sizing process. In this design report, the sweep angle, thickness ratio, taper ratio, dihedral angle, and airfoils will be determined. Then, the type and size of high lift devices will be determined to meet the requirements for lift co-efficient. To determine the wing planform schematic, all the determined values will be used in AAA program.

6.1) WING PLANFORM DESIGN:

Fixed-wing aircraft can have different number of wings like monoplane, biplane, triplane, quadruplane, and multiplane. The wing must be rigid and strong to support itself. The several types of wing support can be used. The wing support types are cantilevered, braced, closed wing, rigid, and flexible. The wing planform is the shape of the wing when viewed from above or below. Nowadays almost all the monoplane has cantilevered support because all the structure is buried under the aerodynamic skin which provides low drag as well. On the other hand, in braced support, the wings are supported by external structure.

The overall configuration for proposed aircraft is conventional (that means tail aft) with low-wing configuration. The wing area, S ($=175.52 \text{ ft}^2$) and aspect ratio, A ($=10$) is already known from the performance sizing. Using these known characteristics, the remaining planform design characteristics can be determined. The overall structural wing configuration for proposed aircraft is cantilever wing with the low wing.

6.1.1) Sweep Angle-Thickness Ratio Combination:

The distinct types of sweep are as follows:

- Zero or negligible sweep
- Aft sweep (Positive sweep)
- Forward sweep (Negative sweep)
- Variable sweep (Symmetrically variable sweep)
- Oblique sweep (Asymmetrically variable sweep)

The variable and oblique sweep are suitable choices for missions where there is a requirement for supersonic cruise, subsonic cruise and for high 'g' maneuvering. The wing geometric data for single engine propeller driver airplane are as follows:

Type	Dihedral Angle, Γ_w	Incidence Angle, i_w	Aspect Ratio, A	Sweep Angle, $\Lambda_{c/4}$	Taper Ratio, λ_w	Max. Speed, V_{max}	Wing Type
	deg.	root/tip deg.		deg.		kts	
CESSNA							
Skywagon 207	1.7	1.5/-1.5	7.4	0	0.69	182	brcd/high
Cardinal RG	1.5	4.1/0.7	7.3	0	0.73	156	ctl/high
Skylane RG	1.7	0.8/-2.8	7.4	0	0.67	187	brcd/high
PIPER							
Cherokee Lance	7.0	2/-1	6.2	0	1.0	188	ctl/low
Cher. Warrior	7.0	2/-1	7.2	5	0.67	152	ctl/low
Turbo Sarat.SP	6.8	NA	7.3	0	0.68	195	ctl/low
Bellanca							
Skyrocket	2	2	6.7	0	0.57	287	ctl/low
Grumman Am.							
Tiger	5	1.4	7.1	0	1.0	148	ctl/low
Rockwell Commander 112A	7	2	7.0	-2.5	0.50	180	ctl/low
Trago Mills							
SAH-1	5	3/1	7.5	0	0.54	202	ctl/low
Scottish Aviation							
Bullfinch	6.5	1.2	8.4	0	0.57	150	ctl/low
Robin HR100/4	6.3	4.7	5.4	0	1.0	180	ctl/low
Socata Rallye							
135E	7	4	7.6	0	1.0	148	ctl/low
Fuji FA-200	7	2.5	6.3	0	1.0	123	ctl/low
Gen Avia P15P	6	4	7.7	0	0.49	167	ctl/low

ctl = cantilever brcd = braced (strutted)

Figure 66 Wing Geometric Data for Single Engine Propeller Driven Airplane

Since all the single engine propeller driven aircraft has zero or negligible sweep, the proposed aircraft will feature the zero-sweep angle. The other reason for selecting zero-sweep angle is due to the fact that the proposed aircraft is not designed for supersonic application and/or it is designed for low subsonic speed, the drag reduction through swept wing is not necessary.

The thickness ratio should be between 0.1 and 0.2. Figure (67) shows that the thickness ratio for single engine propeller driven aircraft is as high as 15 percent.

Type	Wing Area	Wing \bar{c}	Wing Airfoil	Hor. Tail Area S_h	S_e/S_h	x_h	\bar{V}_h	Elevator Chord
	S	\bar{c}	root/tip	S_h				root/tip
	ft ²	ft	NACA*	ft ²		ft		fr. c_h
CESSNA Skywagon 207	174	4.55	2412	44.9	0.45	16.2	0.92	.48/.47
Cardinal RG Skylane	174	4.79	64A215/64A412	35.0	1.00	14.3	0.60	stabilator
PIPER Cherokee	174	4.52	2412	38.8	0.41	14.3	0.71	.47/.39
Lance	173	5.25	63,415	34.6	1.00	16.1	0.61	stabilator
Warrior	170	4.44	65,415	26.5	1.00	13.5	0.48	stabilator
Turbo Saratoga SP	178	4.71	NA	36.2	1.00	16.2	0.70	stabilator
Bellanca Skyrocket	183	5.30	63,215	42.6	0.38	13.8	0.61	.36/.42
Grumman Tiger	140	4.44	NA	37.6	0.28	12.6	0.76	0.39
Rockwell Commander	152	4.58	63415	31.2	0.34	10.9	0.49	.33/.44
Trago Mills SAH-1	120	3.94	2413.6	22.0	0.46	17.8	0.83	0.46
Scottish Aviation Bullfinch	129	3.97	63,615	27.5	0.58	11.9	0.63	0.45

* Unless otherwise indicated.

Figure 67 Thickness Ratio Values for Single Engine Propeller Driven Airplane

As thickness ratio increases, the co-efficient of lift also increases at low speed. The thickness ratio also influences the critical Mach number. As the thickness ratio decreases, the critical Mach number increases. The thickness ratio cannot be less than 0.1 to allow enough room for the wing structure and it should not be more than 0.2 because the profile drag of the wing is going to be too high.

The following airfoil thickness ratios are selected for the proposed aircraft:

at the wing centreline: 0.14

at the wing tip: 0.12

6.2) AIRFOIL SELECTION:

For any airplane, the airfoil is the heart because it can affect the cruise speed, take-off and landing distances, stall speed, handling qualities, and overall aerodynamic efficiency during all phases of flight. The geometry of an airfoil can be seen from following figure (69).

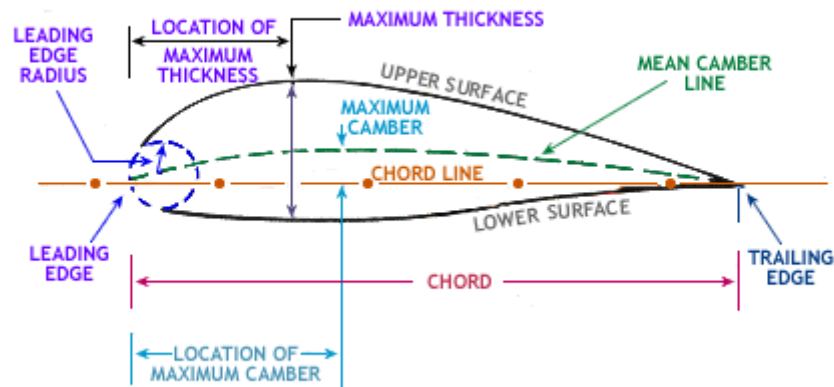


Figure 68 Airfoil Geometry

To prevent a drag-producing bow-shock in supersonic flow, the designed airfoil should have a sharp leading-edge. Most of the airfoil have a blunt trailing edge with small finite thickness because it is difficult to build a perfectly sharp trailing edge. The pressure difference between upper and lower surface generate the net lifting force.

In the 1930's, the NACA developed 'four-digit' airfoil followed by 'five-digit' and 'six-digit' airfoil. The six-digit series were designed for increased laminar flow, which is widely used for high-speed-wing design. A 'supercritical' airfoil is designed to minimize upper surface shock, which helps to increase the critical Mach number.

For proposed electric aircraft, a different type of airfoil were examined for different Reynolds number. Lift and drag characteristics were used to choose an airfoil which meets performance requirements. The chosen airfoil for the proposed aircraft is NACA 63412. It is shown in below figure (70).

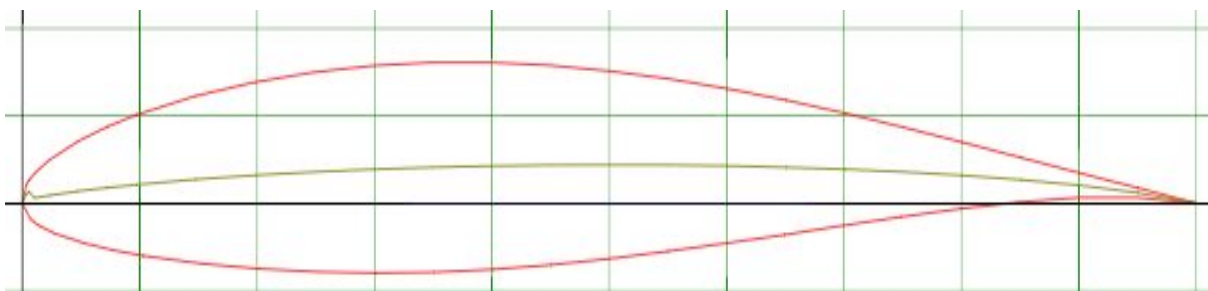


Figure 69 NACA 63412 Airfoil

The above airfoil is also plotted using XFLR5 software and analyse. The graph of co-efficient of lift, co-efficient of drag versus angle of attack is also plotted for two different Reynolds number. The XFLR5 plotted image is as follows:

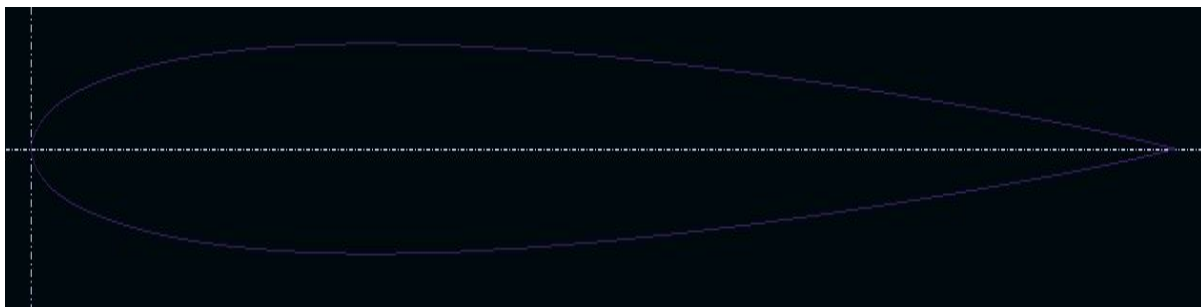


Figure 70 NACA 63412 Plot Using XFLR5

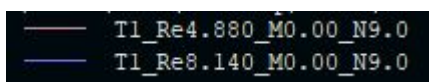


Figure 71 Reynolds Number for NACA 63412

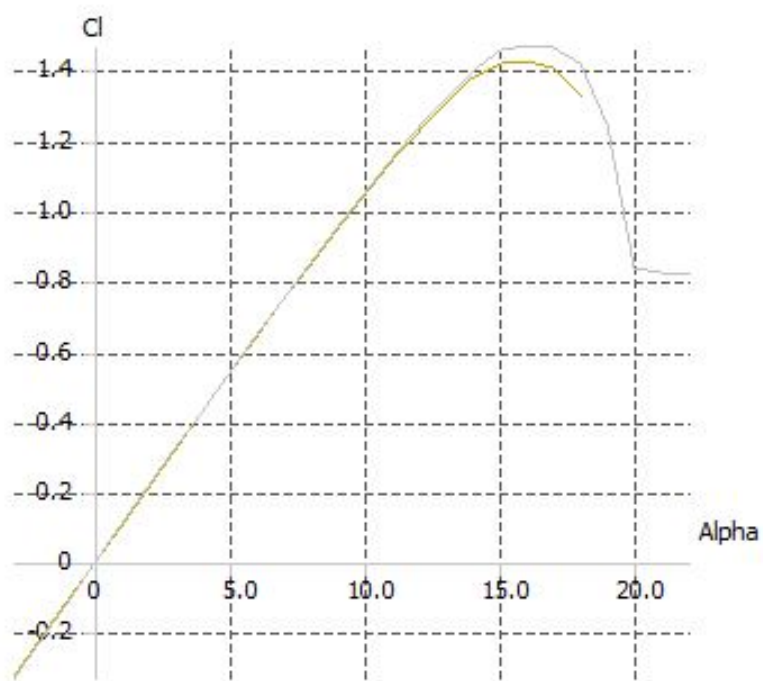


Figure 72 Co-efficient of lift versus angle of attack for NACA 63412

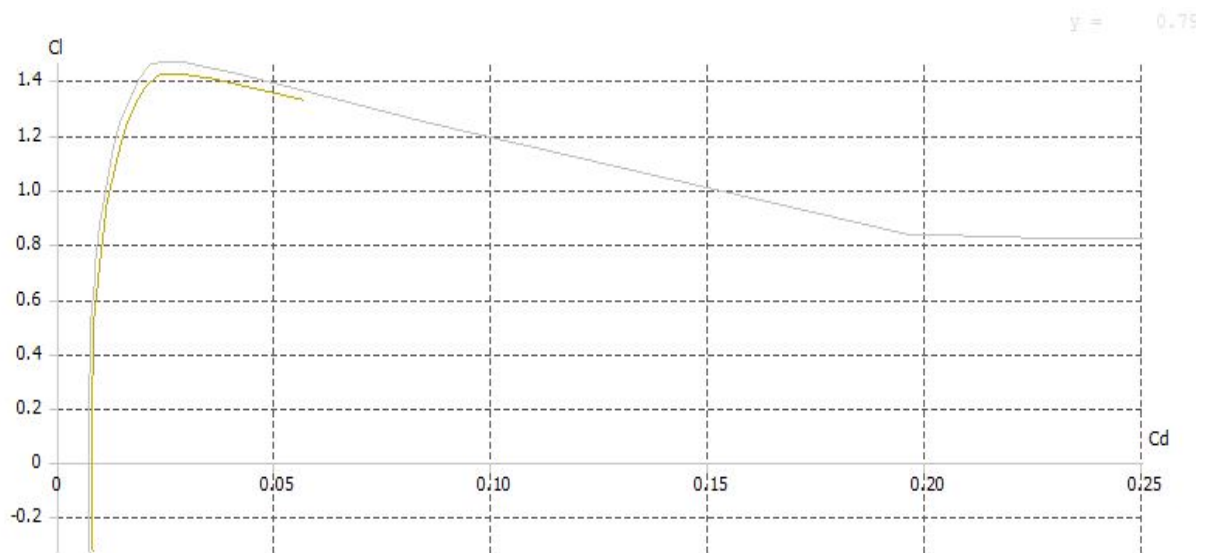


Figure 73 Co-efficient of lift versus co-efficient of drag for NACA 63412

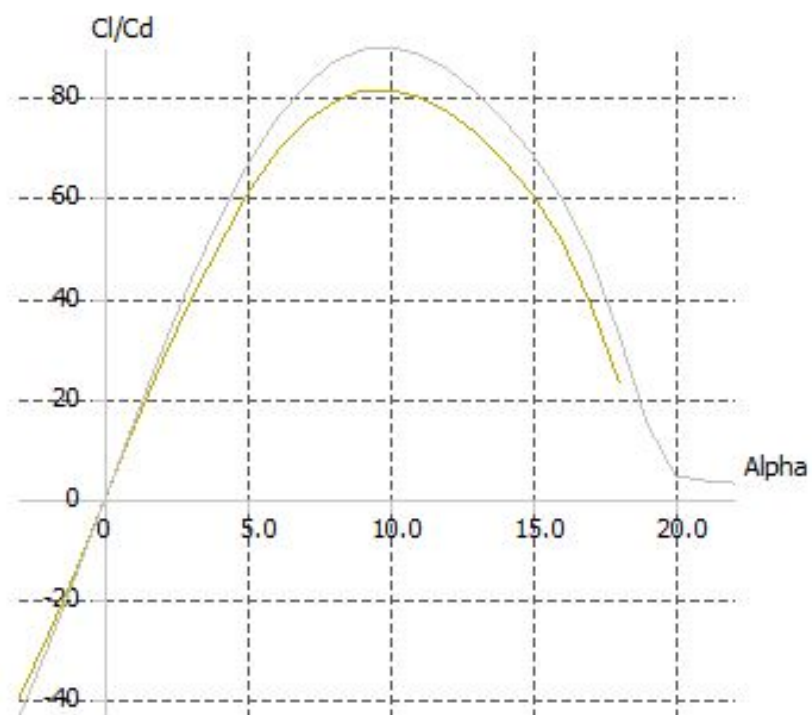


Figure 74 Co-efficient of lift/Co-efficient of drag versus alpha for NACA 63412

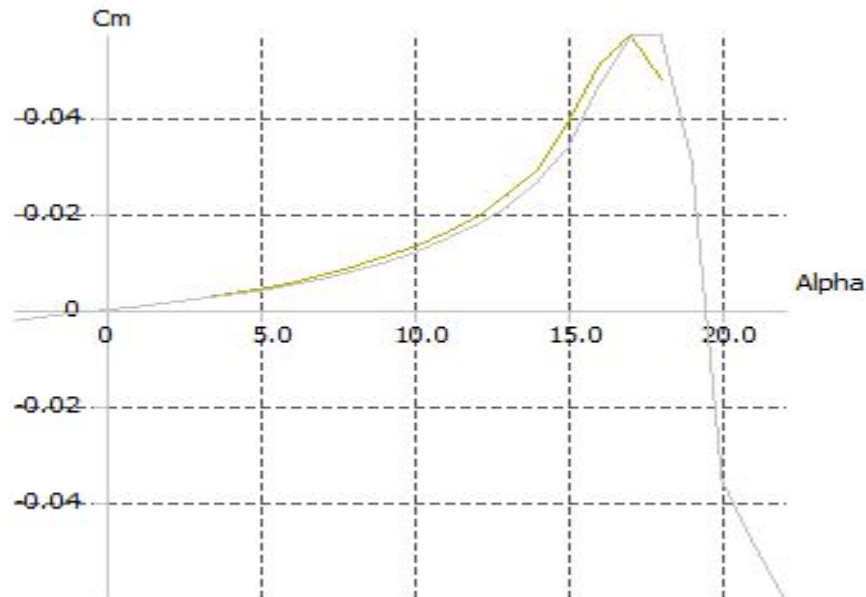


Figure 75 Pitching Moment Co-efficient versus angle of attack for NACA 63412

From the above graph of C_L versus alpha (angle of attack), it can be seen that the proposed airfoil can produce C_L of 1.48 (@Root), 1.45 (@Tip) and when it reaches to critical angle of attack, the lift drops off. The co-efficient of drag is also around 0.025 when the lift is maximum.

As mentioned earlier, figure (67) shows the wing geometric data for single engine propeller driven airplane. From that, the incidence angle is chosen as 3 degrees, the dihedral angle will be 7 degrees and the taper ratio of 0.60 is chosen.

6.3) DESIGN OF HIGH-LIFT DEVICES:

High lift device is a component on aircraft's wing that increases the lift of wing. High lift devices can be classified as follows:

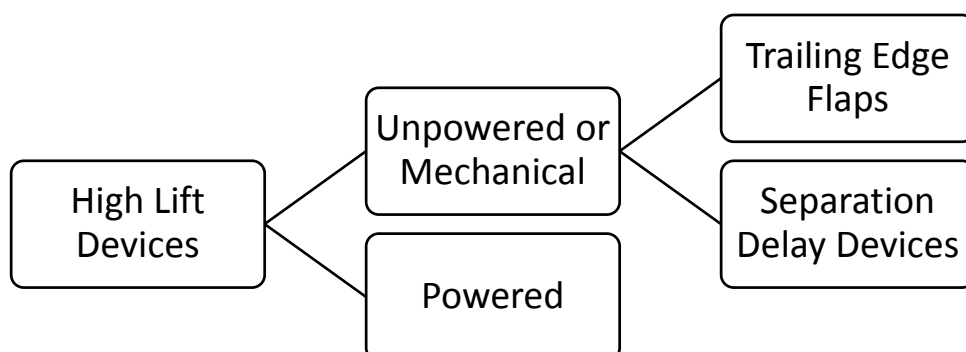


Figure 76 Types of High-Lift Devices

The trailing edge flaps operates by increasing the circulation about the airfoil. The separation delay devices include leading edge flaps, slots or slots and boundary layer control.

The powered lift devices include internal and external blown flaps, deflected slipstream and upper surface blowing, jet flap, fan-in-wing, tilt wing, direct jet lift, and augments wing.

The following section will provide the estimation of high lift devices for the proposed electric aircraft which can provide enough lift at take-off and landing mission requirements. The values of lift co-efficient for take-off and landing is already calculated in performance sizing (chapter 4). The proposed electric aircraft has $C_{L_{max_{clean}}} = 1.7$, $C_{L_{max_{TO}}} = 1.9$ and $C_{L_{max_L}} = 2.0$. The wing planform is already selected for proposed airplane and it was found that: $A = 10$, $S = 175.52 \text{ ft}^2$, $b = 41.9 \text{ feet}$, Sweep angle = 0° , Taper ratio = 0.60, thickness ratio = 0.14, incidence angle = 3° , dihedral angle = 7° , $C_r = 5.23 \text{ feet}$, $C_t = 3.14 \text{ feet}$.

The proposed electric airplane is a moderately short-coupled airplane. Therefore,

$$C_{L_{max_W}} = 1.06 * C_{L_{max}} \quad (6.1)$$

$$C_{L_{max_W}} = 1.06 * 1.7$$

$$C_{L_{max_W}} = 1.80$$

The proposed electric airplane has no sweep, so

$$C_{L_{max_W}} = k_\lambda * \frac{C_{l_{max_r}} + C_{l_{max_t}}}{2} \quad (6.2)$$

Where, $k_\lambda = 0.92$ (from Roskam)

$$C_{l_{max_r}} + C_{l_{max_t}} = 3.91 \quad (6.3)$$

Now, the section maximum lift co-efficient is calculated from Reynold's number.

Reynold's number at root:

$$R_{n_r} = \frac{\rho * V * C_r}{\mu} \quad (6.4)$$

$$R_{n_r} = \frac{1.2255 \left(\frac{kg}{m^3} \right) * 74.59 \left(\frac{m}{s} \right) * 5.23(\text{feet})}{1.79 * 10^{-5} (Pa S)}$$

$$R_{n_r} = 8.14 * 10^6$$

Reynold's number at tip:

$$R_{n_t} = 4.88 * 10^6$$

Now, from the figure (8) it follows that for this airfoil:

$$C_{l_{max_r}} + C_{l_{max_t}} = 1.48 + 1.45$$

$$C_{l_{max_r}} + C_{l_{max_t}} = 2.93 \quad (6.5)$$

By comparing equation (6.3) & (6.5), the design wing planform under consideration is delivering the required value of clean maximum lift co-efficient.

Now, the incremental values of maximum lift co-efficient which need to be produced by the high lift devices:

$$\text{Take-off: } \Delta C_{L_{max_{TO}}} = 1.05 * (C_{L_{max_{TO}}} - C_{L_{max}}) = 1.05 * (1.9 - 1.7) = 0.21$$

$$\text{Landing: } \Delta C_{L_{max_L}} = 1.05 * (C_{L_{max_L}} - C_{L_{max}}) = 1.05 * (2.0 - 1.7) = 0.315$$

The above lift increments are not very high. So, it is speculated that a small plain flap will be enough.

The required incremental section lift co-efficient value with flaps down can be calculated as:

$$\Delta C_{L_{max}} = (\Delta C_{L_{max}}) \left(\frac{S}{S_{wf}} \right) K_{\Lambda} \quad (6.6)$$

Where,

$$K_{\Lambda} = \left(1 - 0.08(\cos\frac{\Lambda_c}{4})^2 \right) (\cos\frac{\Lambda_c}{4})^{\frac{3}{4}} = 0.92$$

$$\frac{S_{wf}}{S} = \text{flap size parameter}$$

The flap size parameter values can be assumed at this point, which is as follows:

	Take-off flaps		Landing flaps	
$\frac{S_{wf}}{S}$	0.3	0.6	0.3	0.6
$\Delta C_{L_{max}}$	0.64	0.32	0.96	0.48

It was already assumed that the plain flap will be sufficient. The plain flap geometry is assumed as follows: $z_{fh} = 0.1, \frac{c_f}{c} = 0.25, \delta_{f_{TO}} = 15 \text{ deg.}, \delta_{f_L} = 40 \text{ deg.}$

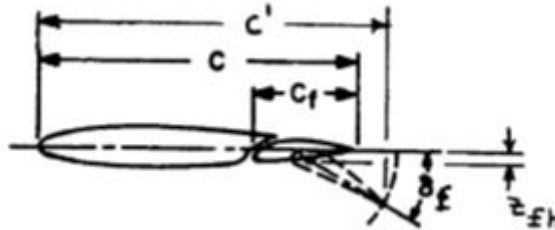


Figure 77 Flap Geometry

The required incremental section lift co-efficient value which the flap must generate can be calculated as:

$$\Delta C_L = \left(\frac{1}{K} \right) \Delta C_{L_{max}} \quad (6.7)$$

Where,

$K=0.75$, which is found from following figure:

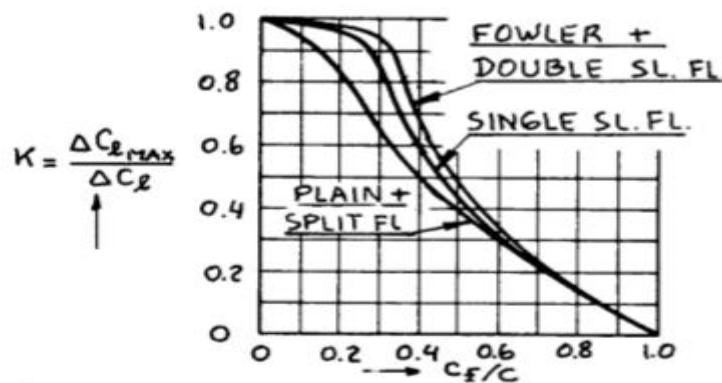


Figure 78 Value of K based on flap chord ratio

The incremental section lift co-efficient, ΔC_L , for plain flap is calculated from:

$$\Delta C_L = C_{L\delta_f} * \delta_f * K' \quad (6.8)$$

Where, $C_{L\delta_f}$ and K' is found from following figures:

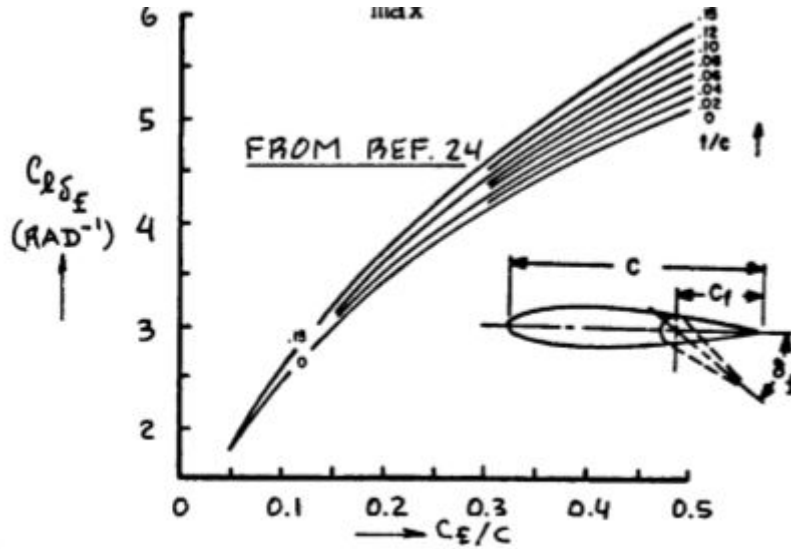


Figure 79 Effect of Thickness Ratio and Flap Chord Ratio on $C_{L\delta_f}$

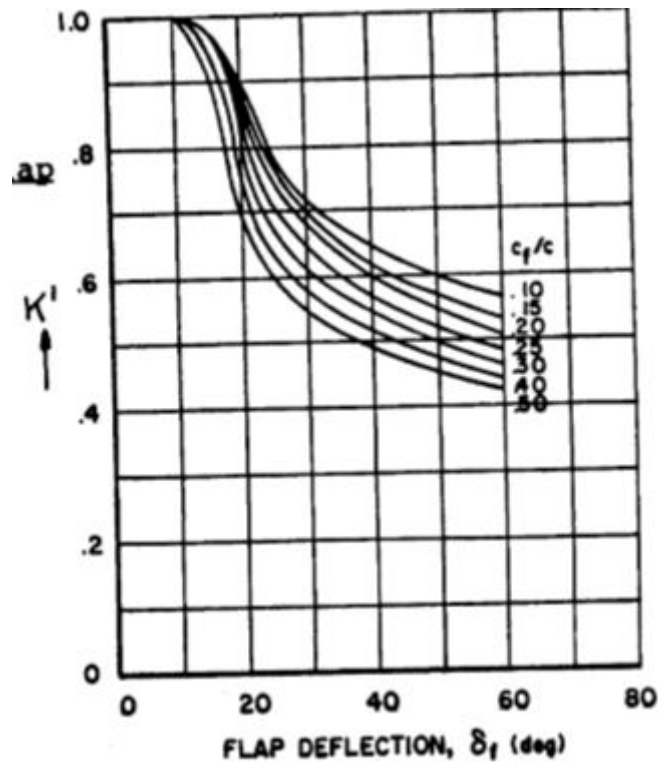


Figure 80 Effect of Flap Chord Ratio and Flap Deflection on K'

Take-off: From equation (6.8), $\Delta C_L = (4.1) * (0.2618) * (0.98) = 1.05$

From equation (6.7), $\Delta C_{L_{max}} = (0.75) * (1.05) = 0.78$

Landing: From equation (6.8), $\Delta C_L = (4.1) * (0.6981) * (0.56) = 1.60$

From equation (6.7), $\Delta C_{L_{max}} = (0.75) * (1.60) = 1.20$

It is seen that the value of $\Delta C_{L_{max}}$, for take-off and landing, is much more than needed with the previously assumed values of $\frac{S_{wf}}{S}$. Thus, the plain flap is sufficient to produce required lift co-efficient.

The flap geometry are as follows:

$$\frac{S_{wf}}{S} = 0.3, \frac{c_f}{c} = 0.25, \delta_{f_{TO}} = 15 \text{ deg.}, \delta_{f_L} = 40 \text{ deg.}$$

6.4) DESIGN OF THE LATERAL CONTROL SURFACES:

The lateral control surfaces are responsible for the lateral stability of the aircraft. The ailerons are used to generate a rolling motion and hinged on the outboard portion of a wing. The lift force of the wing is applied to aerodynamic centre which is at some distance from the aircraft centre of gravity. These unequal forces create a torque and the aircraft rotates about its centre of gravity.

The data for single engine propeller driven airplane is provided in Roskam as follows:

Type	Wing Area S ft ²	Wing Span b ft	Vert. Tail Area S _v ft ²	S _r /S _v	x _v ft	\bar{v}_v	Rudder Chord root/tip fr.c _v	S _a /S	All. Span Loc. in/out fr.b/2	All. Chord in/out fr.c _w
CESSNA										
Skywagon 107	174	35.8	16.0	0.44	18.0	0.046	.46/.46	0.10	.61/.94	.25/.23
Cardinal RG	174	35.5	17.4	0.37	13.5	0.038	.35/.43	0.11	.65/.97	.38/.37
Skylane RG	174	35.8	18.6	0.37	15.8	0.047	.41/.42	0.11	.47/.96	.17/.24
PIPER										
Cherokee										
Lance 175	175	32.8	19.8	0.31	15.3	0.037	.26/.50	0.064	.56/.88	0.20
Warrior 170	170	35.0	11.5	0.36	19.2	0.026	.29/.52	0.078	.48/.96	.27/.24
Turbo Saratoga SP	178	36.2	15.9	0.29	15.2	0.038	.23/.58	0.057	.52/.84	0.19
Bellanca										
Skyrocket 183	183	35.0	18.1	0.33	13.2	0.037	.28/.40	0.076	.60/1.0	.25/.22
Grumman										
Tiger 140	140	31.5	8.4	0.43	12.6	0.024	.36/.46	0.055	.56/.92	0.24
Rockwell										
Commander 151	151	32.8	17.0	0.28	11.4	0.039	.30/.46	0.072	.64/.97	.27/.36
Trigo Mills										
SAB-1 120	120	30.7	17.1	0.40	18.6	0.086	.35/.54	0.080	.58/.97	.25/.29
Scottish Aviation										
Bullfinch 129	129	33.8	22.7	0.39	11.9	0.062	.35/.56	0.073	.61/.95	.23/.30

Figure 81 Aileron Data for Single Engine Propeller Driven Airplane

The data in above table suggest that following aileron dimensions are appropriate:

Aileron chord ratio: 0.24 – 0.26

Aileron span ratio: 0.57 – 0.94

6.5) DRAWINGS:

The wing parameters are as follows:

Table 22 Wing Parameters

Wing Parameter	
Wing Span	41.9 feet
Wing Area	175.52 feet ²
Aspect Ratio	10
Taper Ratio	0.60
Dihedral Angle	7 degrees
Sweep Angle	0 degrees
Thickness Ratio	0.14 (at the wing centreline) 0.12 (at the wing tip)
Root Chord	5.23 feet
Tip Chord	3.14 feet
Aileron Chord Ratio	0.24 – 0.26
Aileron Span Ratio	0.57 – 0.94
Airfoil	NACA 63412
Wing Type	Cantilever
Wing Fuselage Attachment	Low Wing

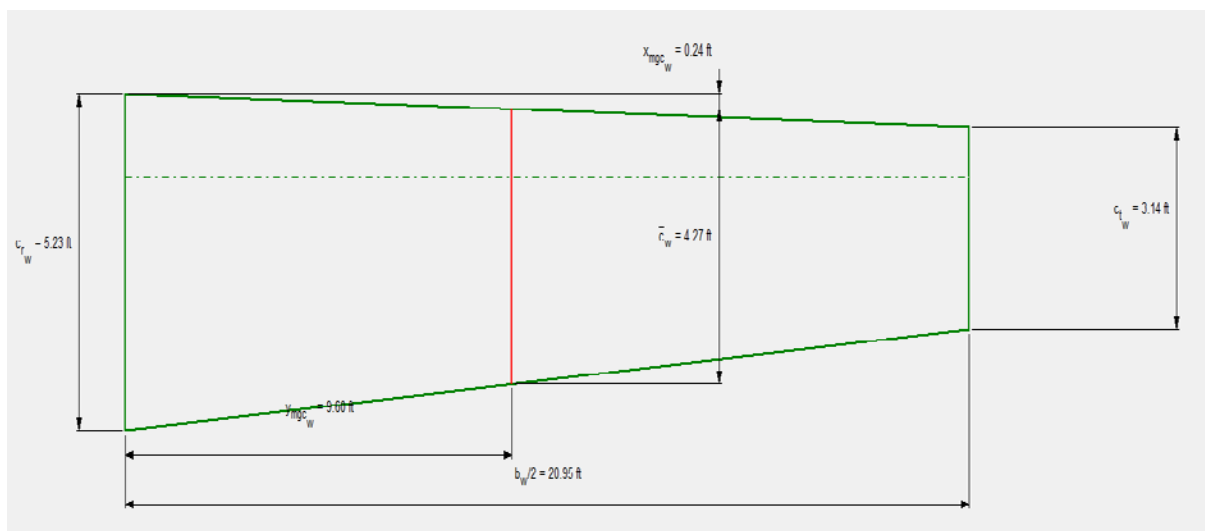


Figure 82 Wing Planform using AAA Program

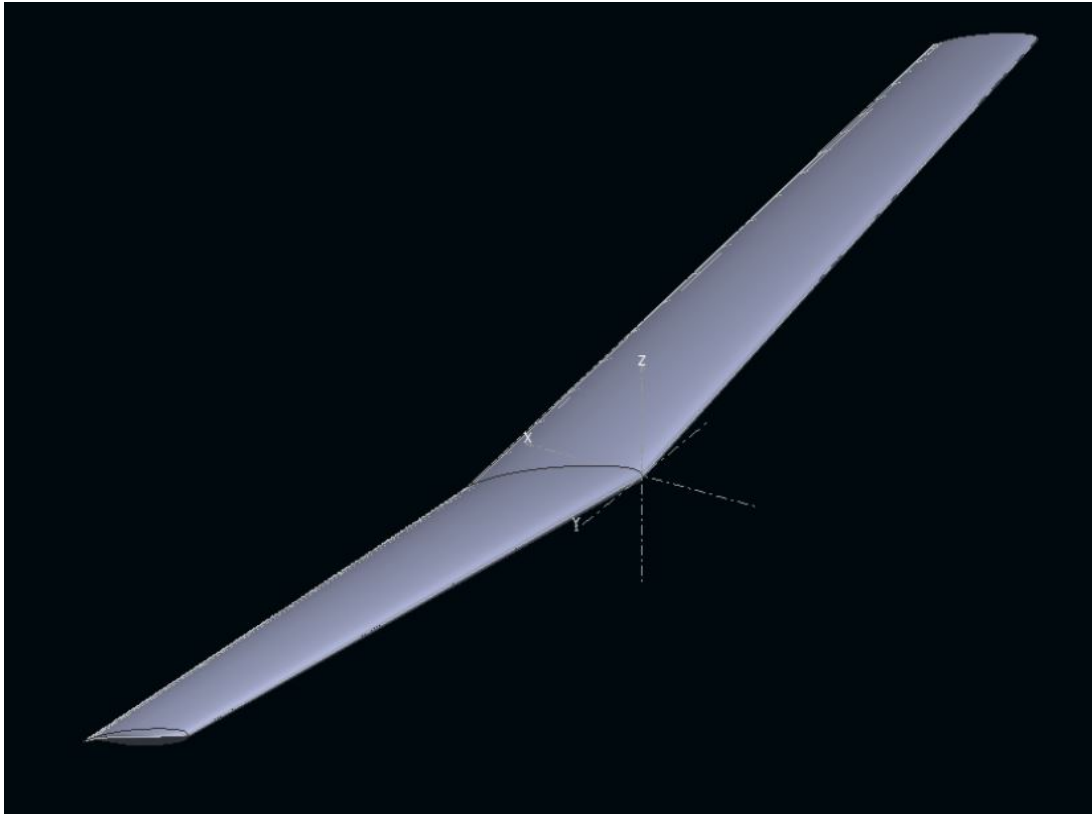


Figure 83 3-D View of Wing using XFLR5

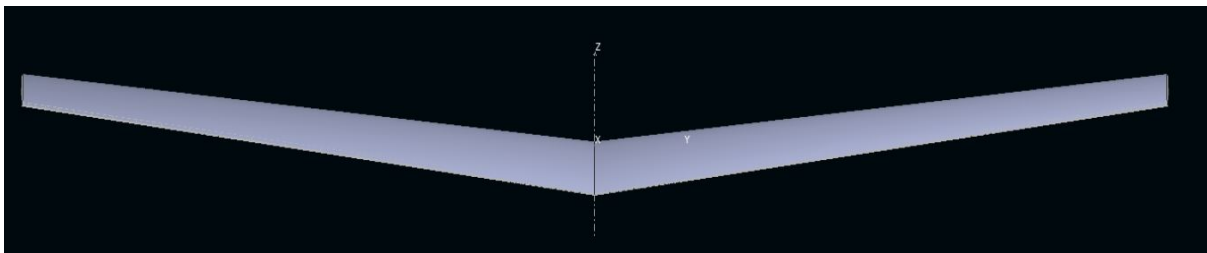


Figure 84 Front View of Wing using XFLR5

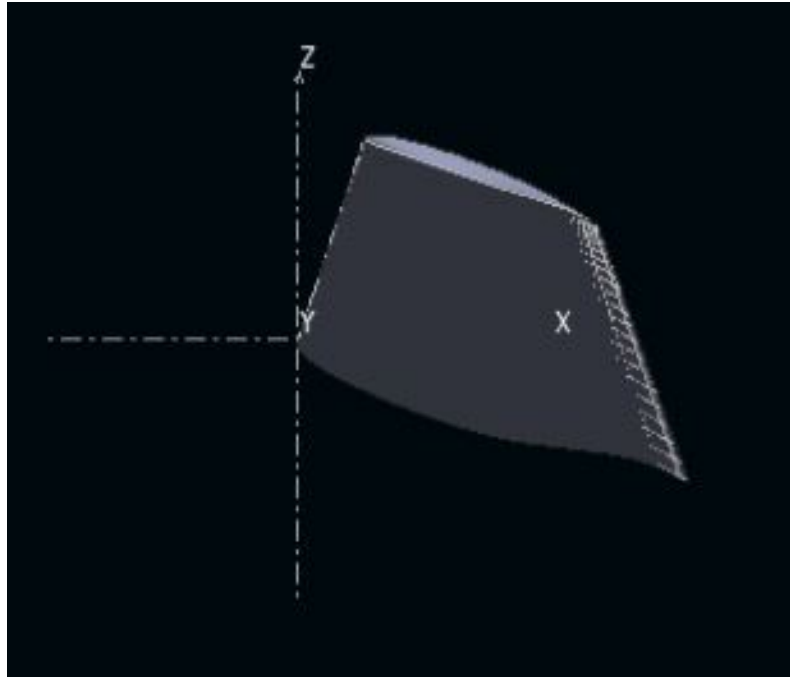


Figure 85 Side View of Wing using XFLR5

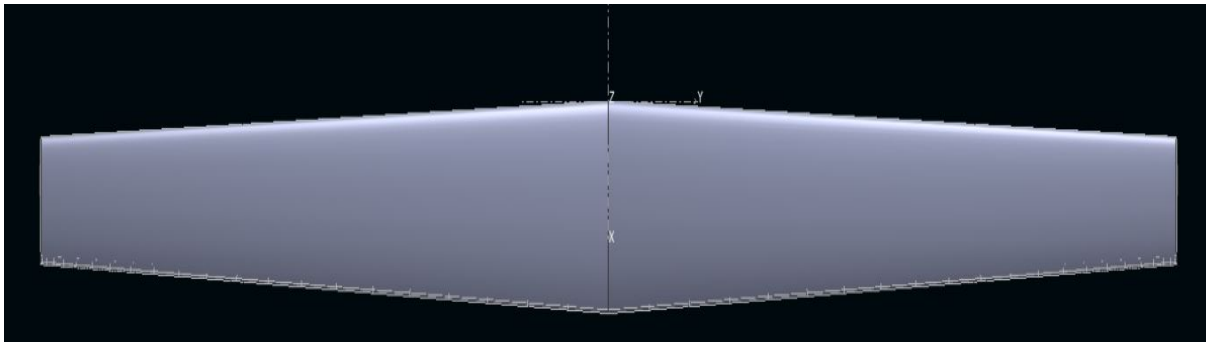


Figure 86 Top View of Wing using XFLR5

6.6) DISCUSSION:

The benchmark data provided in Roskam is used to compare and design the wing parameters. The proposed aircraft is single engine propeller driven general aviation aircraft with low wing so, it doesn't require sweep (zero sweep). The taper ratio is chosen as 0.60 which gives the root and tip chord of around 5.23 feet, 3.14 feet respectively. Almost all the general aviation low wing aircraft have dihedral which gives lateral stability to the aircraft. The dihedral and incidence angle are chosen as 7 degrees and 3 degrees respectively.

Through the calculation of the proposed airplane, the incremental section lift coefficient was calculated and it was found that proposed aircraft does not require any substantial lift devices (high lift devices). The coefficient of lift requirement for proposed aircraft during take-off is 1.9 and landing is 2.0. The calculations verified that an additional lift does not require. The airfoil is substantial to provide lift. The chosen airfoil for proposed electric aircraft is NACA 63412.

CHAPTER 7

DESIGN OF THE EMPENNAGE AND THE LONGITUDINAL AND DIRECTIONAL CONTROLS

The empennage is known as the tail which provides stability during flight. Almost all aircraft have an empennage integrating vertical and horizontal stabilizing surfaces which stabilise the flight dynamics of yaw and pitch. The elevator is usually hinged to horizontal stabilizer which controls the pitch (the nose up and down motion). The yaw motion (side-to-side motion) is restricted by the vertical stabilizer with hinged mounted rudder at the rear section.

The shape of the empennage surfaces is like wing planforms. The tail configurations are classified as follows:

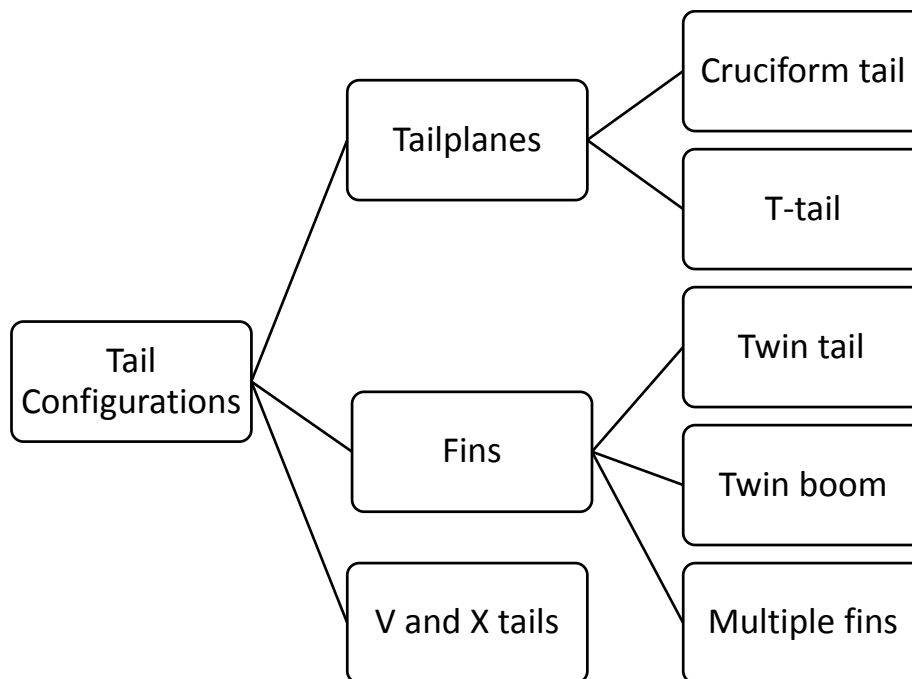


Figure 87 Tail Configurations

The wing planform is already known from wing sizing process. In this design report, the selected empennage configuration will be determined. Then, the size of horizontal and vertical stabilizer will be determined to meet the requirements. In the end, the cross-checking analysis will be provided using AAA program.

7.1) OVERALL EMPENNAGE DESIGN:

An aircraft can have different type of tail configuration. The vertical tail provides directional stability and control while the horizontal tail provides longitudinal control and stability. The sizing of both tail depends on many factors like:

- Landing and take-off
- Manoeuvrability
- High speed

The overall configuration for proposed aircraft is conventional (that means tail aft) with T-tail. By using T-tail, the tail plane is kept well out of the disturbed airflow which gives smoother and faster airflow to the elevators. The effective aspect ratio of aircraft increases using T-tail.

7.1.1) Empennage Disposition Calculations:

The location of the empennage components on the airplane will be decided in this portion. By keeping empennage area as small as possible, the airplane weight and drag will be reduced as much as possible. The location of the empennage components is decided using empennage moment arms x_h , x_v and x_c as defined in figure (89). For the proposed electric aircraft, $x_h = 14.75 \text{ ft}$ and $x_v = 14.80 \text{ ft}$ are gestimated.

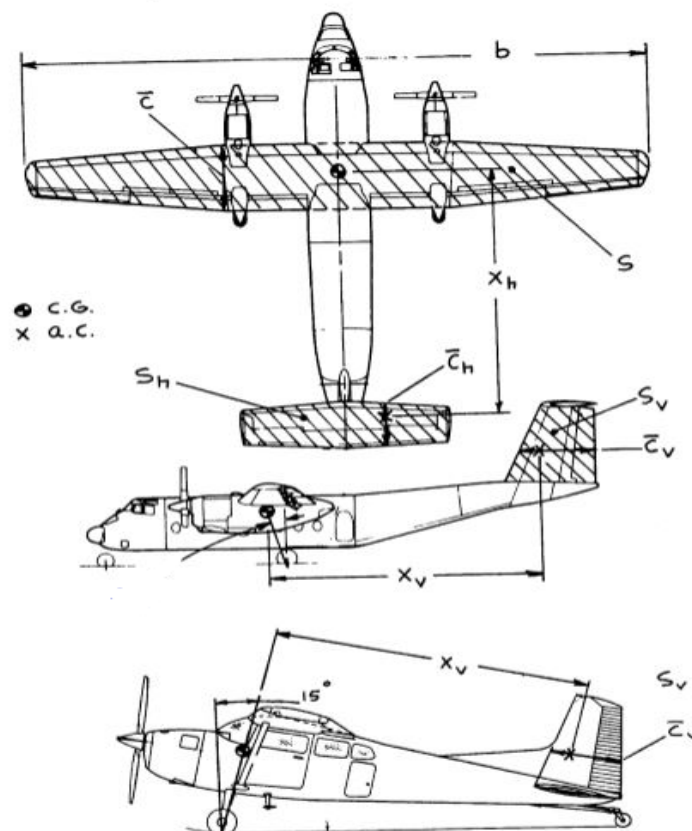


Figure 88 Empennage Moment Arms

7.2) DESIGN OF THE HORIZONTAL STABILIZER:

The design of horizontal stabilizer means deciding on the magnitude of S_h (Horizontal Stabilizer Area). The so-called \bar{V}_h -method is used to size the stabilizer. The tail volume co-efficient is calculated as follows:

$$\bar{V}_h = \frac{x_h S_h}{S \bar{c}} \quad (7.1)$$

If the \bar{V}_h is too small, the aircraft's pitch behaviour will be very sensitive to the centre of gravity location. The following figure (90) represents the values of horizontal tail volume co-efficients for proposed single engine propeller driven aircraft:

Type	Wing Area S ft ²	Wing mc \bar{c} ft	Wing Airfoil root/tip NACA*	Hor. Tail Area S _h ft ²	S _e /S _h	x _h ft	\bar{V}_h	Elevator Chord root/tip fr.c _h
CESSNA Skywagon 207	174	4.55	2412	44.9	0.45	16.2	0.92	.48/.47
Cardinal RG	174	4.79	64A215/64A412	35.0	1.00	14.3	0.60	stabilator
Skylane RG	174	4.52	2412	38.8	0.41	14.3	0.71	.47/.39
PIPER Cherokee								
Lance	175	5.25	65,415	34.6	1.00	16.1	0.61	stabilator
Warrior	170	4.44	65,415	26.5	1.00	13.5	0.48	stabilator
Turbo Saratoga SP	178	4.71	NA	36.2	1.00	16.2	0.70	stabilator
Bellanca Skyrocket	183	5.80	63,215	42.6	0.38	13.8	0.61	.36/.42
Grumman Tiger	140	4.44	NA	37.6	0.28	12.6	0.76	0.39
Rockwell Commander	152	4.58	63415	31.2	0.34	10.9	0.49	.33/.44
Trago Mills SAH-1	120	3.94	2413.6	22.0	0.46	17.8	0.83	0.46
Scottish Aviation Bullfinch	129	3.97	63,615	27.5	0.58	11.9	0.63	0.45

Figure 89 Single Engine Propeller Driven Airplanes: Horizontal Tail Volume Data

For the proposed aircraft the following values are selected: $\bar{V}_h = 0.61$ and $\frac{S_e}{S_h} = 0.45$.

The reason for selecting lower volume co-efficient is the lower wing loading of the proposed aircraft. After selecting all the values, the tail areas can be computed from equation (7.1) as follows:

$$S_h = \frac{\bar{V}_h S \bar{c}}{x_h} = 30.41 \text{ ft}^2$$

The planform geometry of horizontal tail includes the dihedral angle, incidence angle, aspect ratio, sweep angle, taper ratio and airfoil. For preliminary sizing, parameters are selected from following figure (91):

Type	Dihedral Angle, Γ_h deg.	Incidence Angle, i_h deg.	Aspect Ratio, A_h	Sweep Angle, $\Delta_{c/4h}$ deg.	Taper Ratio, λ_h
Single Engine Prop. Driven	0	-5 - 0 or variable	4.0 - 6.3	0 - 10	0.45 - 1.0

Figure 90 Planform Design Parameters for Horizontal Tail

The following choices are made:

1. Aspect ratio: 5.0
2. Span: 12.33 ft
3. Sweep angle: 0 deg.
4. Taper ratio: 0.50
5. Thickness ratio: 0.10
6. Airfoil: NACA 0012
7. Dihedral: 0 deg.
8. Incidence angle: Variable

Basically, the aircraft centre of gravity changes during the cruising flight, the airfoil must create a positive and sometimes a negative lift. This requirement necessitates the tail-plane to behave similar in both positive and negative angle of attack. Due to that, almost all horizontal airfoil are symmetric.

In addition, it is desired that the wing must stall before the tail and horizontal tail never stalls. Also, the tail incidence is determined to satisfy trim design requirement when no control surface is deflected. The tail aspect ratio has influences on the aircraft lateral stability and control, aircraft performance, tail aerodynamic efficiency, and aircraft centre of gravity. For, single engine propeller driven aircraft, it is desirable to have an aspect ratio such that the tail span is longer than the propeller diameter. The difference between tail taper ratio and wing taper ratio is that the elliptical lift distribution is not a requirement for tail. Therefore, the main motivation behind the tail taper ratio value is to lower the tail weight.

The horizontal tail sweep angle is often the same as wing sweep angle. In a similar way, the horizontal tail dihedral angle is often the same as wing sweep angle. The tail dihedral angle is different than the wing dihedral angle. There are reasons for such difference including a need for the aircraft lateral stability adjustment, a need for lateral control adjustment, and a need for a reduction in aircraft height and operational requirements.

7.3) DESIGN OF THE VERTICAL STABILIZER:

The design of vertical stabilizer means deciding on the magnitude of S_v (Vertical Stabilizer Area). The so-called \bar{V}_v -method is used to size the stabilizer. The tail volume co-efficient is calculated as follows:

$$\bar{V}_v = \frac{x_v S_v}{S b} \quad (7.2)$$

If the \bar{V}_v is too small, the aircraft will tend to oscillate or 'wallow' in yaw as the pilot gives rudder or aileron inputs. The following figure (92) represents the values of vertical tail volume co-efficients for proposed single engine propeller driven aircraft:

Type	Wing Area S ft ²	Wing Span b ft	Vert. Tail Area S _v ft ²	S _r /S _v	x _v ft	\bar{V}_v	Rudder Chord root/tip fr.c _v	S _a /S	Ail. Span Loc. in/out fr.b/2	Ail. Chord in/out fr.c _w
CESSNA Skywagon 207	174	35.8	16.0	0.44	18.0	0.046	.46/.46	0.10	.61/.94	.25/.22
Cardinal RG	174	35.5	17.4	0.37	13.5	0.038	.35/.43	0.11	.65/.97	.38/.37
Skylane RG	174	35.8	18.6	0.37	15.8	0.047	.41/.42	0.11	.47/.96	.17/.24
PIPER Cherokee Lance	175	32.8	13.8	0.31	15.3	0.037	.26/.50	0.064	.56/.88	0.20
Warrior	170	35.0	11.5	0.36	13.2	0.026	.29/.52	0.078	.48/.96	.27/.24
Turbo Saratoga SP	178	36.2	15.9	0.29	15.2	0.038	.23/.58	0.057	.52/.84	0.19
Bellanca Skyrocket	183	35.0	18.1	0.33	13.2	0.037	.28/.40	0.076	.60/1.0	.25/.22
Grumman Tiger	140	31.5	8.4	0.43	12.6	0.024	.36/.46	0.055	.56/.92	0.24
Rockwell Commander	152	32.8	17.0	0.28	11.4	0.039	.30/.46	0.072	.64/.97	.27/.36
Trigo Mills SAB-1	120	30.7	17.1	0.40	18.6	0.086	.35/.54	0.080	.58/.97	.25/.29
Scottish Aviation Bullfinch	129	33.8	22.7	0.39	11.9	0.062	.35/.56	0.073	.61/.95	.23/.30

Figure 91 Single Engine Propeller Driven Airplanes: Vertical Tail Volume Data

For the proposed aircraft the following values are selected: $\bar{V}_v = 0.047$ and $\frac{S_r}{S_v} = 0.37$.

The reason for selecting lower volume co-efficient is the lower wing loading of the proposed aircraft. After selecting all the values, the tail areas can be computed from equation (2) as follows:

$$S_v = \frac{\bar{V}_v S \bar{b}}{x_v} = 23.35 \text{ ft}^2$$

The planform geometry of vertical tail includes the dihedral angle, incidence angle, aspect ratio, sweep angle, taper ratio and airfoil. For preliminary sizing, parameters are selected from following figure (93):

Type	Dihedral Angle, Γ_v deg.	Incidence Angle, i_v deg.	Aspect Ratio, λ_v	Sweep Angle, $\Delta_c/4_v$ deg.	Taper Ratio, λ_v
Single Engine Prop. Driven	90	0	0.9 - 2.2	12 - 42	0.32 - 0.58

Figure 92 Planform Design Parameters for Vertical Tail

The following choices are made:

1. Aspect ratio: 1.6
2. Span: 6.11 ft
3. Sweep angle: 15 deg.
4. Taper ratio: 0.40
5. Airfoil: NACA 0012
6. Dihedral: 90 deg.
7. Incidence angle: 0 deg.

Basically, the vertical tail airfoil selection is responsible for the generation of the vertical tail lift co-efficient. To insure the symmetry of the aircraft about x-z plane, the vertical airfoil section must be symmetric.

The vertical tail incidence must be initially zero because to maintain the symmetry about x-z plane, the vertical tail is not required to produce any lift to maintain the directional trim in a normal flight condition. But, in a propeller driven aircraft the vertical tail is required to generate a lift and cancels the rolling moment (the aircraft is going to roll as a reaction to the rotation of the propeller and its shaft). Therefore, the vertical tail has about 1-2 degrees of incidence to insure the prevention of aircraft roll in a reaction to propeller revolution.

The horizontal tail location and efficiency are functions of vertical tail aspect ratio. The vertical tail aspect ratio must be large enough to keep the horizontal tail out of the wing wake when the wing stalls. The main purpose of vertical tail taper ratio is to reduce the bending stress on the vertical tail root and to allow the vertical tail to have a sweep angle.

The yawing moment arm is increased as the sweep angle of the vertical tail increased which improves the directional control of the aircraft. As the proposed aircraft has T-tail, an increase in vertical tail sweep angle increases the horizontal tail moment arm which improves the aircraft longitudinal stability and control. An aircraft with one vertical tail does not require any dihedral angle.

7.4) EMPENNAGE DESIGN EVALUATION:

The geometry created in AAA is shown in below figure (94). The output parameters are $\Lambda_{LE} = 3.8 \text{ deg.}$, $\Lambda_{TE} = -11.2 \text{ deg.}$, $Y_{mgc} = 2.74 \text{ ft}$, and $X_{mgc} = 0.18 \text{ ft}$, $\bar{C}_h = 2.55 \text{ ft}$.

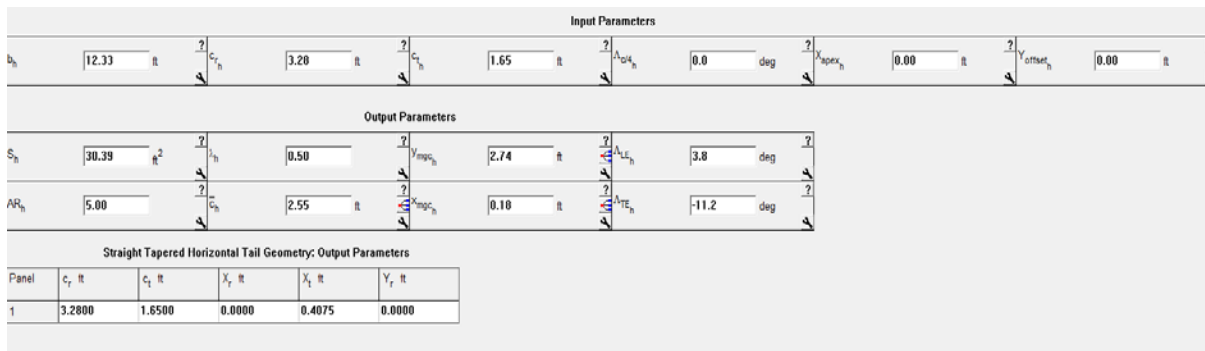


Figure 93 The AAA Input Parameters for Horizontal Tail: Proposed Aircraft

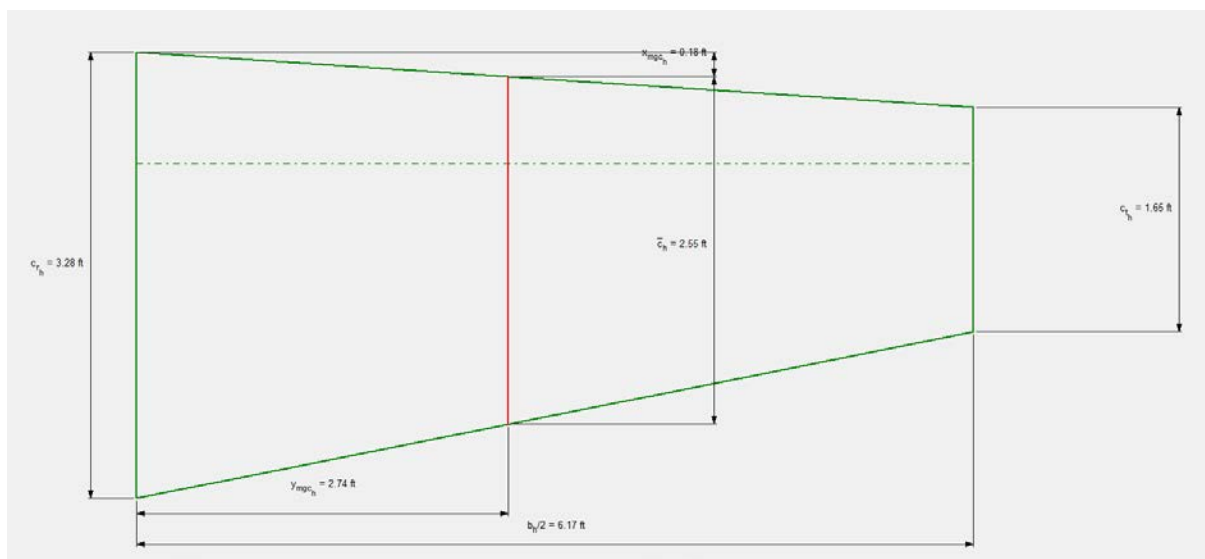


Figure 94 The Horizontal Tail: Proposed Aircraft

The geometry created in AAA is shown in below figure (96). The output parameters are $\Lambda_{LE} = 21.5 \text{ deg.}$, $\Lambda_{TE} = -7.6 \text{ deg.}$, $Z_{mgc} = 2.62 \text{ ft}$, and $X_{mgc} = 1.05 \text{ ft}$, $\bar{C}_h = 4.05 \text{ ft}$.

Input Parameters							
b_v	6.11 ft	c_{1v}	5.45 ft	c_{2v}	2.18 ft	Λ_{2E_v}	15.0 deg
x_{apex_v}	0.00 ft	z_{apex_v}	0.00 ft				
Output Parameters							
S_v	23.31 ft ²	λ_v	0.40	z_{mgc_v}	2.62 ft	Λ_{LE_v}	21.9 deg
AI_v	1.60	\bar{c}_v	4.05 ft	x_{mgc_v}	1.05 ft	Λ_{TC_v}	-7.6 deg
Straight Tapered Vertical Tail Geometry: Output Parameters							
Panel	c_r ft	c_1 ft	λ_1 ft	λ_2 ft	Z_r ft		
1	5.4500	2.1800	0.0000	2.4547	0.0000		

Figure 95 The AAA Input Parameters for Vertical Tail: Proposed Aircraft

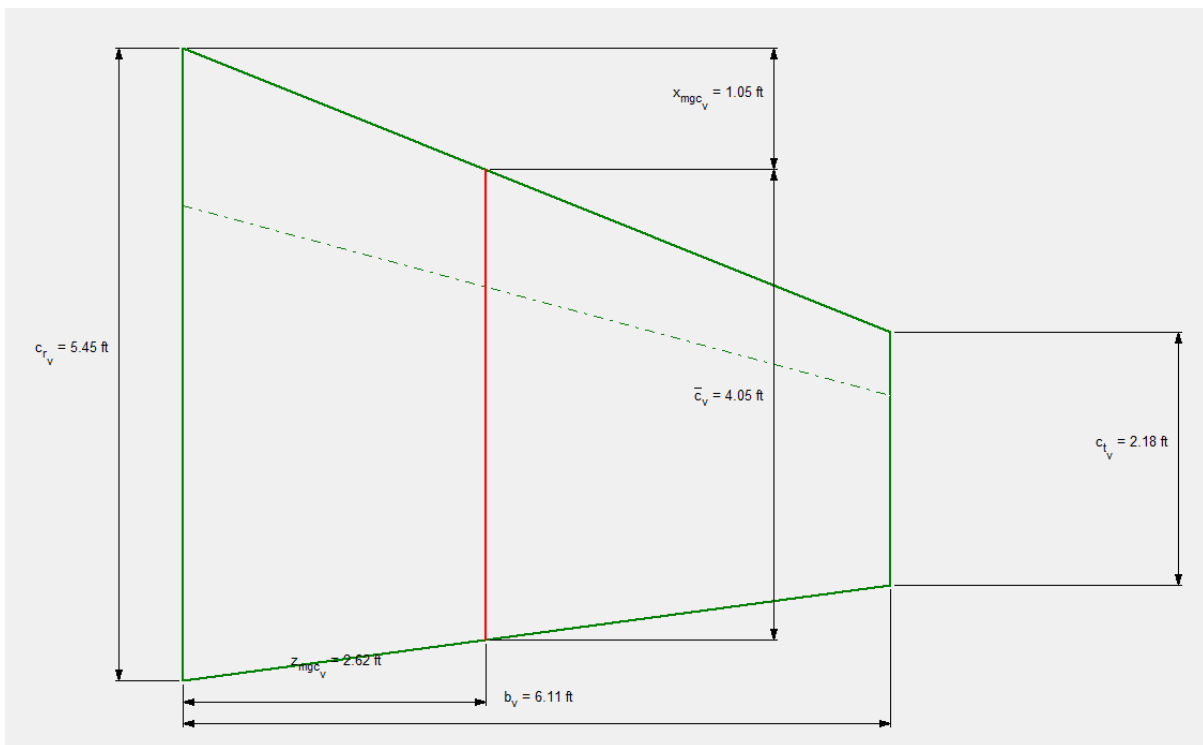


Figure 96 The Vertical Tail: Proposed Aircraft

For both horizontal and vertical tail, the airfoil chosen is NACA-0012 symmetric. The geometry is as follows:

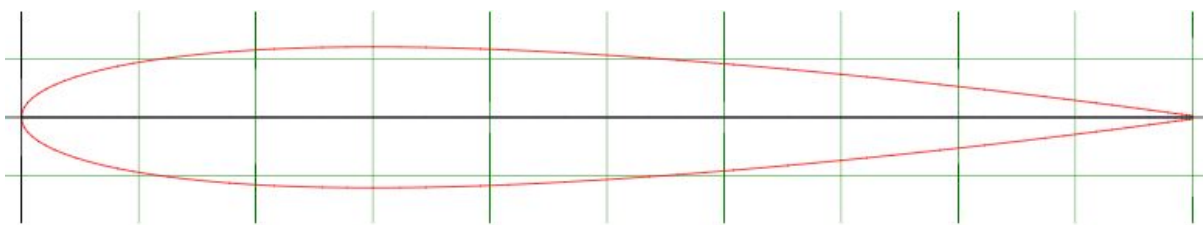


Figure 97 NACA-0012 Airfoil

The main performance parameter for an empennage is that its main wing should stall first before the horizontal tail. The stall angle of wing is around 18.5 degrees while the stall angle of attack for proposed horizontal tail airfoil is at about 19 degrees.

7.5) DESIGN OF THE LONGITUDINAL AND DIRECTIONAL CONTROLS:

The elevator is hinged to the back of the horizontal stabilizer and it is moveable. It controls the pitching moment (nose up and down movement) of the aircraft. The rudder is mounted on back of the vertical stabilizer which is also moveable and controls the yawing moment (nose left and right movement). The horizontal and vertical stabilizer areas are already calculated in section 7.3 & 7.4, respectively. The elevator and rudder areas can be found as follows:

$$\frac{S_e}{S_h} = 0.45 \quad \& \quad \frac{S_r}{S_v} = 0.37$$

Where, $S_h = \text{Horizontal stabilizer area} = 30.41 \text{ ft}^2$

$S_v = \text{Vertical stabilizer area} = 23.35 \text{ ft}^2$

So,

$$S_e = 13.68 \text{ ft}^2 \quad \& \quad S_r = 8.64 \text{ ft}^2.$$

The elevator and rudder outlines are drawn into the planforms of figure (100).

The design is also done in AAA. The elevator design is shown in below figure (100).

Input Parameters							
AR_h	5.00	γ_h	0.50	$(c_e/c_p)_h$	40.00 %	$(\eta_e/c)_e$	15.00 %
S_h	30.41 ft^2	$\Delta\alpha_h$	0.0	$(c_e/c_p)_v$	40.00 %	$(\eta_e/c)_e$	15.00 %
						η_{v_e}	90.00 %

Elevator Airfoils		
Panel	Root Airfoil	Tip Airfoil
1	naca0012.dat	naca0012.dat

Output Parameters							
c_{r_e}	1.25	c_{l_e}	0.19	c_{d_e}	1.06	c_{m_e}	34.00 %
c_{l_e}	0.72	c_{d_e}	0.11	S_e	9.73 ft^2	Balance c_e	0.18

Figure 98 The AAA Input Parameters for Elevator: Proposed Aircraft

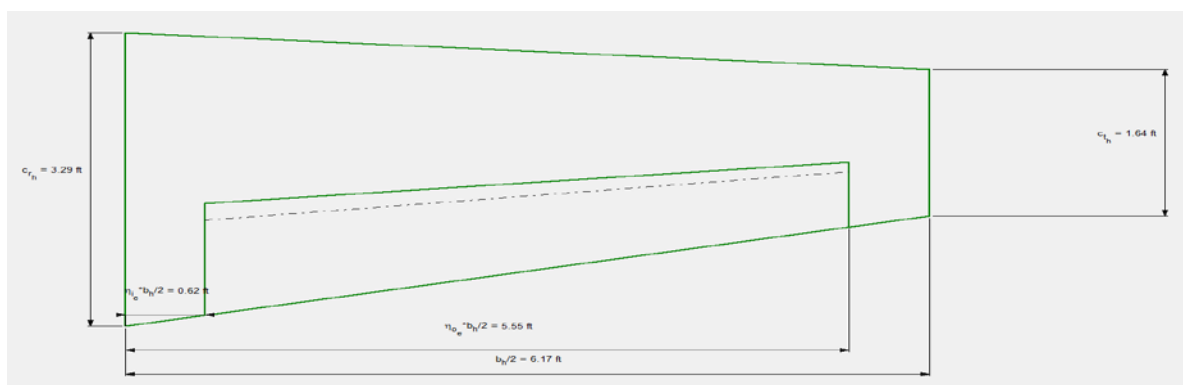


Figure 99 The Elevator Design: Proposed Aircraft

Input Parameters									
AR_v	1.60	λ_v	0.40	$(c_r/c_v)_i$	35.0 %	$(w/c)_r$	15.00 %	m_{c_r}	10.0 %
S_v	23.35 ft ²	Λ_{c_v}	15.0 deg	$(c_r/c_v)_o$	25.0 %	$(w/c)_{i,r}$	15.00 %	m_{c_r}	90.0 %

Rudder Airfoils		
Panel	Root Airfoil	Tip Airfoil
1	naca0012.dat	naca0012.dat

Output Parameters										
c_{r_r}	1.000 ft	c_{r_v}	0.27 ft	c_{r_t}	1.53 ft	c_r/c_v	27.5 %	C_r	1.31	Coordinates Undefined
c_{t_r}	0.63 ft	c_{b_r}	0.09 ft	c_{r_r}	0.53 ft	S_r	5.92 ft ²	Balance _r	0.18	

Figure 100 The AAA Input Parameters for Rudder: Proposed Aircraft

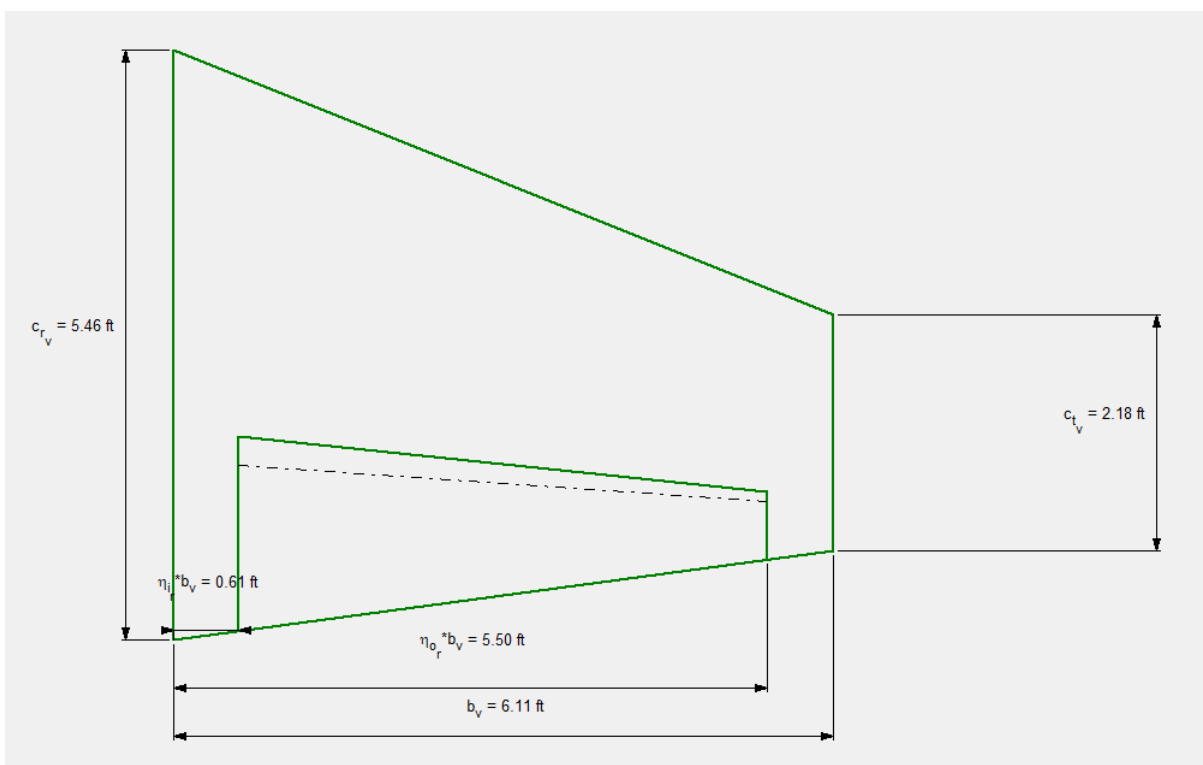


Figure 101 The Rudder Design: Proposed Aircraft

7.6) DRAWINGS:

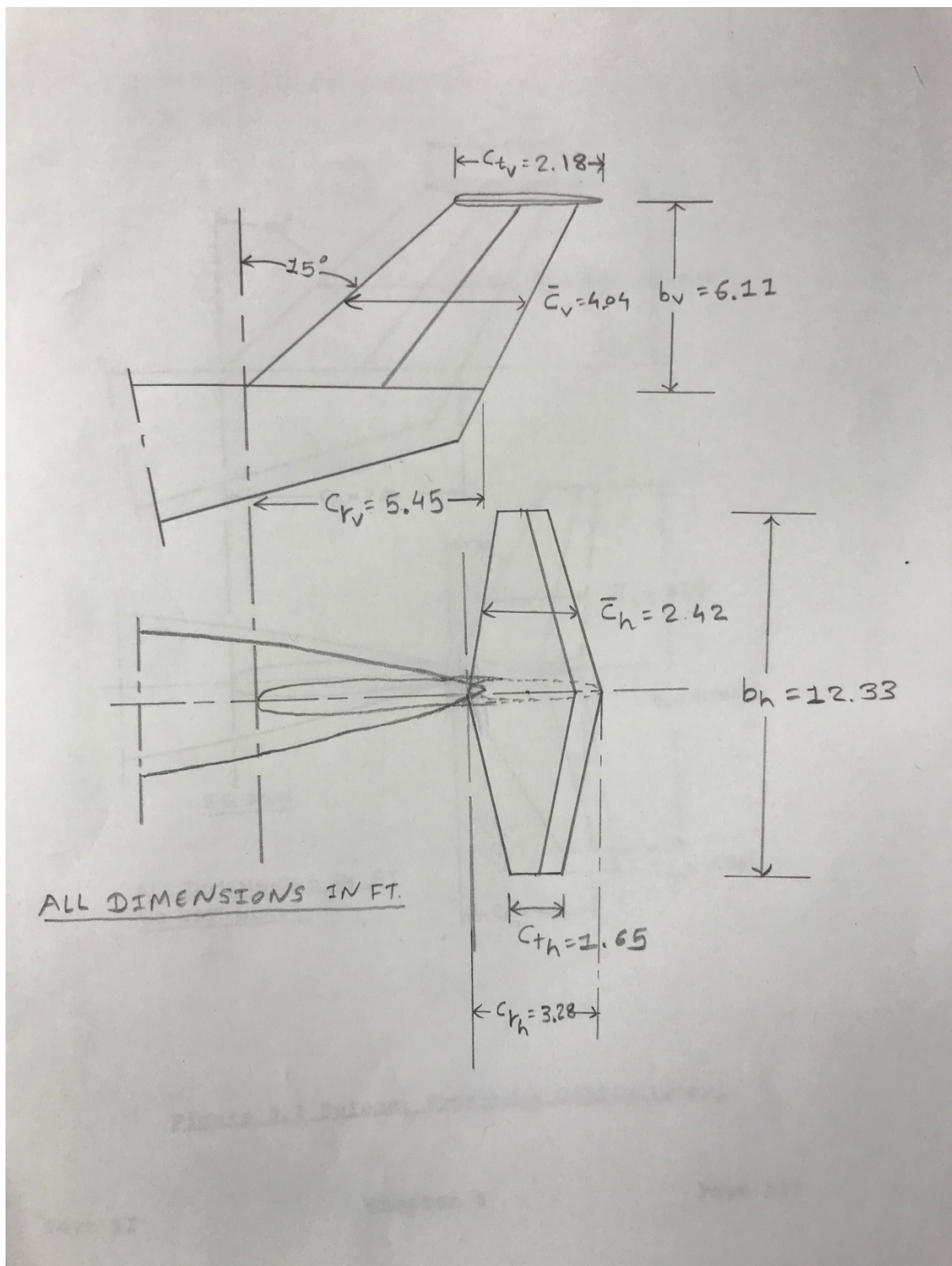


Figure 102 Empennage Configuration for Proposed Aircraft

7.7) DISCUSSION:

The T-tail configuration is chosen, and all the parameters are chosen based on gasoline aircraft data. The empennage design is done by comparing the data for similar types of aircraft provided in Roskam. The chosen control surface ratios are consistent with the ratios provided by Roskam. Thus, for proposed aircraft the ratios are $\frac{S_e}{S_h} = 0.45$ & $\frac{S_r}{S_v} = 0.37$. These values are quite reasonable. The AAA values are also like the manually calculated values.

The proposed aircraft empennage is modelled after guessing the volume co-efficient for horizontal and vertical stabilizer. The locations are decided by guessing the moment arms for both stabilizer. It will be iterated to determine the aerodynamic centre.

CHAPTER 8

LANDING GEAR DESIGN, WEIGHT AND BALANCE ANALYSIS

The preliminary aircraft sizing, wing and empennage configurations has already been obtained from previous reports. Almost all the key design parameters are locked at this stage. The next major component needs to be designed is landing gear. The landing gear supports an aircraft during taxi, take-off, and land. The following landing gear parameters are decided here:

1. Number, type and size of tires
2. Length and diameter of strut
3. Preliminary disposition

The landing gear has main gear and secondary gear. The closest gear to the aircraft cg is called as main gear. The landing gear preliminary parameters can be seen in following figure:

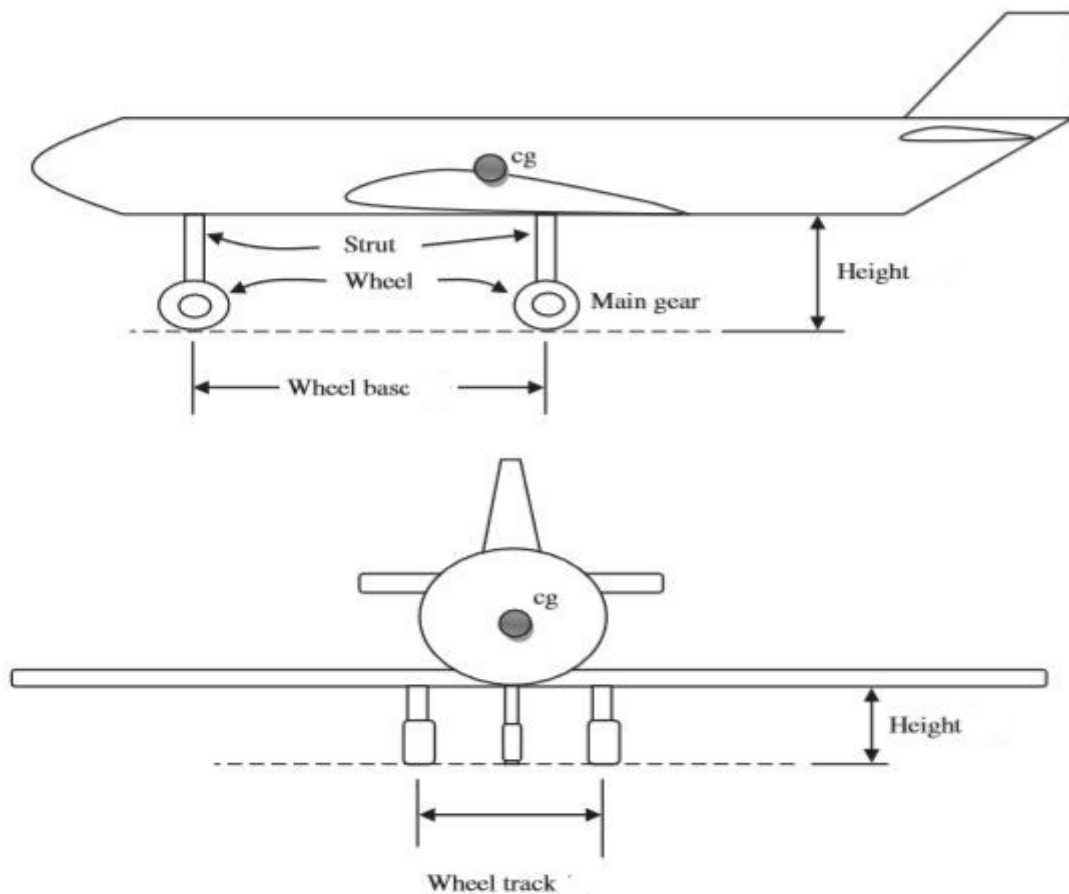


Figure 103 Landing Gear Parameters

As decided in performance sizing, the cruise speed of proposed electric aircraft is less than the 150 knots, so the retractable landing gear does not require. A fixed tricycle landing gear is selected for proposed electric aircraft. The reason behind selecting such kind of configuration is because it leads to fewer parts, less weight, low cost, design is easy, and more longitudinally stable.

8.1) ESTIMATION OF THE CENTRE OF GRAVITY LOCATION FOR THE AIRPLANE:

It is better to have rough idea about the centre of gravity of overall airplane before proceeding into the landing gear analysis. In this section, the centre of gravity locations for all major components are determined. At this stage, all the estimations are done just to get an idea about the landing gear disposition. A detailed analysis will be discussed in later sections to get somewhat accurate centre of gravity location.

The class I method for weight estimation is highly relies on the assumption that it is possible to express each component weight as a fraction of take-off (W_{TO}) or empty (W_E) or flight design gross weight (GW). For almost all the civil airplanes, take-off weight and flight design gross weight are same.

From preliminary sizing, all the weight values are known as:

$$W_{TO} = 3335 \text{ lbs}, W_E = 1715 \text{ lbs}, W_{PL} = 820 \text{ lbs}, W_{Battery} = 800 \text{ lbs}.$$

For reasons of brevity, only major component weights are considered. The following table lists the major weight fractions for similar airplanes.

Table 23 The Weight Fractions for Similar Airplanes

Type	Cessna 210A	Beech J-35	Rockwell 112TCA	Cessna 210J	Proposed Electric Plane
Wing Group/GW	0.090	0.131	0.113	0.099	0.090
Empennage Group/GW	0.024	0.020	0.033	0.025	0.020
Fuselage Group/GW	0.109	0.069	0.121	0.120	0.069
Landing Gear Group/GW	0.071	0.071	0.055	0.056	0.055
Fixed Equipment Weight/GW	0.094	0.115	0.151	0.099	0.094
Power Plant/GW	0.199	0.201	0.189	0.171	0.171
Empty Weight/GW	0.598	0.628	0.705	0.578	0.578

Using these average weight fractions from table (24), the component weight summary can be determined as follows:

Table 24 The Major Component Weight Summary for Proposed Electric Aircraft

Component	First weight estimate (lbs)	Adjustment	Class I weight (alum.) (lbs)	Class I weight (compos.) (lbs)
Wing	300	-70	230	196
Empennage	67	103	170	145
Fuselage	230	170	400	340
Landing Gear	183	57	240	240
Power Plant	570	-320	250	250
Fixed Eqp.	313	112	425	425
Empty Weight	1664	51	1715	1596
Payload			820	820
Battery			800	800
Take-off Gross Weight			3335	3216

The difference in empty weight is due to round-off errors in the weight fractions used and the major saving factor for proposed electric aircraft is engine weight. All traditional gasoline powered aircraft has almost 3 times more engine weight than the proposed electric aircraft. An assumption of 15 percent weight reduction is applied to wing, empennage, and fuselage for using the composites as the primary structural materials.

The first step in class I weight and balance analysis is the breakdown of weights calculated in class I weight data. The typical class I weight breakdown data are as follows:

Table 25 Component Weight Breakdown and Coordinate Data: Proposed Aircraft

Component	Weight (lbs)	X (in.)	WX (lbs) (in.)	Y (in.)	WY (lbs) (in.)
Wing	230	128	29,440	0	0
Empennage: V.T.	60	266	15,960	0	0
Empennage: H.T.	110	279	30,690	0	0
Fuselage	400	122	48,800	0	0
Landing Gear: Nose	48	54	2,592	0	0
Landing Gear: Main	192	132	25,344	0	0
Fixed Equipment	425	122	51,850	0	0
Power Plant	250	24	6,000	0	0
Batteries: Fuselage- Baggage	300	150	45,000	0	0
Batteries: Fuselage	500	123	61,500	0	0
Passenger: Front Row	350	102	35,700	0	0

Passenger: Rear Row	350	149	52,150	0	0
Luggage	120	170	20,400	0	0

The following figure (105) shows the approximately cg locations for major components. The following figure (106) shows the preliminary arrangement for all components with their centres of gravity. Also, table (26) provides some guidance for locating component cg's of major weight group. It is also lists the x and y coordinates of all weight components.

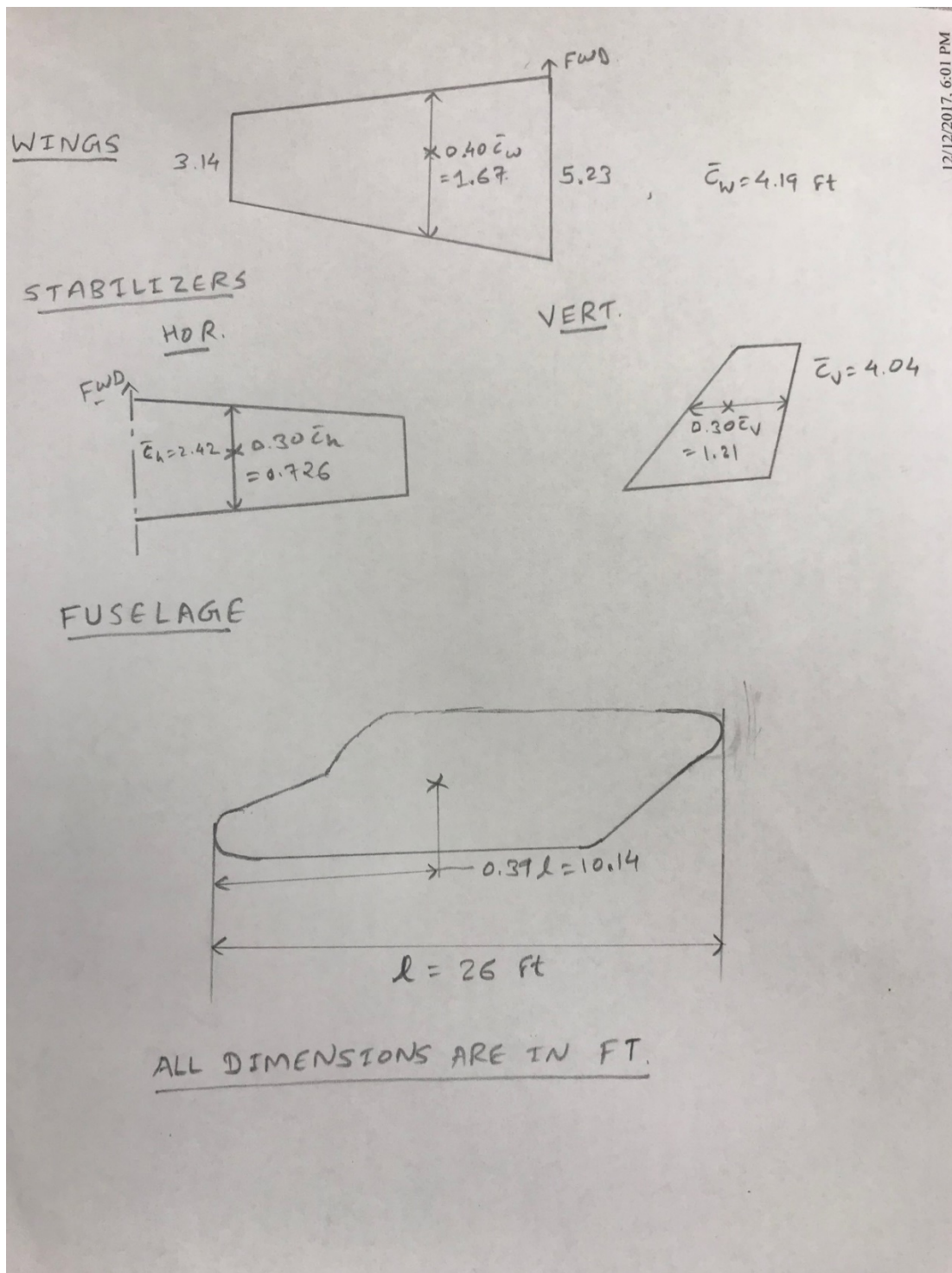


Figure 104 The C.G. Location for Major Component

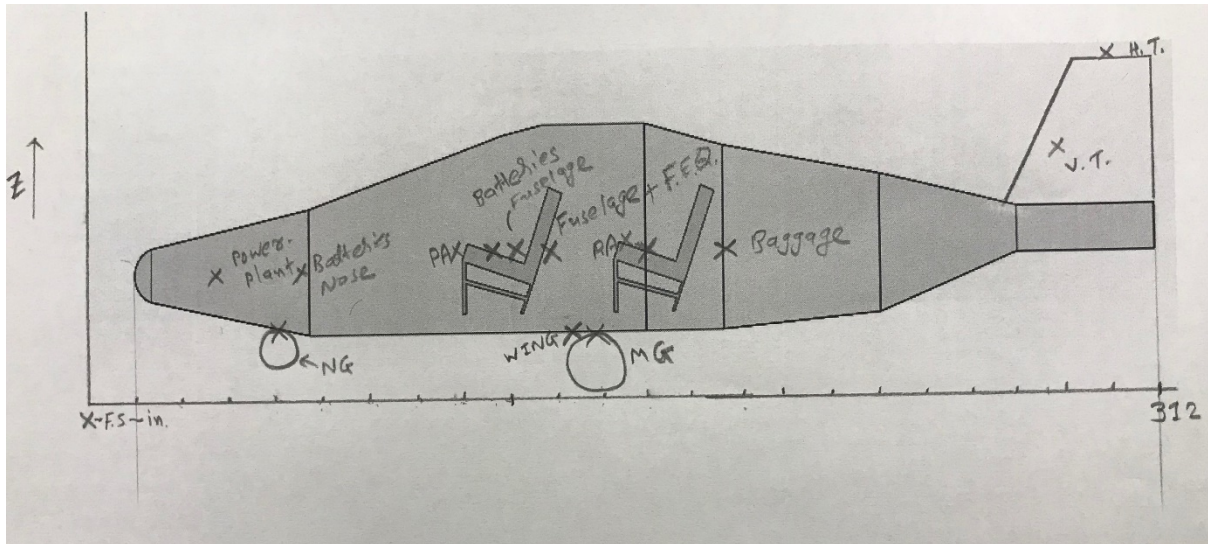


Figure 105 General Arrangement for Proposed Aircraft

From all the calculated weight and c.g. locations, the weight-c.g. excursion diagram can be drawn as follows:

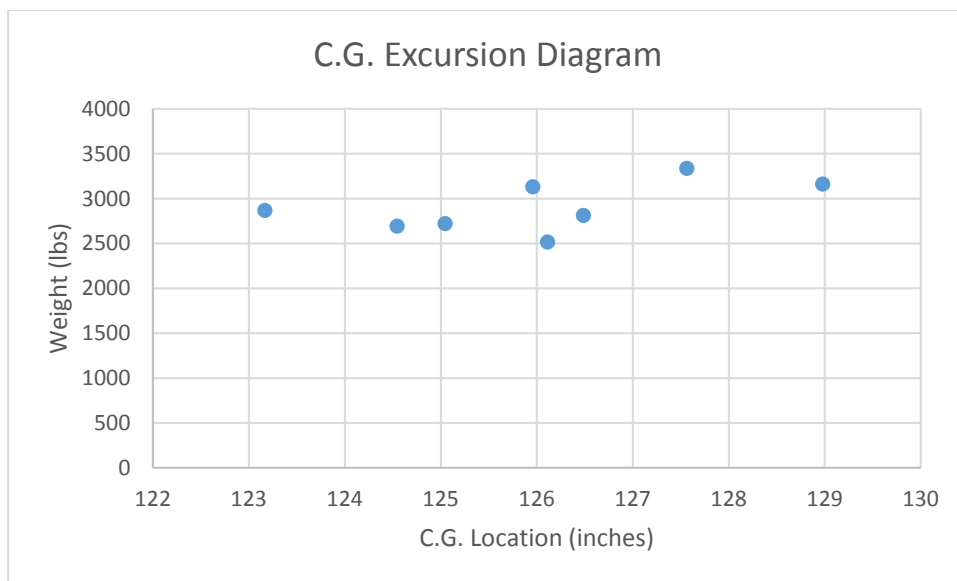


Figure 106 Proposed Aircraft: Weight-C.G. Excursion Diagram

From above figure (107), it follows that the c.g. limits are:

Most forward c.g. occurs at $W = 2865$ lbs, F.S. = 123.16 in.

Most aft c.g. occurs at $W = 3160$ lbs, F.S. = 128.97 in.

The c.g. range of the proposed electric plane is 6 inches.

8.2) LANDING GEAR DESIGN:

Since proposed electric airplane is single propeller driven general aviation aircraft; the landing gear is chosen as fixed tricycle configuration. The main wheels are placed usually aft of the cg and carry much of the aircraft weight and load. Two main wheels are placed at the same distance from the c.g. in the x and y axis. The nose gear is placed far from the c.g.; hence it carries a small load. The height for both wheels are same because the aircraft should be level on the ground, but the main gears often have larger wheels.

This nose gear configuration is directionally stable on ground and during taxiing. Also, the pilot view is much better compare to tail gear. After calculating the weight and balance data, the next step is associated with the landing gear strut disposition. There are two geometric criteria which needs to be considered in deciding the strut disposition:

- Tip-over Criteria: For tricycle landing gears, the main landing gear must be behind the aft cg and it is located at an angle of 15 deg. (longitudinal tip-over criteria). The longitudinal and lateral tip-over criteria is shown in following figure (108).

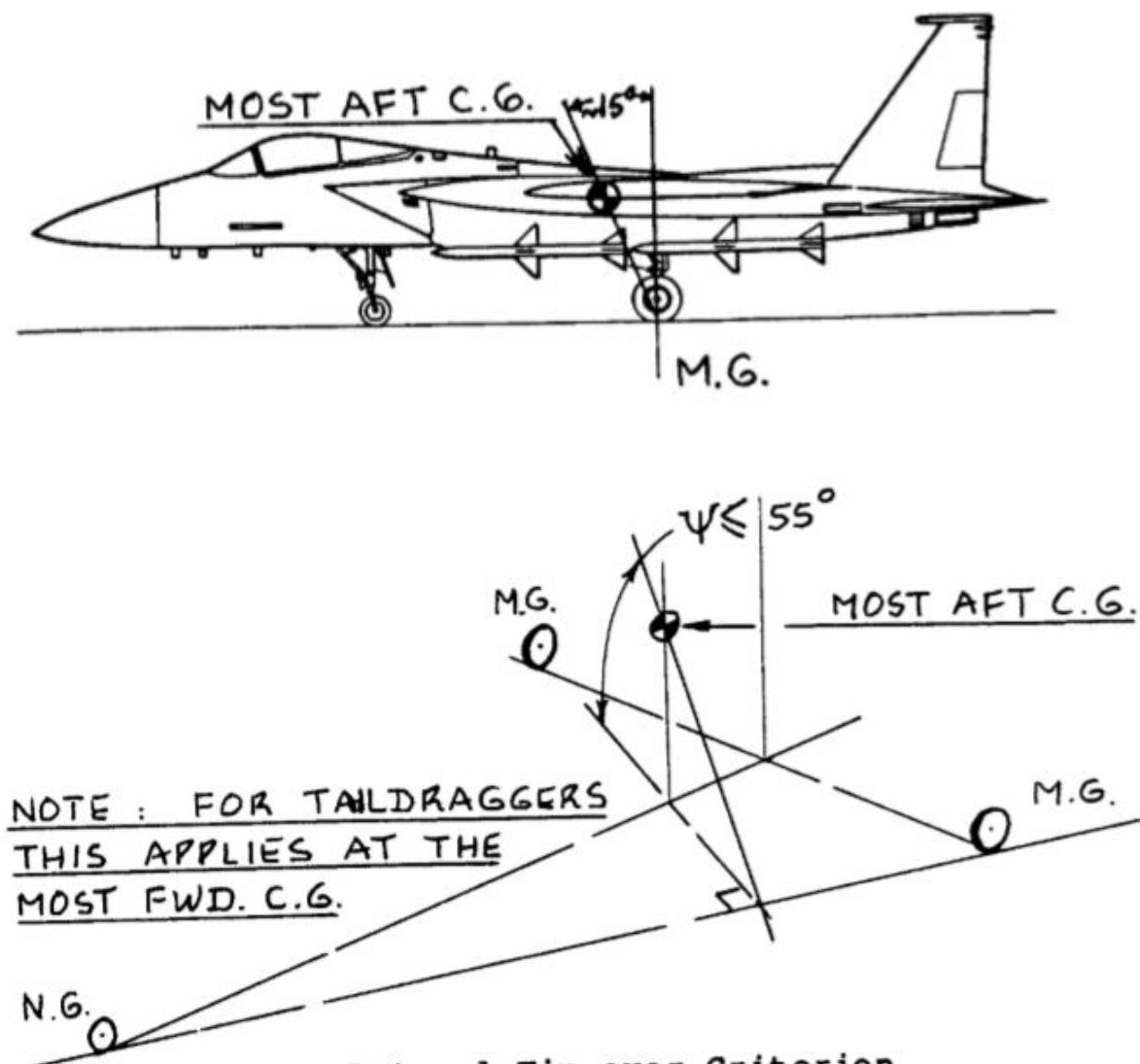


Figure 107 Tip-over Criteria for Landing Gear Placement

- Ground Clearance Criteria: Both lateral and longitudinal ground clearance angle applies to tricycle gear configuration. It is shown in following figure (109).

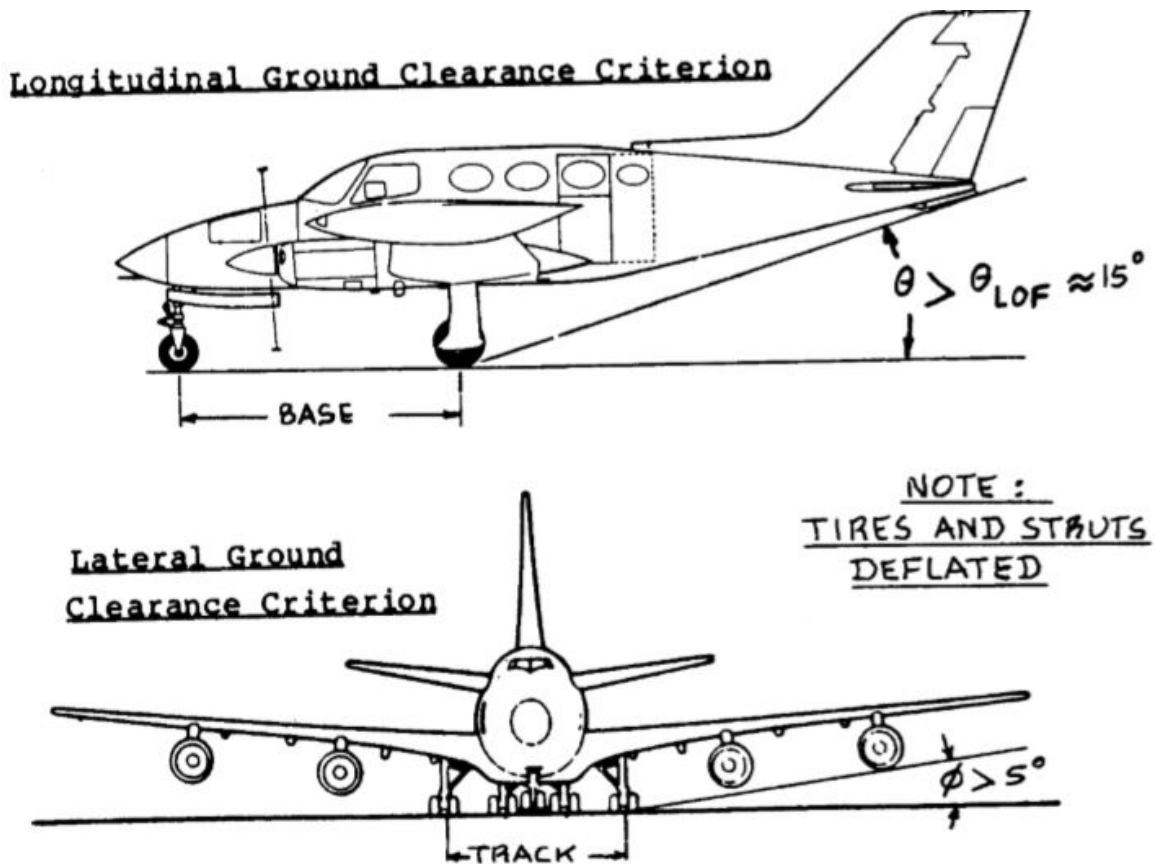


Figure 108 Ground Clearance Criteria for Gear Placement

By considering all the above-mentioned factors the strut disposition is shown in following figure (110):

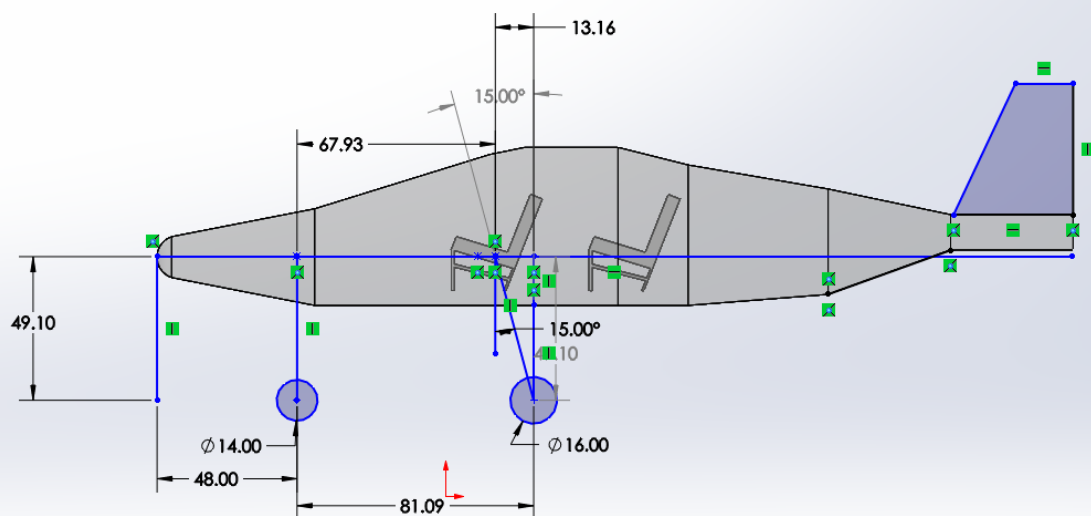


Figure 109 Proposed Aircraft: Landing Gear Arrangement

From the strut disposition, the maximum static load per strut can be found as follows:

$$\text{Nose wheel strut: } P_n = \frac{W_{TO} * l_m}{l_m + l_n} = 551.51 \text{ lbs}$$

$$\text{Main gear strut: } P_m = \frac{W_{TO} * l_n}{\text{number of strut} * (l_m + l_n)} = 1391.743 \text{ lbs}$$

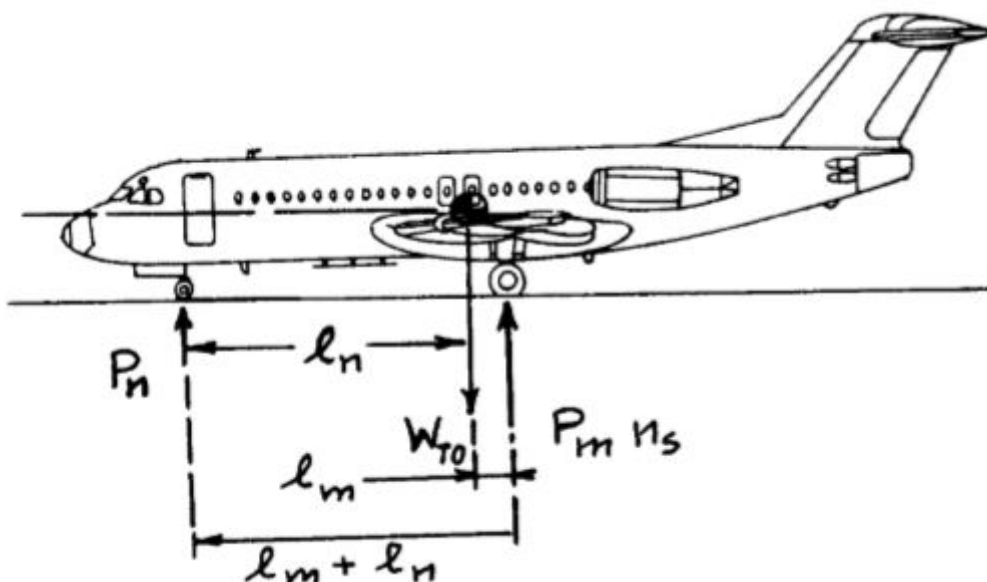


Figure 110 Geometry for Static Load Calculation

Now, the gear load ratios are found: $\frac{P_n}{W_{TO}} = 0.17$, $\frac{P_m}{W_{TO}} = 0.83$.

For airplanes in this category, it is quite reasonable to assume that one nose wheel tire and one main gear tire per strut are acceptable choices. The following tire sizes are acceptable choices:

Nosewheel tire: $D_t \times b_t = 14 \times 5$ with 22 psi.

Main gear tire: $D_t \times b_t = 16 \times 6$ with 19 psi.

The tires are drawn into the above figure (110).

8.3) WEIGHT AND BALANCE ANALYSIS:

For the weight and balance analysis, the landing gear position is known. The following table shows the new moment arm data for landing gear.

Table 26 Revised Moment Arm: Proposed Aircraft

Component	Weight (lbs)	X (in.)	WX (lbs) (in.)	Y (in.)	WY (lbs) (in.)
Wing	230	128	29,440	0	0
Empennage: V.T.	60	266	15,960	0	0

Empennage: H.T.	110	279	30,690	0	0
Fuselage	400	122	48,800	0	0
Landing Gear: Nose	48	48	2,304	0	0
Landing Gear: Main	192	129	24,768	0	0
Fixed Equipment	425	122	51,850	0	0
Power Plant	250	24	6,000	0	0
Batteries: Fuselage Baggage	300	150	45,000	0	0
Batteries: Fuselage	500	123	61,500	0	0
Passenger: Front Row	350	102	35,700	0	0
Passenger: Rear Row	350	149	52,150	0	0
Luggage	120	170	20,400	0	0

The new cg location is calculated for some configuration which is as follows:

Table 27 New C.G. Location for Different Configuration: Proposed Aircraft

Weight (lbs)	C.G. (inches)	Configuration
3335	127.30	4 people, 4 bags
2515	125.77	0 people, 0 bags
2690	124.38	1 in front, 0 bags
2720	124.88	1 in front, 1 bag
2865	123.01	2 in front, 0 bags
3160	128.84	1 in front, 2 in back, 4 bags
3130	125.81	2 in front, 1 in back, 3 bags
2810	126.32	1 in front, 4 bags

From all the calculated weight and c.g. locations, the weight-c.g. excursion diagram can be drawn as follows:

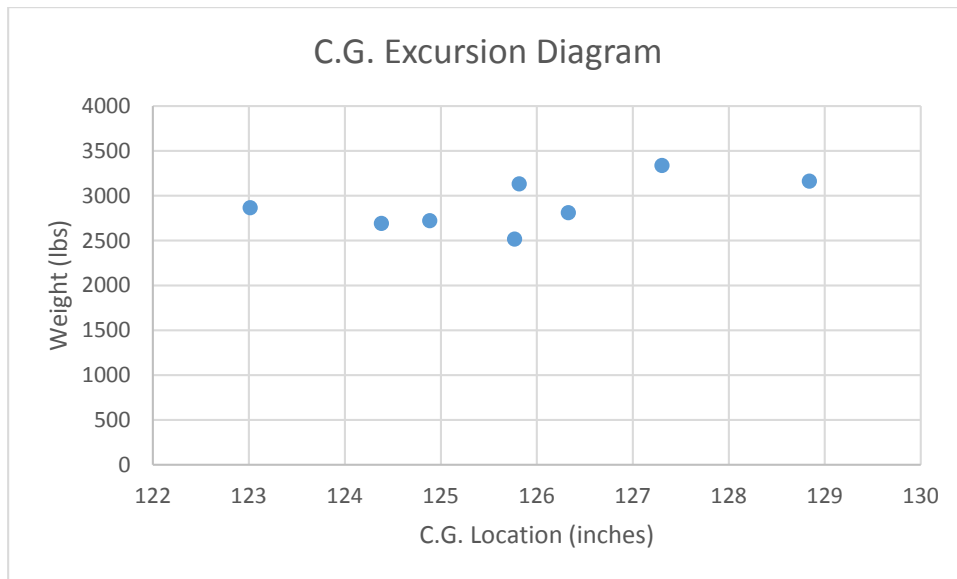


Figure 111 Proposed Aircraft: Weight-C.G. Excursion Diagram

From above figure (112), it follows that the c.g. limits are:

Most forward c.g. occurs at $W = 2865$ lbs, F.S. = 123.01 in.

Most aft c.g. occurs at $W = 3160$ lbs, F.S. = 128.84 in.

The c.g. range of the proposed electric plane is 6 inches.

8.4) DISCUSSION:

The initial component breakdown has been using similar types of aircraft component weights given by Roskam. The initial C.G. and placement of landing gear are determined by assuming the landing gear moment arms. Based on the most aft C.G. location, the actual placement of landing gear has been done by satisfying tip over criterion and ground clearance criterion. Also, one of the major factor which needs to be considered for propeller driven airplanes is the clearance between propeller tip and ground.

The C.G. location determined in above section might change afterwards. The C.G. determination is an iterative process as it is changes with change in the size of horizontal tail. The stability and control analysis will give the final location of C.G., the empennage location and size as well as the landing gear location.

CHAPTER 9

STABILITY AND CONTROL ANALYSIS / WEIGHT AND BALANCE- STABILITY AND CONTROL CHECK

In this design report, class I stability and control analysis will be done by following steps provide by Roskam in Airplane Design Part II. This will allow to calculate the characteristics like static longitudinal stability and static directional stability. There are two types of stability: static and dynamic. The static stability deals with the initial tendency of vehicle to return to equilibrium after being disturbed while the dynamic stability deals with the time history of the vehicle's motion after it initially responds to its static stability (John D. Anderson, Jr., Introduction to Flight, 1978).

The dynamically stable aircraft must always be statically stable. On contrary, static stability is not sufficient to ensure dynamic stability. An aircraft control means the study of deflections of the ailerons, elevators, and rudder necessary to make the airplane do what we want and of the amount of force that must be exerted by the pilot to deflect these controls.

Also, the x-plots for longitudinal and directional stability will be determined to check for any change in tail areas. This will be done by using a factor called static margin. An iteration might need to re-size the empennage and landing gear.

9.1) STATIC LONGITUDINAL STABILITY:

The static longitudinal stability is calculated by plotting the aerodynamic centre and centre of gravity change as function of horizontal tail area. The aircraft aerodynamic centre can be found from following equation:

$$\bar{x}_{ac_A} = \frac{\bar{x}_{ac_{wf}} + \frac{C_{L_{ah}} \left(1 - \frac{\partial \epsilon_h}{\partial \alpha}\right) \left(\frac{S_h}{S}\right) \bar{x}_{ac_h}}{C_{L_{awf}}}}{F}$$

Where,

$$F = 1 + \frac{C_{L_{ah}} \left(1 - \frac{\partial \epsilon_h}{\partial \alpha}\right) \left(\frac{S_h}{S}\right)}{C_{L_{awf}}}$$

The calculated values for above equation are as follows: $x_{ac_{wf}} = 1.28 \text{ ft}$, $C_{L_{ah}} = 4.311$, $\left(1 - \frac{\partial \epsilon_h}{\partial \alpha}\right) = 0.66$, $x_{ac_h} = 14.48 \text{ ft}$, $C_{L_{awf}} = 5.25$.

The following graph shows the longitudinal x-plot. The centre of gravity movement is very slow compared to aerodynamic centre movement. For the proposed aircraft, the longitudinal x-plot is stable, and it follows that the horizontal area needs to be increased for 10% static margin. The new horizontal tail area for proposed aircraft is 38.70 ft².

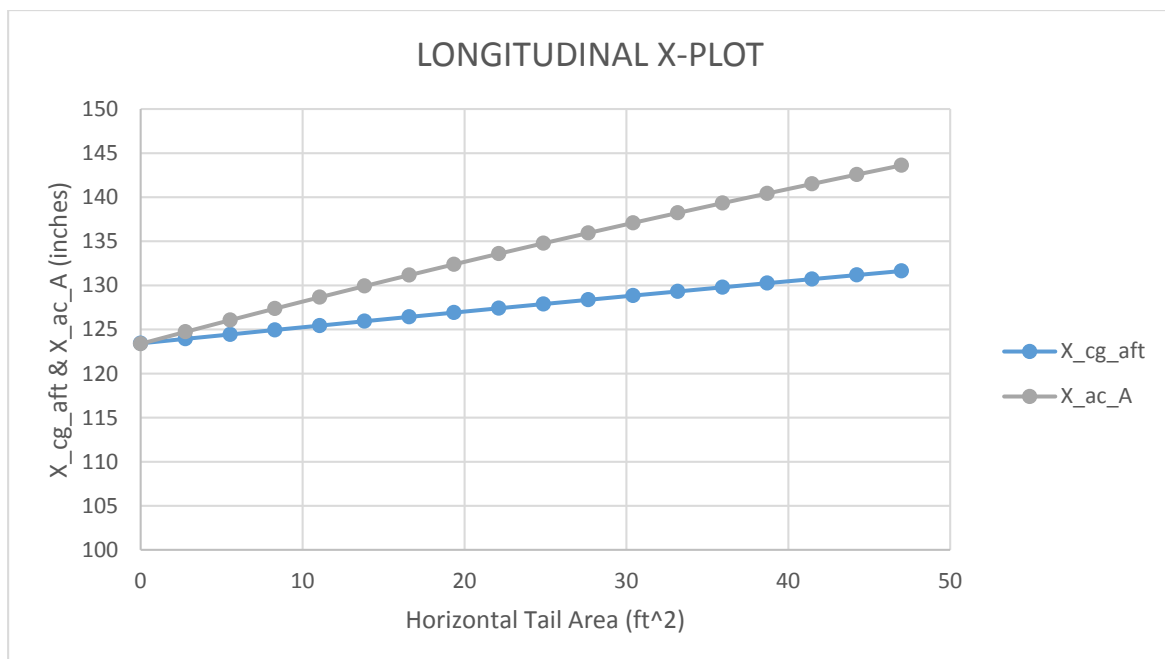


Figure 112 The Longitudinal X-Plot: Proposed Aircraft

9.2) STATIC DIRECTIONAL STABILITY:

The static directional plot is analysed in this section. The following equation shows the relationship between the vertical tail area and side slip moment co-efficient. This equation is used to plot the x-plot.

$$C_{n_\beta} = C_{n_{\beta wf}} + C_{L_{av}} \left(\frac{S_v}{S} \right) \left(\frac{x_v}{b} \right)$$

Where,

$$C_{n_{\beta wf}} = -57.3K_N \left(\frac{S_{fs} l_f}{Sb} \right)$$

The directional x-plot is shown below:

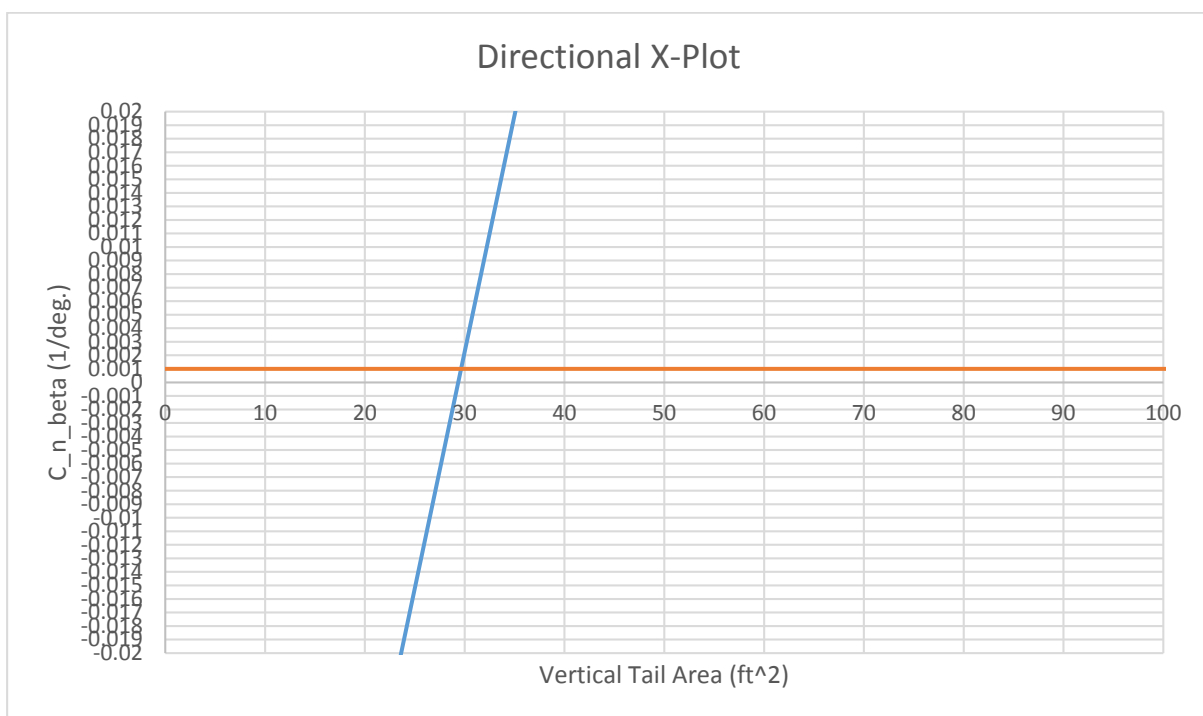


Figure 113 The Directional X-Plot: Proposed Aircraft

The desired value for $C_{n_\beta} = 0.0010$. From the plot, the $C_{n_\beta} = -0.004$ and the difference is around 0.005. Thus, the airplane needs to have de facto directional stability. The required sideslip to rudder feedback gain can be calculated from below equation:

$$k_\beta = \frac{\Delta C_{n_\beta}}{C_{n_{\delta_r}}} \quad \& \quad \Delta C_{n_\beta} = 0.0010 - C_{n_\beta}$$

Thus, $k_\beta = 0.01 \text{ deg}$. And this yields for the rudder deflection angle. This is well within the allowable value of 5 deg. Thus, the vertical tail area resulting in the lowest value of C_{n_β} which is consistent and the smallest possible vertical tail area. This new vertical tail area is 30 ft².

The proposed aircraft is single engine propeller driven aircraft. Thus, the one engine inoperative requirement does not apply.

9.3) EMPENNAGE DESIGN-WEIGHT AND BALANCE-LANDING GEAR DESIGN-LONGITUDINAL STATIC STABILITY AND CONTROL CHECK:

The horizontal stabilizer area does not meet the 10% static margin difference, so the horizontal stabilizer does need to be resized. To get 10% static margin the new horizontal area is 38.70 ft². Also, the vertical stabilizer needs to change to provide required side slip moment co-efficient. The new area required for vertical stabilizer is 30 ft².

9.4) DISCUSSION:

The stability and control analysis done in this report is only class I analysis. The sizing of the proposed aircraft needs to be re-iterate. The current aircraft does show longitudinal stability as well as directionally stable. The static margin requirement does not meet for proposed aircraft. The components need to be rearranged according to the required C.G. travel so that static margin of 10% is achieved for longitudinal stability. This would affect the C.G. location and hence the control derivatives for directional x-plot too. After arranging the component, the new x-plot is developed. The new required horizontal tail area is increased from 30 ft² to 38.70 ft². The directional stability provided here is with current C.G. of the aircraft. The iteration for proposed aircraft will be explored further in class II sizing.

CHAPTER 10

DRAG POLAR ESTIMATION

In the previous chapters, the design analysis of wing, empennage, and landing gear have been detailed. The aircraft design is almost locked in the previous reports. The drag is a crucial factor in improving the aerodynamics of the aircraft. The drag is calculated in terms of the wetted area of all aircraft components. The drag due to different aircraft components will be calculated and documented in this design report.

10.1) AIRPLANE ZERO-LIFT DRAG:

The airplane zero lift drag is calculated from total wetted area of an airplane. The 3D view of an aircraft is necessary to calculate the wetted area. The wetted area of an airplane is the integral of airplane perimeter versus distance from nose to tail. The major components which contributed to the wetted area are as follows:

- Wing
- Vertical Tail
- Horizontal Tail
- Fuselage

The wetted area for above mentioned components can be calculated as follows:

a) Wetted Area for Wing Planform:

For straight tapered wing the wetted area is found from:

$$S_{wet_W} = 2 * S_{exp.W} * \left\{ 1 + 0.25 * \left(\frac{t}{c} \right)_r * \frac{1 + \tau\lambda}{1 + \lambda} \right\} \quad (10.1)$$

$$\text{Where, } \tau = \frac{\left(\frac{t}{c} \right)_r}{\left(\frac{t}{c} \right)_t} = \frac{0.14}{0.12} = 1.16 \text{ and } \lambda = \frac{C_t}{C_r} = 0.60.$$

$$S_{wet_W} = 364.06 \text{ ft}^2$$

b) Wetted Area for Vertical Tail:

From above equation (10.1),

$$S_{wet_{V.T.}} = 61.80 \text{ ft}^2$$

c) Wetted Area for Horizontal Tail:

From above equation (10.1),

$$S_{wet_{H.T.}} = 79.72 \text{ ft}^2$$

d) Wetted Area for Fuselage:

For Fuselage with cylindrical mid-sections:

$$S_{wet_{fus}} = \pi D_f l_f \left(1 - \frac{2}{\lambda_f} \right)^{\frac{2}{3}} \left(1 + \frac{1}{\lambda_f^2} \right) \quad (10.2)$$

$$S_{wetFuselage} = 553.51 \text{ ft}^2$$

The total wetted area for proposed aircraft is 1059.13 ft^2 . The approximately calculated wetted area was 900 ft^2 . The wing and empennage usually intersect a fuselage, so it is necessary to subtract the areas of intersection from the wetted area of a fuselage. But still the difference is not within 10 percent. However, since it is a significant increase, the impact of any change in cruise L/D needs to be evaluated.

From the below figure (115), it is seen that for a single propeller aircraft a value of $C_f = 0.0060$ is attainable.

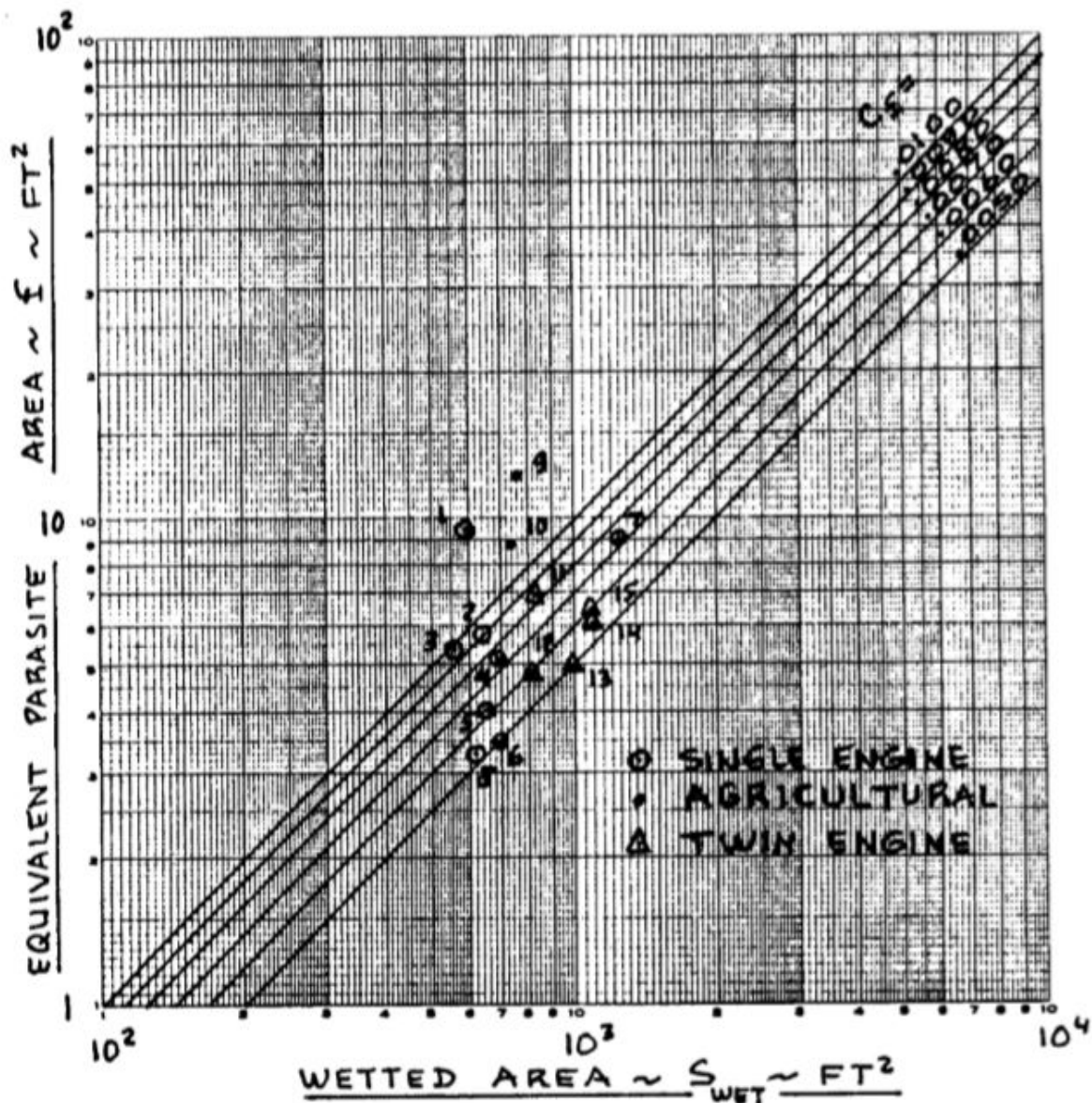


Figure 114 The Equivalent C_f Value

With the wetted area of 1000 ft^2 this implies a value of $f = 8 \text{ ft}^2$. The zero lift drag coefficient for proposed electric aircraft at low subsonic speed now calculated from $C_{D_0} =$

$$\frac{8}{175.52} = 0.045.$$

10.2) LOW SPEED DRAG INCREMENTS:

10.2.1) Flap Drag Increment for Take-off and Landing:

The flap drag increment are as follows:

Table 28 Flap Drag Increment

Configuration	ΔC_{D_0}	Aspect Ratio	e
Take-off flaps	0.010	10	0.80
Landing flaps	0.055	10	0.75

10.2.2) Landing Gear Drag Increment for Take-off and Landing:

The landing gear drag increment is as follows:

Table 29 Landing Gear Drag Increment

Configuration	ΔC_{D_0}	Aspect Ratio	e
Landing Gear	0.015	10	No effect

10.3) COMPRESSIBILITY DRAG:

The compressibility drag effects are negligible when the aircraft travels at very low subsonic speed. The proposed aircraft cruises at Mach 0.22, so the compressibility effect is neglected here. It can also be seen in following figure (116).

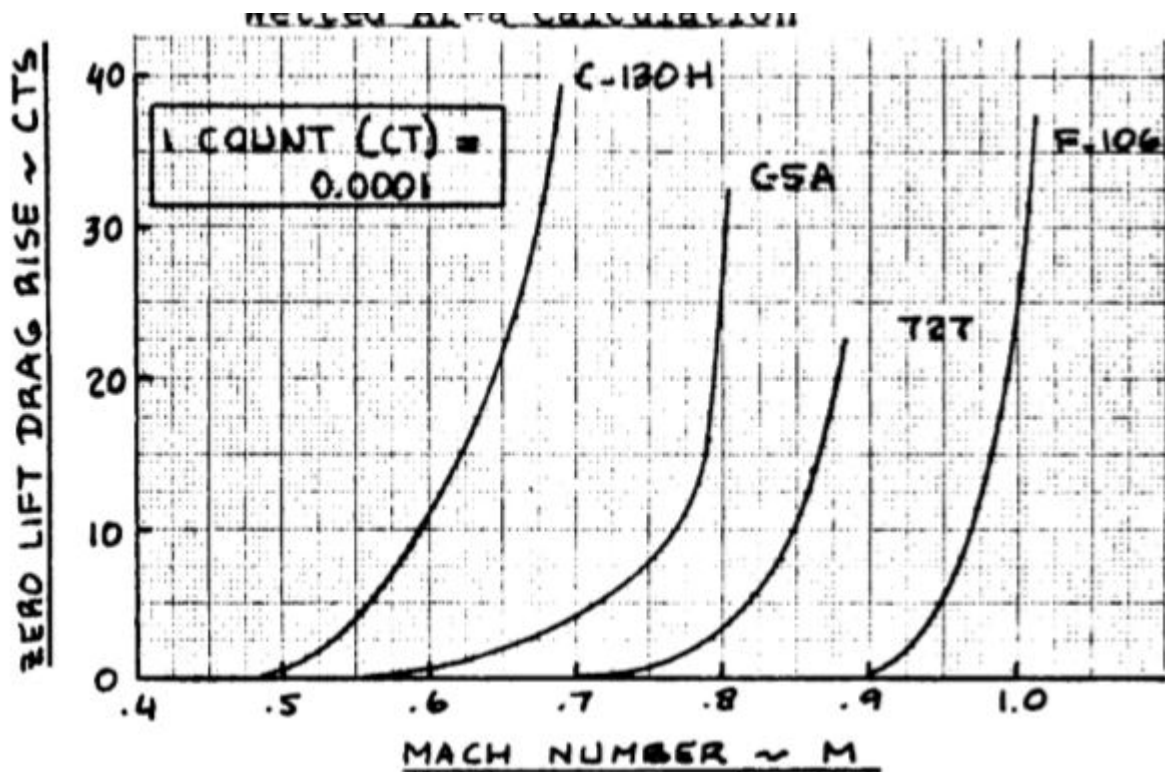


Figure 115 Compressibility Drag Behaviour

10.4) AIRPLANE DRAG POLARS:

The following data are obtained:

Table 30 Zero Lift Drag Coefficient: Proposed Airplane

W_{TO}	$(W/S)_{TO}$	S	S_{wet}	f	C_{D_0}
3335 lbs	19	175.52	1000	8	0.045

From above data, the drag polars are calculated as follows:

Table 31 Drag Polars: Proposed Aircraft

Configuration	Aspect Ratio	e	Drag Polar
Clean	10	0.80	$C_D = 0.045 + 0.0398C_L^2$
Take-off, flaps	10	0.80	$C_D = 0.055 + 0.0398C_L^2$
Landing, flaps	10	0.75	$C_D = 0.100 + 0.0424C_L^2$
Landing gear	10	No effect	$C_D = 0.060 + 0.0398C_L^2$

The new L/D values are:

Table 32 The New L/D Values: Proposed Aircraft

Configuration	L/D
Clean	11
Take-off, flaps with landing gear	8
Landing, flaps with landing gear	7

The L/D is decreased from 12 to 11. Thus, from the sensitivity study it is concluded that the range will be decreased by 22 nautical miles. The AAA calculated drag polars are as follows:

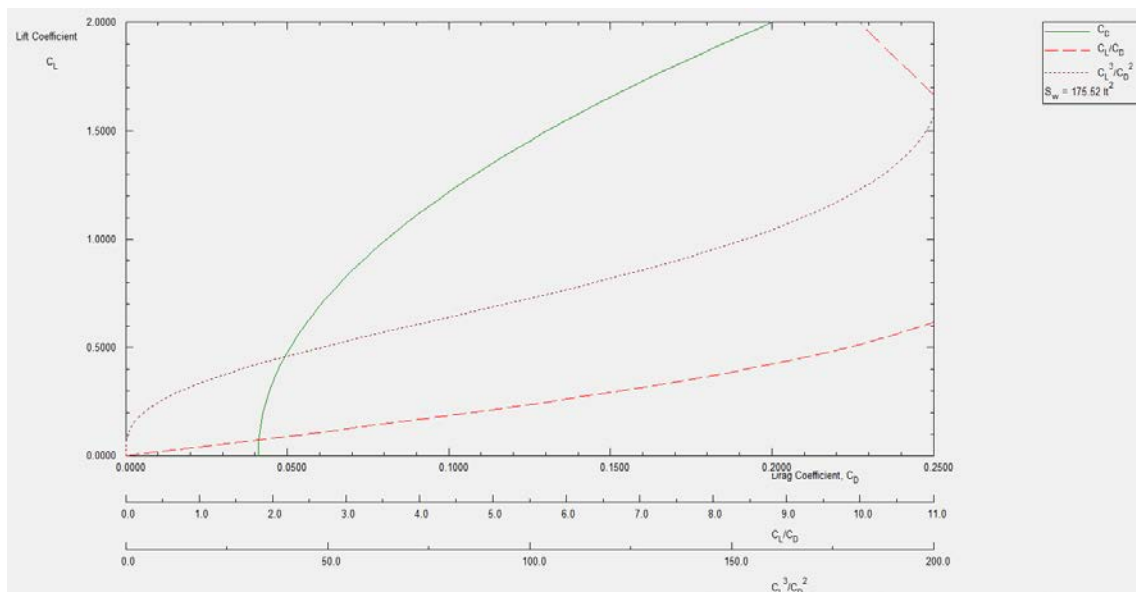


Figure 116 Clean Configuration Drag Polar

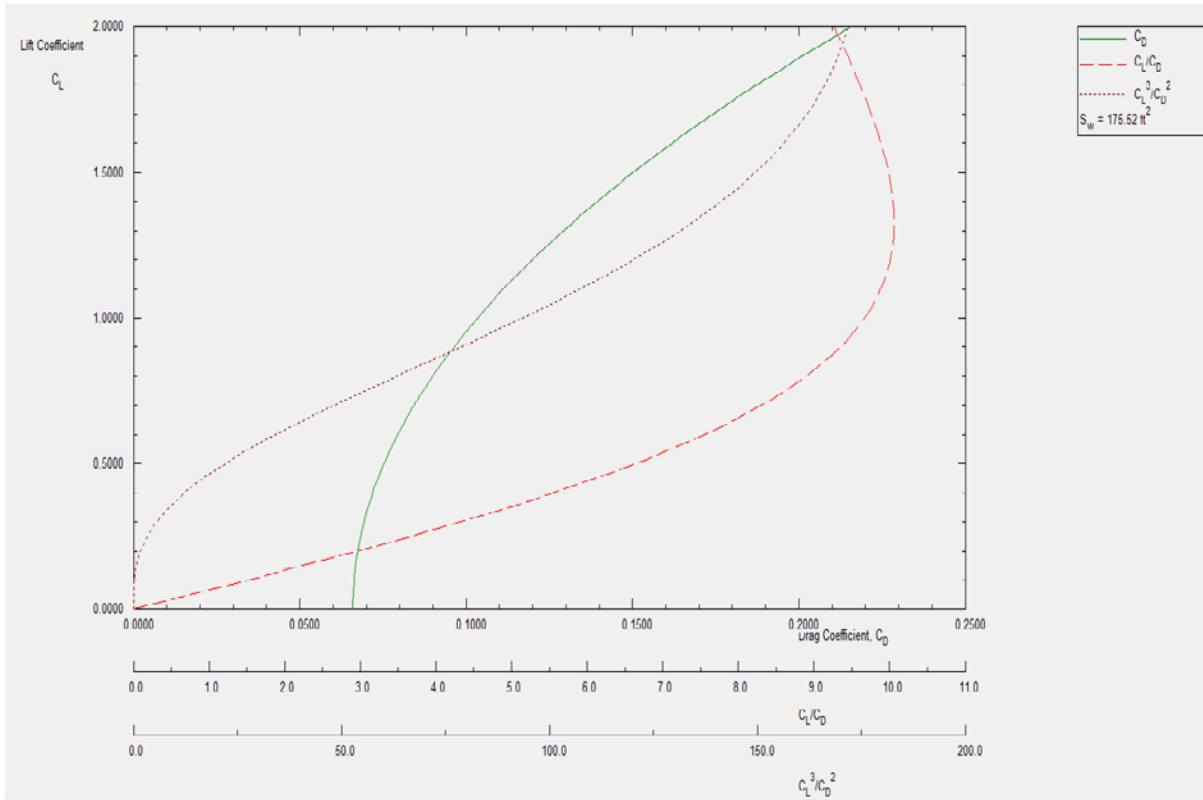


Figure 117 Take-off Flaps with Landing Gear Down Drag Polar

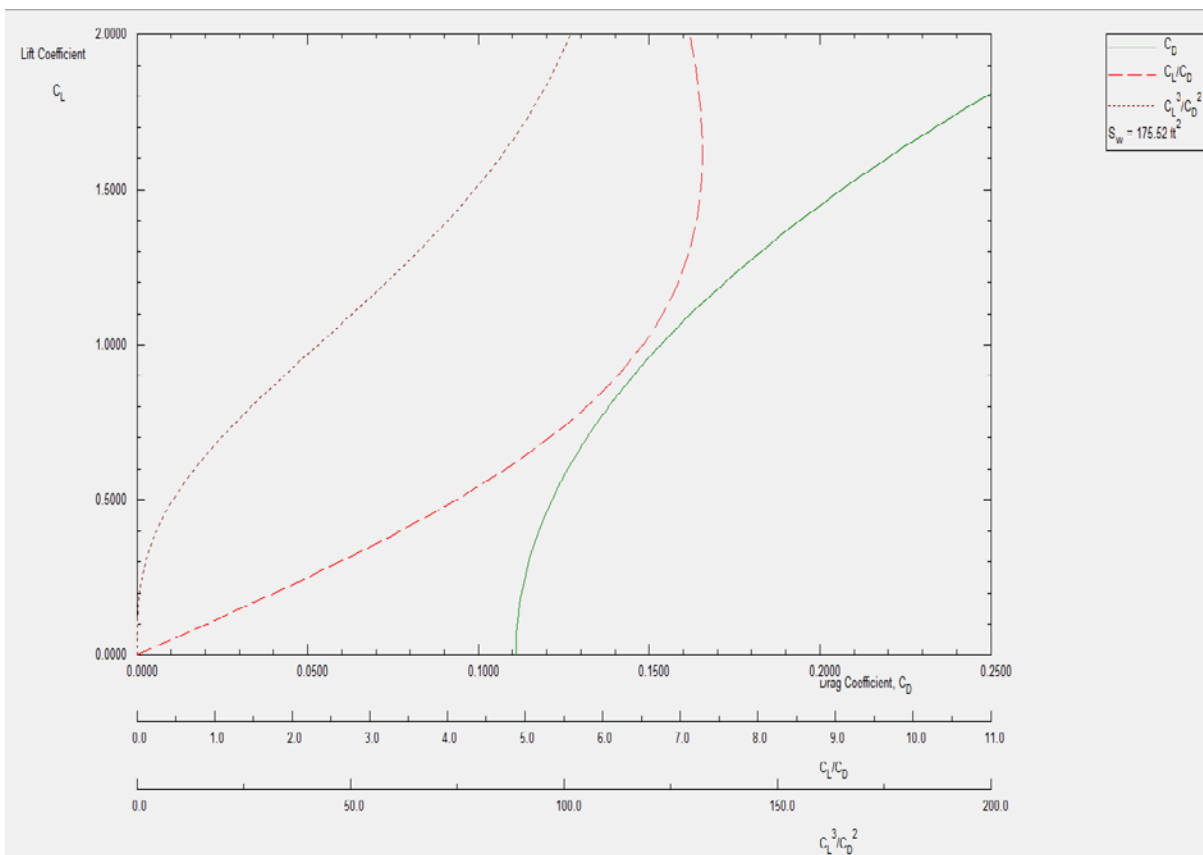


Figure 118 Landing Flaps with Landing Gear Down Drag Polar

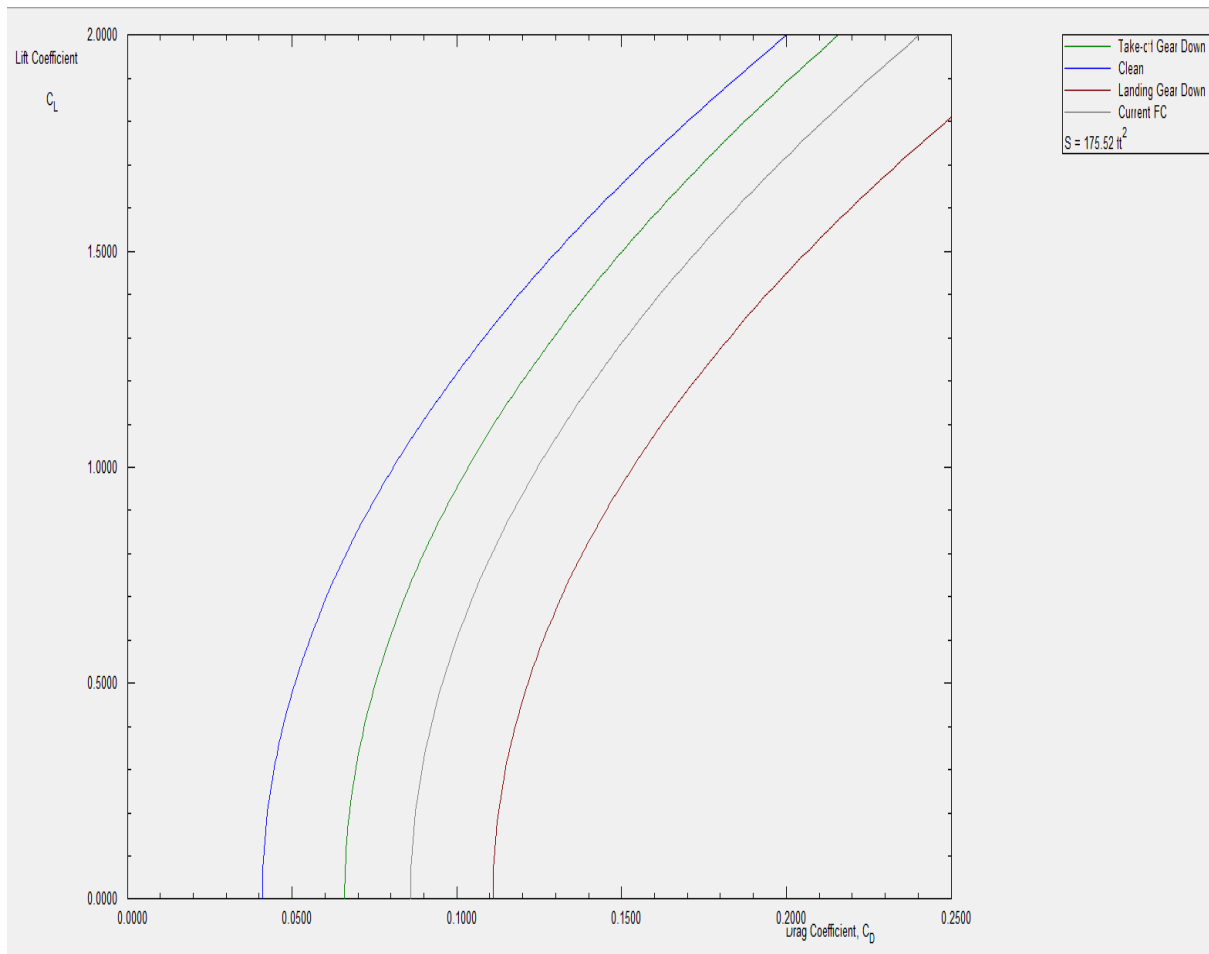


Figure 119 All Drag Polar Conditions

10.5) DISCUSSION AND CONCLUSION:

The component wise drag calculation is described in above sections. The calculations are done based on the class I drag polar calculation methods, which considers only certain components. Also, there are few assumptions has been made during calculations. The drag increments due to flaps and landing gear are assumed from the pre-defined range given in Roskam. The values are based on old technologies, which might change for new materials and designs.

The last step in the preliminary aircraft design is the drag polar. The aerodynamic behaviour can be understood from calculated drag values. The class II sizing can be done based on above calculated values.

CHAPTER 11

CONCLUSIONS AND RECOMMENDATIONS

11.1) DRAWING & SUMMARY OF MOST IMPORTANT DESIGN PARAMETERS:

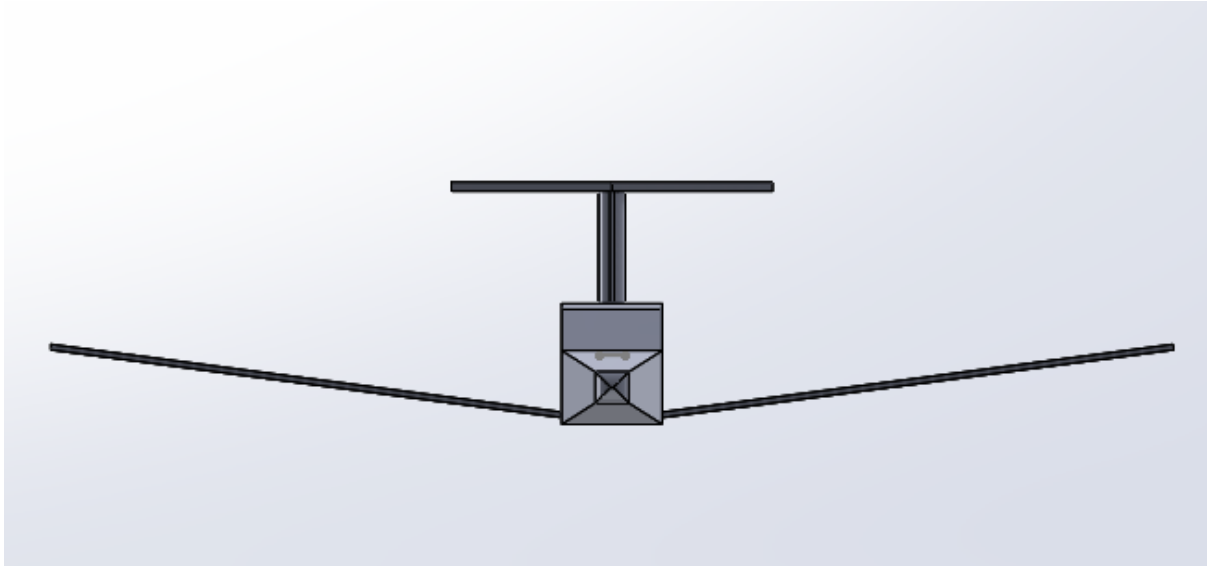


Figure 120 Front View: Proposed Aircraft

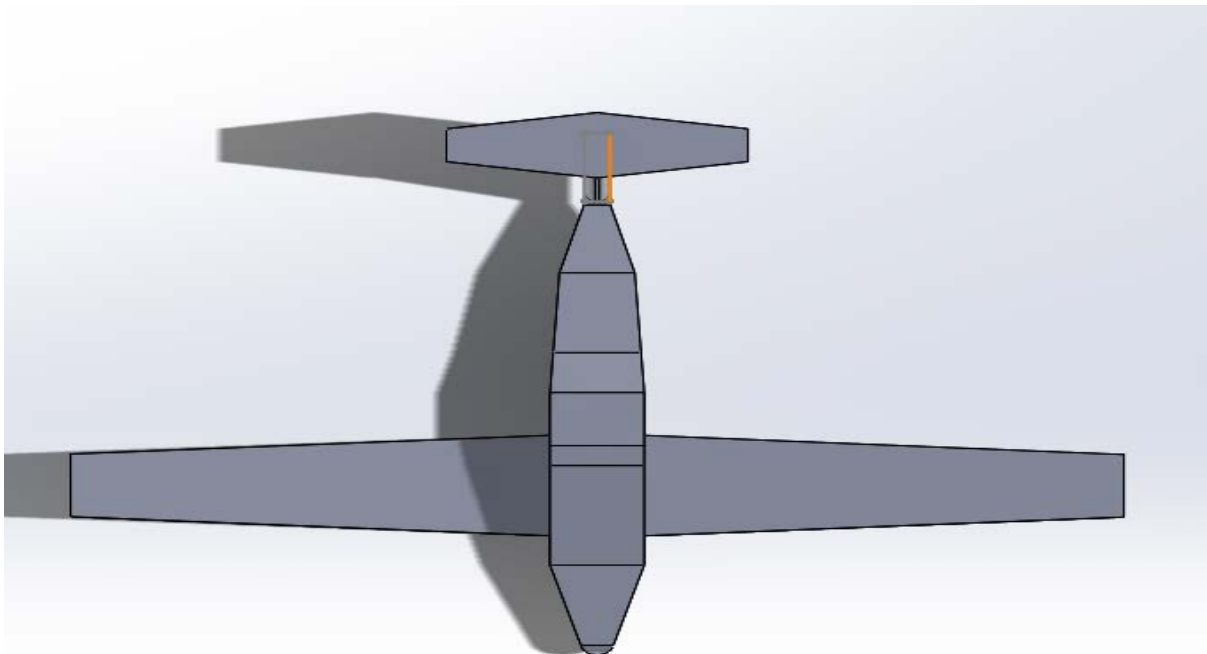


Figure 121 Top View: Proposed Aircraft

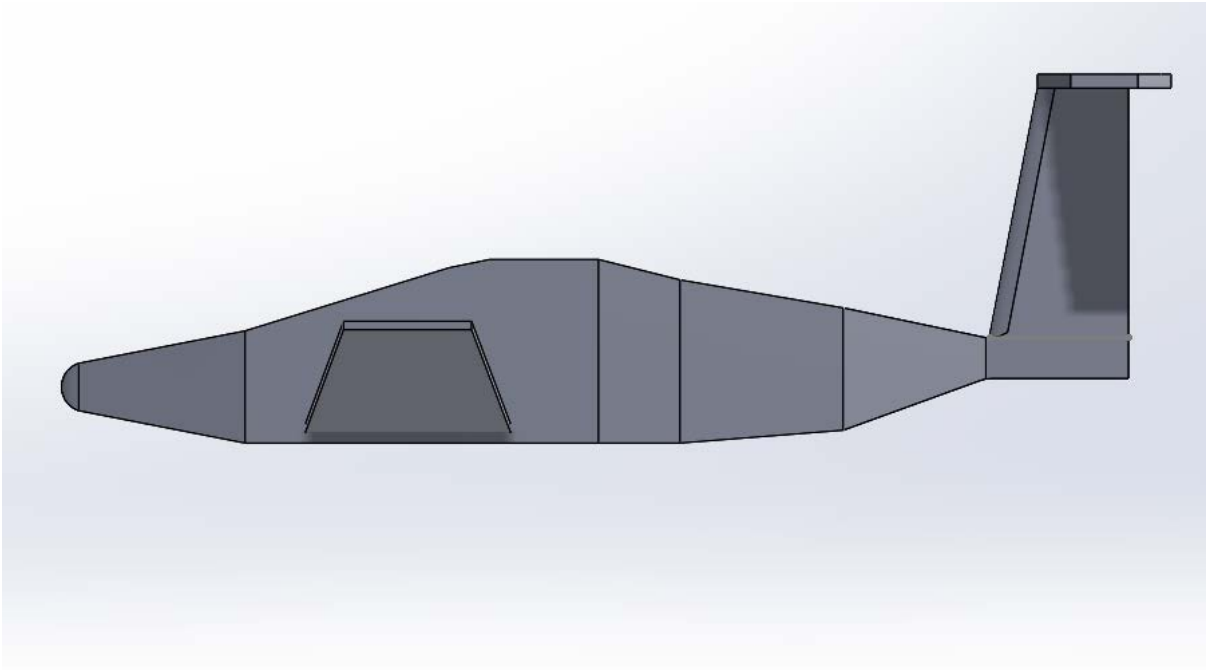


Figure 122 Side View: Proposed Aircraft

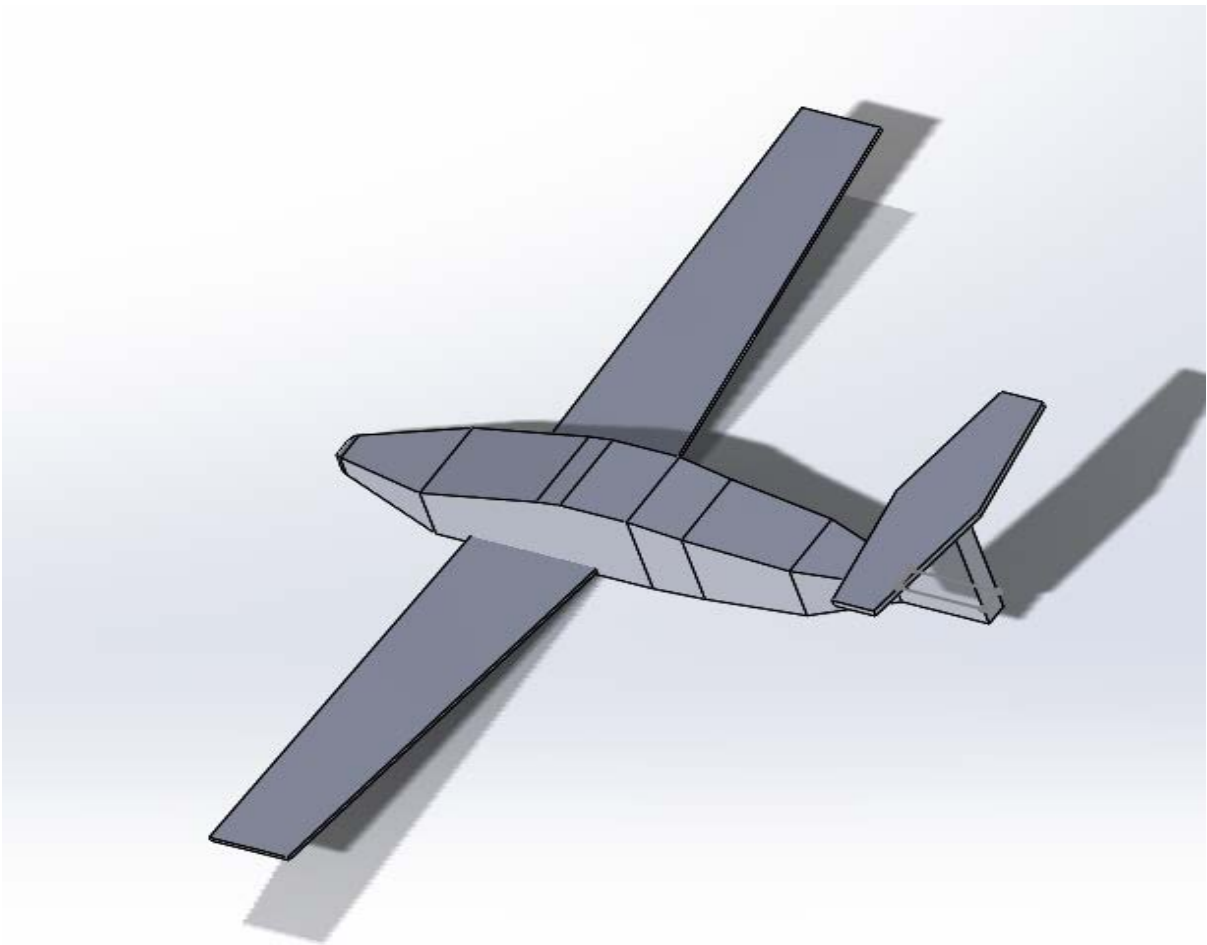


Figure 123 Isometric View: Proposed Aircraft

Table 33 Geometric Parameters: Proposed Aircraft

	WING	HORIZONTAL TAIL	VERTICAL TAIL
Area	175.52 ft ²	38.70 ft ²	30 ft ²
Span	41.9 ft.	13.91 ft.	6.92 ft.
Aspect Ratio	10	5	1.6
Sweep Angle	0 deg. (c/4)	0 deg. (c/4)	15 deg. (L.E.)
Taper Ratio	0.60	0.50	0.40
Thickness Ratio	0.12	0.12	0.12
Airfoil	NACA 63412	NACA-0012	NACA-0012
Dihedral Angle	7 deg.	0 deg.	90 deg.
Incidence Angle	0 deg.	Variable	0 deg.
Root Chord	5.23 ft.	3.86 ft.	5.65 ft.
Tip Chord	3.14 ft.	1.93 ft.	2.62 ft.
	FUSELAGE		
Total Length	26 ft.		
Diameter	4.5 ft.		
Width	3.75 ft.		
Fineness Ratio	5.78		
Tail Cone Length	13 ft.		
Cabin Length	9 ft.		
Nose Length	4 ft.		

11.2) RECOMMENDATIONS:

The proposed aircraft integrated the propulsion into the fuselage. The motors are also placed in fuselage which enhanced the diameter of propeller. The power source is batteries only so, the power generated from batteries are differ in terms of specific energy, power output and weight. The range for proposed electric aircraft is 400 nm. Ten years from now, if the battery densities have been increased to maximum then the changes for attaining a L/D of 10 are fair. The most crucial factor which affects the range is battery specific energy or battery weight. Also, the component weights can be decreased for proposed electric aircraft because of the development of new composites materials.

The power to weight ratio in an electric aircraft is the weight saving factor that these technologies provide compared to gasoline aircraft. With the improvement in motor technology, an all-electric aircraft can maximize on the range and could also result in long haul travel with further advancements. In short, the further research on the current and future battery trends of batteries will be carried out to further improve the design and performance. An in-depth analysis on the trade studies must be carried out to better understand the customer requirements.

The design point can be varied according to lift co-efficient values. Further research will be done on different airfoil which may generates more lift. The proposed aircraft is longitudinally as well as directionally stable.

11.3) ENVIRONMENTAL / ECONOMIC TRADE-OFFS:

Conventional aircraft have been serving the current aviation needs both for cargo and passenger travel. Depletion of the fossil fuel reserves, increasing levels of carbon emissions is urging us to search for an alternative means to power the aircraft engines or to change the entire aircraft design. There are many proposed solutions like hydrogen, electricity and bio-fuels to replace the conventional jet A-1 fuels. The main motto of aircraft design is to develop a geometrical conceptual description. In the past few decades, airlines have poured lump sum into research, but the innovations are still limited, winglets.

According to EPA (United States Environmental Protection Agency), 27 percent of U.S. greenhouse gas (GHG) emissions is from transportation & it is also the second leading source of GHG emissions in the United States [1]. From that, Aircraft account for 12 percent of all U.S. transportation GHG emissions and 3 percent of total U.S. GHG emissions [2]. The emissions from aviation is contribute about 1 percent of the total air pollution, as states in GAO Repot 2008. Even though this contribution seems small, the air traffic is anticipated to increase at a rate of 60 percent by 2030 [3]. This GHG emissions from aircraft can be controlled by introducing zero-emission propulsion systems in accordance with appropriate airplane design. This can be achieved by designing of an electric airplane by using innovative technologies and noise reduction is also by-product of an electric aircraft.

Aerodynamic Efficiency and Propulsion System are the two factors that affect the sustainability of the aircraft design. But for the conventional aircraft, there has still been a

compromise in one of these factors. An electric aircraft offers great improvements in the propulsion and as well as aerodynamic efficiency. Due to this, electric motors are preferred over the Internal combustion engines for model aircraft back in 1970's which were not fully scaled because of low specific energy of the batteries. However, there is no reason why a fully scalable electric aircraft has not been developed with greatly improved battery efficiencies, especially in this era of rapid electric car development.

Electric batteries pose a design challenge in terms of weight. To meet the mission requirements, an aircraft must be equipped with sufficient power. Since the battery weight is directly proportional to the power output. It requires a motor that produces greater horsepower while keeping the weight minimum. Efficiency of a battery is a major design challenge which current technology limits their full-scale integration. However, in the design chapters all the limitations are carefully addressed, and all the possible design solutions is documented.

The cost involved in manufacturing the electric aircraft is not going to be high except the integration of avionics and other subsystems with batteries. Once the technology gets matured and validated, the cost will automatically decrease.

The main concern for aviation industries, as mentioned earlier, is the price of fuel, which is basically impelling them to look for alternatives to conventional fuel sources. Therefore, the electrical energy, as an alternative to conventional fuel, may boost the global electric aircraft market demand over the forecast period. It can also reduce the noise generation and ground pollution. This results in reducing the global warming, which is also one of the major reason to drive the global electric aircraft.

Below is a graphical representation of the electric aircraft market trends and this clearly portrays a projected market increase up to 4.33% globally [4].

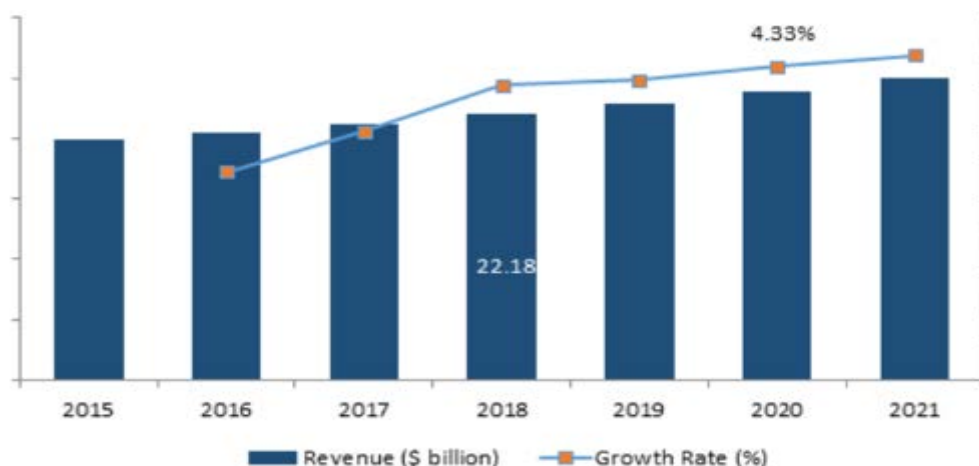


Figure 124 Global Electric Aircraft Market Trends

The technical and economic feasibility of this project is to push the limits of the current technology. Current battery technology is not efficient for long range more capacity airplane. Due to their limited efficiencies, they cannot generate the required power during take-off.

Batteries should be carried on-board to power the aircraft during take-off and this results an additional weight. The electric motor developed by DARPA, just weigh 1.4 lbs and can deliver power output of 7 hp. The design of the battery should have the capabilities to fully utilize the motor power.

11.4) SAFETY / ECONOMIC TRADE-OFFS:

The biggest setback for an electric aircraft is the battery behaviour. Most recent batteries like lithium-ion are vulnerable to explosion due to over-charging or ampere imbalance. The discharge rate needs to be controlled by an electronic speed controller which needs to have robust algorithm. The electric aircraft is a very recent concept and technology and was not feasible in the past due to limitations of battery specific energy and battery weight.

More advanced controllers for voltage, current and discharge rate have been developed to keep the balance between these three factors to avoid explosion of battery during charging and discharging. The high specific energy batteries are expensive and accounts for nearly 40% of the cost of the aircraft. Replacement of such an expensive part is not feasible if the battery life cycle is small.

The only solution to this problem is an advance battery which has a very high specific energy density and low weight. The batteries with most specific energy are Lithium Air, Lithium Sulphur and Aluminium Air + Lithium Ion hybrid system which are currently not available in market, but they would be available around 2020 [5][6]. The aluminium air has already been executed in some forms of transportation.

Current battery technology and expected future battery specific energy is shown in below figure. Currently, large amount of experimental concepts research has been going on and it gives the most promise in terms of specific energy [7].

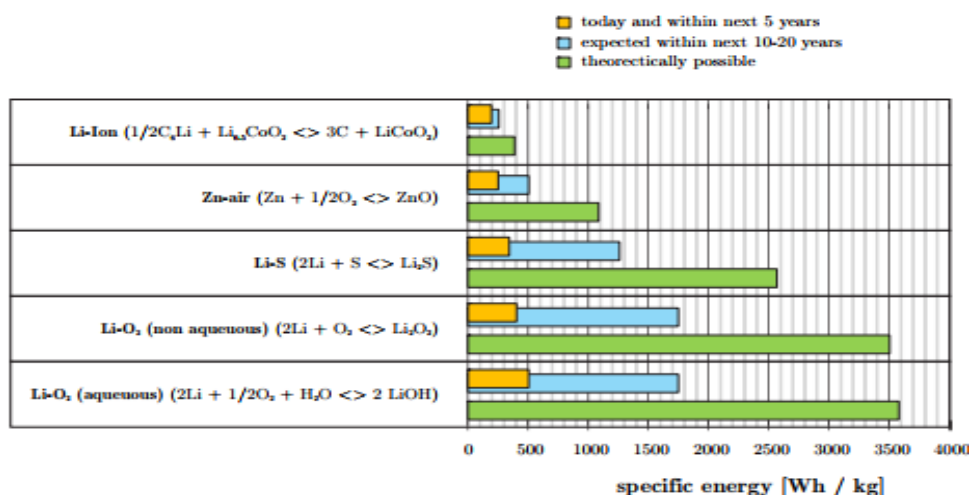


Figure 125 The Current and Future Battery Trends

CHAPTER 12

CLASS II: LANDING GEAR DESIGN

12.1) INTRODUCTION

The purpose of this chapter is to provide an estimate design of landing gear using class II methods. The chapter 8 represents the class I sizing of the landing gear. In this chapter, the same dimensions will be used for class II sizing. The landing gear must be capable of absorbing landing and taxi loads as well as transit part of these loads to the airframe. As mentioned in chapter 8 all geometric clearance and tip-over criteria are satisfied. In this chapter, the proper tire size, shock absorber stroke and strut diameter will be determined. For proposed aircraft, the landing gear is fixed type so, it does not require the design of retraction kinematics.

12.2) DETERMINATION OF ALLOWABLE WHEEL LOADS:

The landing gear layout design must be considered following three types of loads.

- Vertical Landing Gear Loads
- Longitudinal Loads
- Lateral Loads

The vertical landing gear loads depends on the touchdown rate and according to FAR-23 it can be calculated as follows:

$$w_t = 4.4 (W/S)^{1/4}$$

$$w_t = 9.18 \text{ fps} \quad (12.1)$$

And satisfied the requirement (It should be no less than 7 and no more than 10 fps (FAR 23.725)).

The longitudinal and lateral loads resists by the elements called drag-brace and the side-brace respectively. The loads on each landing gear strut as well as the load on each tire may not exceed values which:

- cause structural damage to the gear or to the airplane
- cause tire damage
- cause runway damage

These loads can be calculated based on three types of runway surfaces. The type 1 surfaces include the grassy and gravel surfaces. The type 2 surfaces include the runways with asphalt or tarmacadam and type 3 include the concrete runways. To avoid gear induced surfaces damage for type 1 surfaces the tire pressures should not exceed the values given in following figure:

Description of Surface	Maximum Allowable Tire Pressure	
	kg/cm ²	psi
Soft, loose desert sand	1.8 - 2.5	25 - 35
Wet, boggy grass	2.1 - 3.2	30 - 45
Hard desert sand	2.8 - 4.2	40 - 60
Hard grass depending on the type of subsoil	3.2 - 4.2	45 - 60
Small tarmac runway with poor foundation	3.5 - 5.0	50 - 70
Small tarmac runway with good foundation	5.0 - 6.3	70 - 90
Large, well maintained concrete runways	8.5 - 14	120 - 200

Figure 126 Recommended Tire Pressures for Various Surfaces

The proposed aircraft tire pressures are 22 psi for nosewheel and 19 psi for main gear, which is below the maximum allowable tire pressure.

To avoid surface damage for type 2 and type 3 surfaces the LCN (Load Classification Number) method is used. For landing gears with a single wheel per strut the relationship between its LCN, its load per wheel and its tire pressure is shown in below figure.

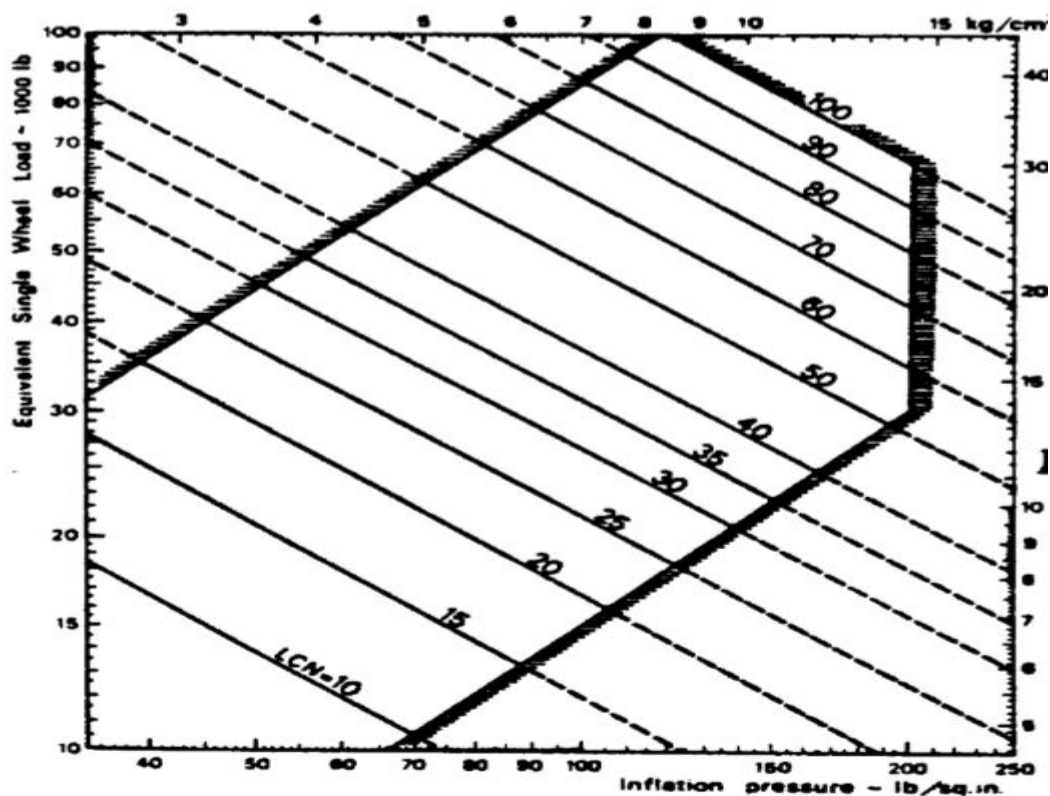


Figure 127 Effect of Tire Pressure and Tire Load on LCN

The LCN value for proposed electric aircraft is found using above figure. As the pressure and load per strut has already been calculated (Nose wheel = 551.51 lbs & Main gear = 1391.74 lbs also pressure is 22 psi & 19 psi respectively), the LCN is less than 10.

12.3) TIRES: TYPES, PERFORMANCE, SIZING AND DATA:

In airplane, the seven tire types are frequently used. The tire manufacturers rate tires in terms of ply rating, maximum allowable static loading, recommended inflation pressure, and maximum allowable runway speed. The new seven tire types are shown in below figure:

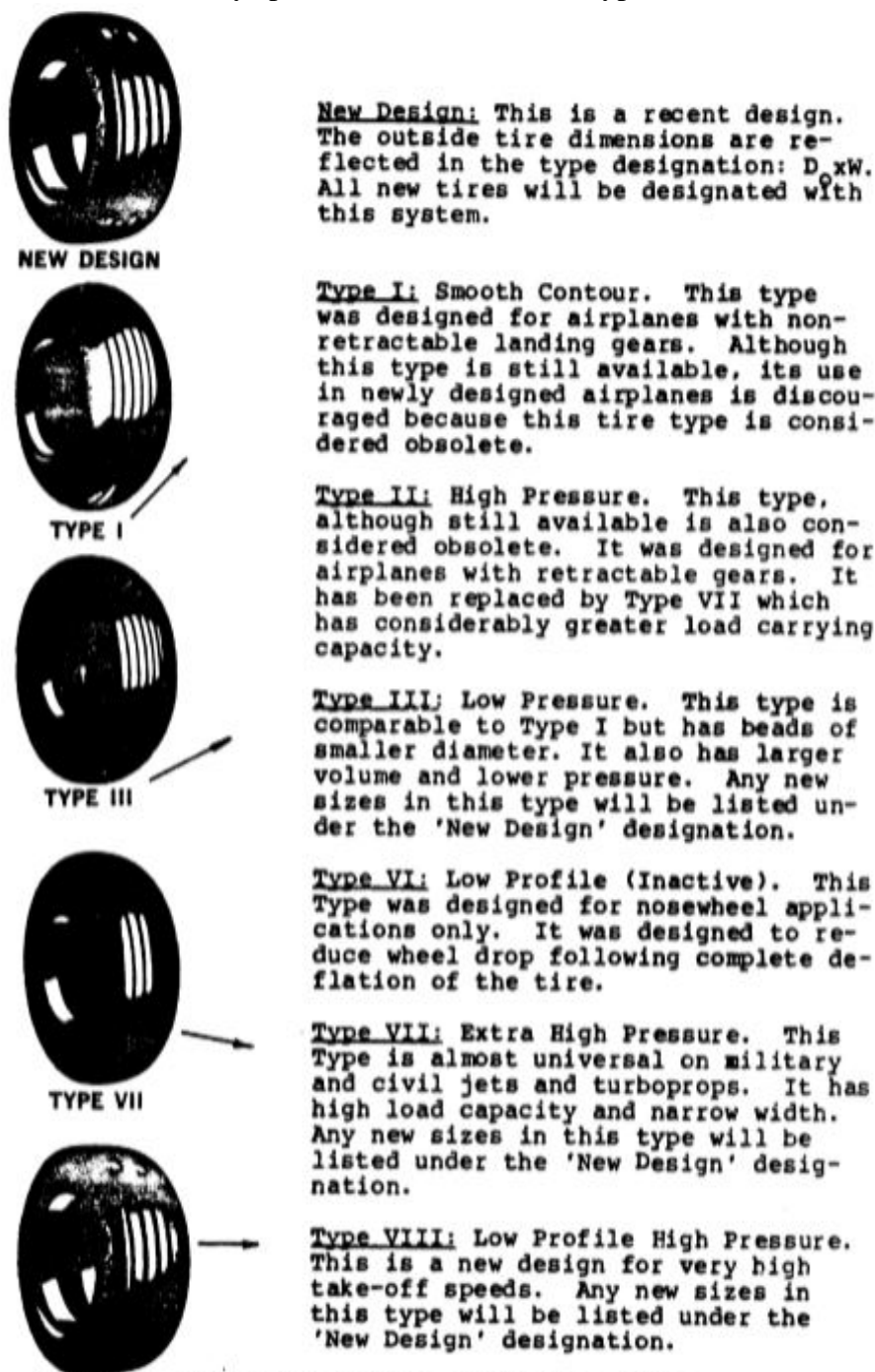


Figure 128 Types of Airplane Tyres

The type III tire is selected for proposed aircraft. The main gear and nose gear dimensions are as follows:

Nosewheel tire: $D_t \times b_t = 14 \times 5$

Main gear tire: $D_t \times b_t = 16 \times 6$

The nosewheel tires are designed for maximum allowable dynamic loads. These dynamic loads are obtained as follows:

Dynamic load = f_{dyn} (static load)

For type III tires the $f_{dyn} = 1.45$ & static load = 551.51 lbs (chapter 8).

Dynamic load = 799.68 lbs

To allow for growth in airplane weight, multiplying the static and dynamic load by 1.25 gives the new static and dynamic load as 639.38 lbs & 999.6 lbs per nose gear tire.

The maximum static load on each main gear is already calculated in chapter as 1391.74 lbs. Now, to allow for growth in airplane weight, multiplying the design load by factor 1.25 gives the new design load as 1739.67 lbs per main gear tire.

Now, the maximum dynamic load per nose gear tyre can also be calculated using following equation:

$$P_{n_{dyt_t}} = \frac{W_{TO} \left(l_m + \frac{a_x}{g(h_{cg})} \right)}{n_t(l_m + l_n)} \quad (12.2)$$

Where, $l_m = 1.7$ inches & $l_n = 79.3$ inches

$\frac{a_x}{g} = 0.35$ for dry concrete with simple brakes

$\frac{a_x}{g} = 0.45$ for dry concrete with anti – skid brakes

$h_{cg} = 58$ inches & $n_t = 1$

$$P_{n_{dyt_t}} = \frac{5689.625}{81} = 70.24 \text{ lbs}$$

$$\text{Static load} = \frac{70.24}{1.45} = 48.44 \text{ lbs}$$

By comparing both static & dynamic load, the maximum value is chosen for further calculation. The load values are as follows:

The design maximum static load per nose gear tire = 639.38 lbs.

The design maximum dynamic load per nose gear tire = 999.6 lbs

The design maximum static load per main gear tire = 1739.67 lbs

Now, using tables provided in Roskam, the list of all tires which meet the load conditions of the airplane are as follows:

Table 34 Tire Data for Nose & Main Gear

NO.	SIZE	PR	LOAD RATING		INFL PRESS, PSI	TIRE O.D., INS	WIDTH, INS	QUALIFIC STATUS
			STATIC, LB.	DYNAMIC, LB.				
1	15x6	4	1250	n/a	45	15.20	6.30	MIL
2	16x4.4	4	1100	n/a	55	16	4.45	MIL
3	15x6	6	1950	n/a	68	15.20	6.30	MIL
4	14.50"	8	2000	n/a	80	14.70	6.24	MIL

The first two rows represent the tire data for nose gear and last two rows represents the tire data for main gear. By considering factors like inflation pressure and large wheel diameter, the chosen tire sizes are as follows:

Main Gear: No.3 15x6 6PR

Nose Gear: No.1 15x6 4PR

12.4) STRUT WHEEL INTERFACE, STRUTS AND SHOCK ABSORBERS:

There are two main parameters for strut-wheel interface. The 'rack' is the angle between the wheel swivel axis and a line vertical to the runway surface. The 'trail' is the distance between the runway-wheel contact point and the point where the wheel swivel axis intersects the ground. Both parameters are shown in following below figure:

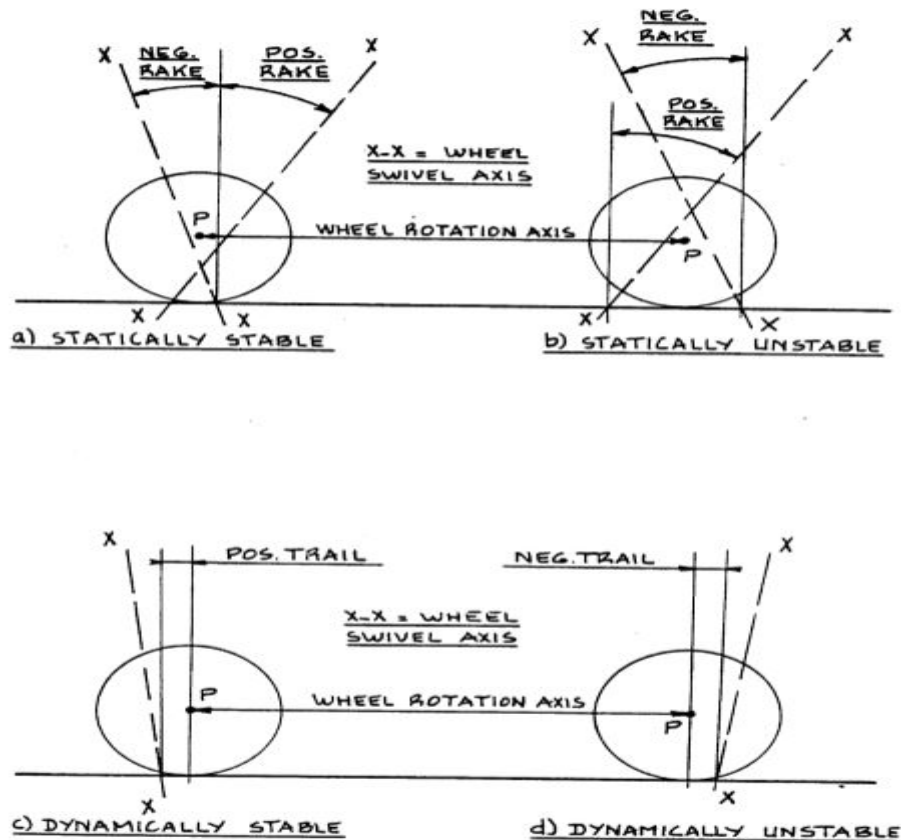


Figure 129 Definition of Rake and Trail

In most airplanes, stable strut-wheel arrangements are used. For the nose gear, the air-oil strut wheel combination is used for proposed aircraft as well as the leaf-type spring gear structure is used. The following figure shows the air-oil strut and spring leaf strut for nose and main landing gear respectively.

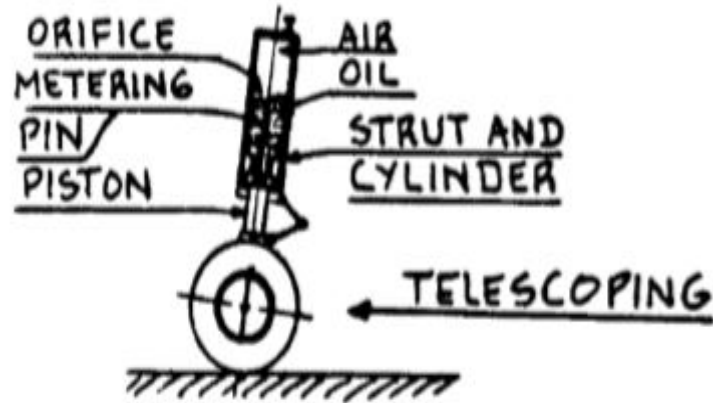


Figure 130 Nose gear Strut: Proposed Aircraft

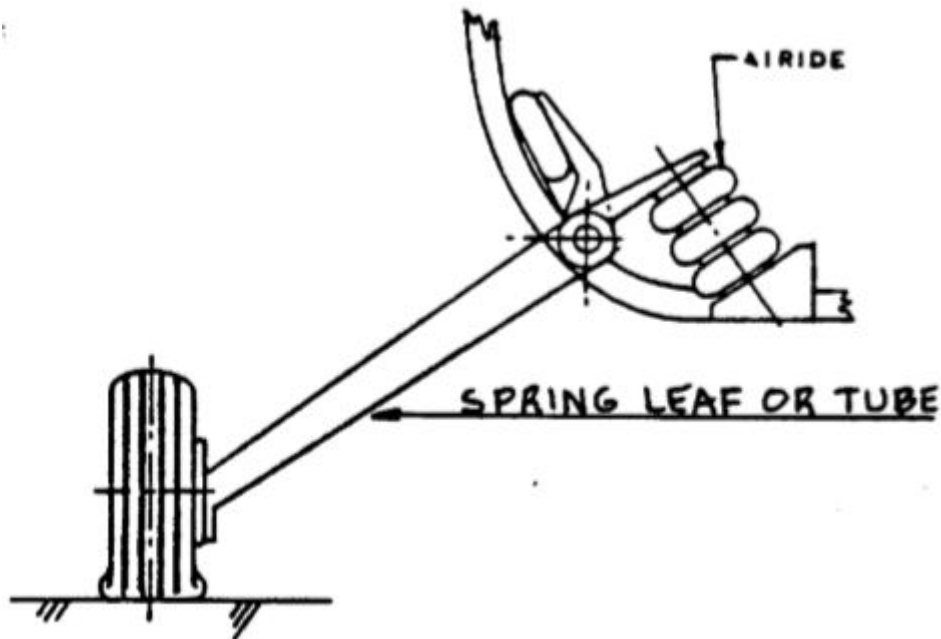


Figure 131 Main Gear Strut: Propose Aircraft

Similar like strut-wheel combination, there are many designs available for shock absorption devices. The main aim for using shock absorption devices are to convert shock energy of landing impact into heat energy. The main devices are tires, shock chords, air springs, cantilever springs, oleo-pneumatic struts, and liquid springs. The most common type of strut is oleo-pneumatic struts which is basically compressed air/nitrogen combined with hydraulic fluid. For proposed aircraft, the oleo-pneumatic strut is chosen, and it is shown in below figure.

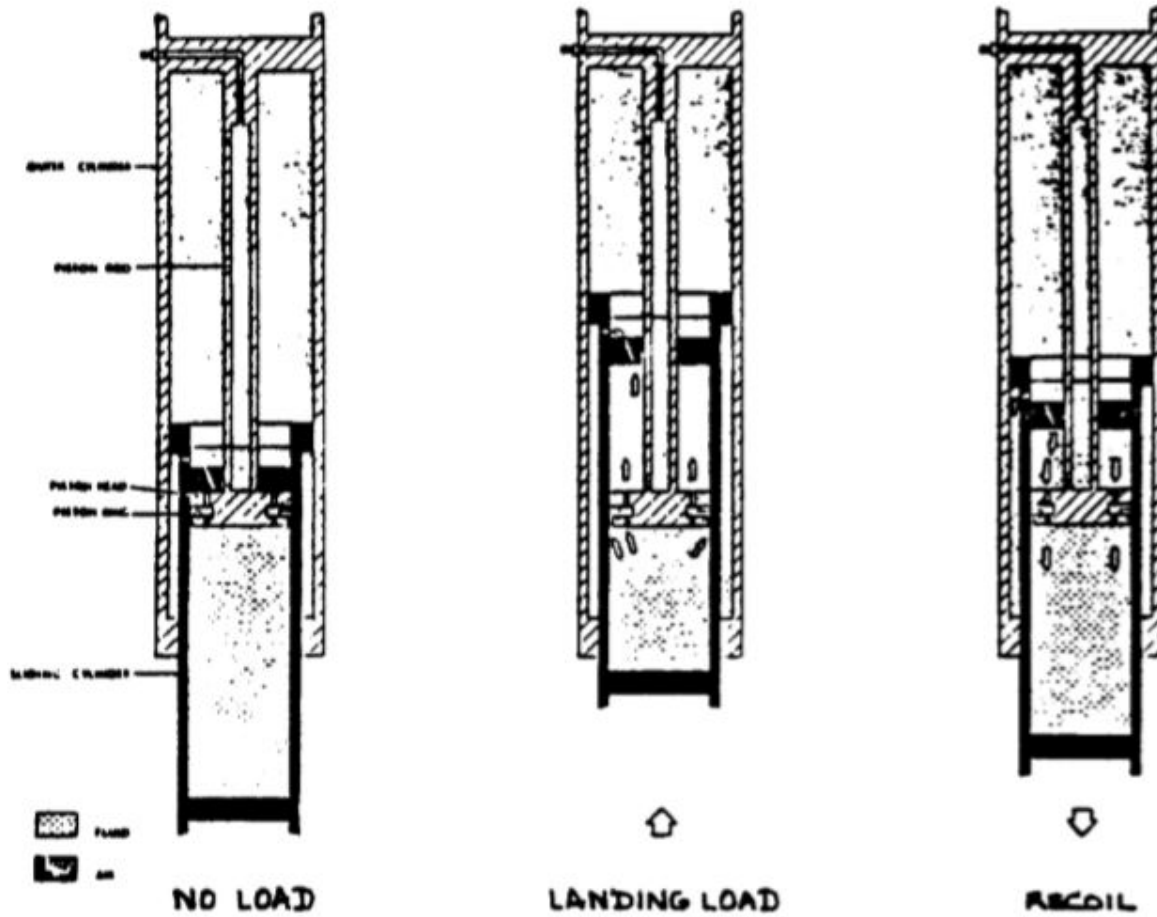


Figure 132 Shock Absorption Device: Proposed Aircraft

SIZING OF STRUTS:

The maximum kinetic energy which needs to be absorbed, when an airplane touches down is calculated from following equation:

$$E_t = 0.5(W_L)(w_t)^2 \quad (12.3)$$

Where, W_L = Landing weight, $w_t = 9.18$ ft/s (calculated in eq. (12.1))

$$E_t = 0.5(3335 \text{ lbs}) \left(9.18 \frac{\text{ft}}{\text{s}}\right)^2$$

$$E_t = 1913.20 \text{ pound - force} \quad (12.4)$$

The total energy calculated in equation (12.4) needs to be absorbed by the landing gear (combination of nose & main landing gear).

A) For Main Landing Gear: At this stage it is convenient to assumed that the entire touch-down energy is absorbed by the main landing gear. The following equation is used:

$$E_t = n_s P_m N_g (\eta_t S_t + \eta_s S_s) \quad (12.5)$$

Where, $W_L = n_S P_m = 3335 \text{ lbs}$

n_S is the number of main gear struts = 2

P_m is the maximum static load per main gear strut

N_g is the landing gear load factor: ratio of maximum load per leg to
the maximum static load per leg = 3

η_t is the tire energy absorption efficiency = 0.47

η_S is the energy absorption efficiency of the shock absorber = 0.80

S_S is the stroke of the shock absorber

S_t is the maximum allowable tire deflection

$$S_t = D_0 - 2(\text{loaded radius})$$

$$S_t = 15.20 - 2(6.20)$$

$$S_t = 2.8 \text{ inches}$$

$$S_S = [\{0.5(W_L/g) (w_t)^2 / (n_S P_m N_g)\} - \eta_t S_t] / \eta_S$$

$$S_S = 4.90 \text{ inches}$$

It is suggested to add one inch to this length:

$$S_{S_{design}} = S_S + 1 = 5.90 \text{ inches}$$

The diameter of the shock absorber is estimated from:

$$d_S = 0.041 + 0.0025(P_m)^{\frac{1}{2}}$$

$$d_S = 0.1452 \text{ inches}$$

B) For the Nose Gear: By following the same procedure as main gear, the stroke of the shock absorber is:

$$S_t = 2.8 \text{ inches}$$

$$S_S = 2.54 \text{ inches}$$

$$S_{S_{design}} = S_S + 1 = 3.54 \text{ inches}$$

$$d_S = 0.12 \text{ inches}$$

CHAPTER 13

CLASS I: AIRPLANE INERTIAS

13.1) INTRODUCTION:

The purpose of this chapter is to provide airplane inertias. The inertia moments are useful whenever it is necessary to calculate undamped natural frequencies for airplanes. The first step is to find radii of gyration. It is obvious that class I method for airplane inertia estimation relies on the assumption that within each category it is possible to identify a radius of gyration for the airplane.

13.2) ESTIMATING MOMENT OF INERTIA WITH RADII OF GYRATION:

For the proposed electric aircraft, the following information are already known:

$$W_{TO} = 3335 \text{ lbs}, W_E = 1715 \text{ lbs}, b = 41.9 \text{ ft.}, L = 26 \text{ ft.}, e = (b + L)/2 = 33.9 \text{ ft.}$$

From the table B2 (Part V, Airplane Design by Jan Roskam, Appendix B), the following airplanes are judged to be comparable in terms of mass distribution: Beech N-35 & Cessna 210K. From this table, the non-dimensional radii of gyration apply to proposed aircraft:

$$\bar{R}_X = 0.25, \bar{R}_Y = 0.37, \bar{R}_Z = 0.39$$

The moment of inertia (@ W_{TO}) is calculated as follows:

$$I_{XX} = (\bar{R}_X * b/2)^2 * \frac{W}{g} = 2840 \text{ slug} * \text{ft}^2$$

$$I_{YY} = (\bar{R}_Y * L/2)^2 * \frac{W}{g} = 2400 \text{ slug} * \text{ft}^2$$

$$I_{ZZ} = (\bar{R}_Z * e/2)^2 * \frac{W}{g} = 4525 \text{ slug} * \text{ft}^2$$

The moment of inertia (@ W_E) is calculated as follows:

$$I_{XX} = \left(\frac{W_E}{W_{TO}}\right) * I_{XX@W_{TO}} = 1460 \text{ slug} * \text{ft}^2$$

$$I_{YY} = \left(\frac{W_E}{W_{TO}}\right) * I_{YY@W_{TO}} = 1234 \text{ slug} * \text{ft}^2$$

$$I_{ZZ} = \left(\frac{W_E}{W_{TO}}\right) * I_{ZZ@W_{TO}} = 2326 \text{ slug} * \text{ft}^2$$

By comparing the above results with the graphs provided in Jan Roskam (Part V, Chapter 3, Figure 3.1 through 3.3), the inertia estimates are reasonable.

CHAPTER 14

V-n DIAGRAMS

14.1) INTRODUCTION:

In this chapter, V-n diagram is constructed using procedure given in Jan Roskam. The V-n diagrams are used to determine design limit and design ultimate load factors as well as the corresponding speeds to which airplane structures are designed. For the FAR-23 certified airplanes, the V-n diagram is shown in below figure:

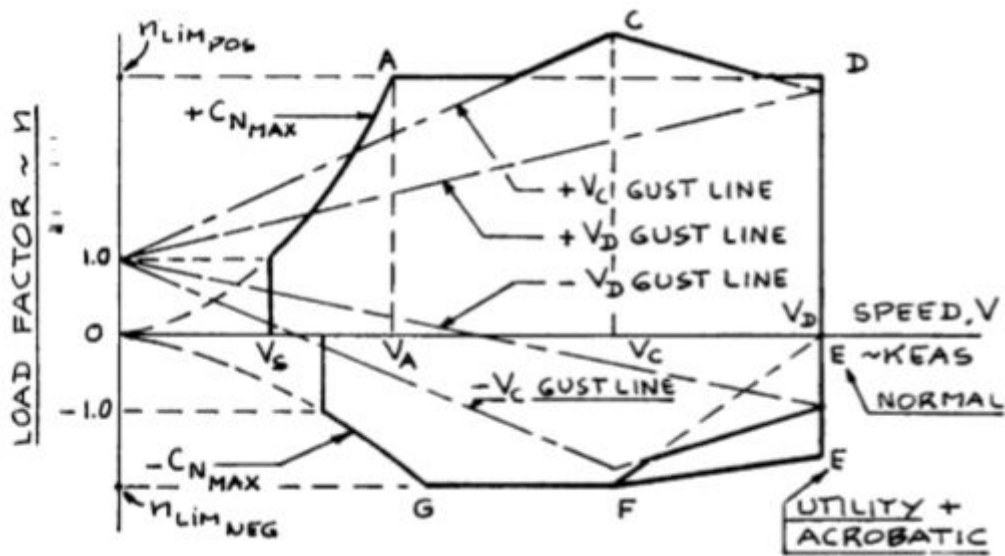


Figure 133 V-n Diagram According to FAR-23

Where, $V_s = +1g$ stall speed or the minimum speed at which the airplane is controllable

$V_C =$ design cruising speed

$V_D =$ design diving speed

$V_A =$ design maneuvering speed

A, B, C, D, E, F, G = Critical points

Note: All speeds are in knots.

14.2) V-n DIAGRAM: PROPOSED AIRPLANE

According to mission specification the proposed aircraft comes under FAR-23 airplane and it will be certified under normal category.

Determination of +1g stall speed, V_S

$$V_S = \left\{ 2 * \frac{\frac{GW}{S}}{\rho * C_{N_{max}}} \right\}^{\frac{1}{2}}, \quad (14.1)$$

Where, GW = flight design gross weight in lbs = 3335

S = wing area in ft² = 175.52

ρ = air density in slugs/ft³ = 0.002378

$C_{N_{max}}$ = maximum normal force co-efficient = $1.1 * C_{L_{max}} = 1.1 * 1.7 = 1.87$

$$V_S = 92 \text{ fps} = 57 \text{ knots}$$

Determination of design cruising speed, V_C

$$V_C = k_c * \left(\frac{GW}{S} \right)^{\frac{1}{2}}, \quad (14.2)$$

Where, $k_c = 33$ for normal and utility category airplanes up to W/S = 20 psf.

$$V_C = 144 \text{ knots}$$

Determination of design diving speed, V_D

$$V_D = 1.25 * V_C = 1.25 * 144 = 180 \text{ knots}$$

Determination of design limit load factor, n_{lim}

The positive, design limit load factor is given by:

$$n_{lim_{pos}} = 2.1 + \left\{ \frac{24000}{GW + 10000} \right\}, \quad (14.3)$$

$$n_{lim_{pos}} = 3.89$$

The negative, design limit load factor is given by:

$$n_{lim_{neg}} = 0.4 * 3.89 = 1.55$$

Determination of gust load factor lines, V_C and V_D

The gust load factor lines are defined by the following equation:

$$n_{lim} = 1 + \frac{K_g U_{de} C_{L\alpha} V}{498 \left(\frac{GW}{S} \right)} \quad (14.4)$$

Where, $K_g = \frac{0.88\mu_g}{5.3 + \mu_g} = 0.72$

Where, $\mu_g = \frac{2 \left(\frac{GW}{S} \right)}{\rho \bar{c} g C_{L\alpha}} = \frac{2 * 20}{0.002378 * 4.27 * 32.2 * 5.084} = 24$

For the V_C gust lines:

$U_{de} = 50$ fps between sea-level and 20,000 ft

$$n_{lim_{gust}} = 1 + 0.0183V$$

For the V_D gust lines:

$U_{de} = 25$ fps between sea-level and 20,000 ft

$$n_{lim_{gust}} = 1 + 0.0091V$$

Determination of design maneuvering speed, V_A

$$V_A = V_S * n_{lim}^{\frac{1}{2}} \quad (14.5)$$

$$V_A = 112.42 \text{ knots}$$

Determination of negative stall speed line

$$V_{S_{neg}} = \left\{ \frac{2 \left(\frac{GW}{S} \right)}{\rho C_{N_{max_{neg}}}} \right\}^{\frac{1}{2}} \quad (14.6)$$

Where, $C_{N_{max_{neg}}} = 1.1 * C_{L_{max_{neg}}} = 1.1 * 1.18 = 1.29$

$$V_{S_{neg}} = 111 \text{ knots}$$

From above calculated data, it is possible to draw the V-n diagram as follows:

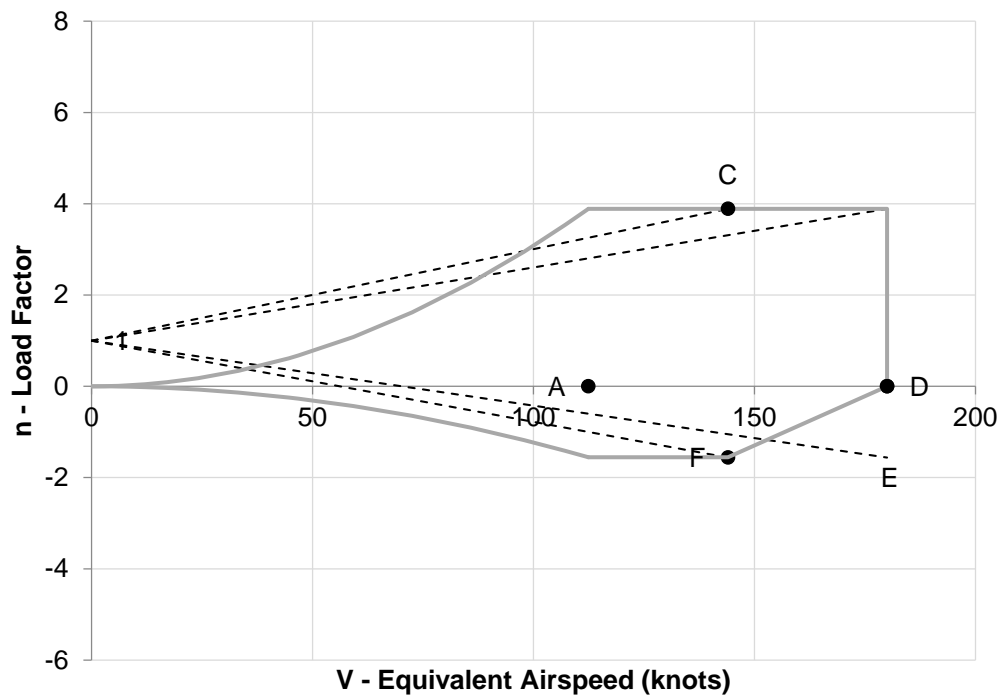


Figure 134 V-n Diagram: Proposed Airplane

CHAPTER 15

CLASS II: WEIGHT ESTIMATES

15.1) STRUCTURE WEIGHT ESTIMATION:

The aircraft structure weight is assumed to consist of the following components: Wing, Empennage, Fuselage, and landing gear. There are mainly three methods available to calculate the structure weights for general aviation airplanes: a) Cessna method, b) USAF method, and c) Torenbeek method. The equations used to calculate structure weights are taken from Part V: Component Weight Estimation, Aircraft design by Jan Roskam. The calculated values are as follows:

Table 35 Class II Structure Weight Estimates: Proposed Aircraft

Component	Methods: Class I	Cessna Method	USAF method	Torenbeek Method	Use as Class II Estimate
Wing	230	665	304	246	361
Horizontal Tail	110	154	45	63	85
Vertical Tail	60	N.A.	25		39
Fuselage	400	N.A.	240	N.A.	320
Landing Gear	240	80	32	N.A.	117
Structure Weight	1040	899	646	309	921

(All Weights are in 'lbs')

15.2) POWERPLANT WEIGHT ESTIMATION:

The airplane powerplant weight is assumed to be consist of the following components: Engines, Battery, Propellers, and Air induction system. There are mainly three methods available to calculate the powerplant weights for general aviation airplanes: a) Cessna method, b) USAF method, and c) Torenbeek method. The equations used to calculate structure weights are taken from Part V: Component Weight Estimation, Aircraft design by Jan Roskam. The calculated values are as follows:

Table 36 Class II Powerplant Weight Estimates: Proposed Aircraft

Component	Methods: Class I	Cessna Method	USAF method	Torenbeek Method	Use as Class II Estimate
Engine	150	100	N.A.	N.A.	125
Battery	800	N.A.	N.A.	N.A.	800
Propellers	50	N.A.	N.A.	N.A.	50
Air Induction System	50	N.A.	N.A.	N.A.	50
Powerplant Weight	1050	N.A.	180	178	1025

(All weights are in 'lbs')

15.3) FIXED EQUIPMENT WEIGHT ESTIMATION:

The airplane fixed equipment weight is assumed to be consist of the following components: Flight Control System, Electrical system, Instrumentation, Oxygen system, and furnishings. There are mainly three methods available to calculate the powerplant weights for general aviation airplanes: a) Cessna method, b) USAF method, and c) Torenbeek method. The equations used to calculate structure weights are taken from Part V: Component Weight Estimation, Aircraft design by Jan Roskam. The calculated values are as follows:

Table 37 Class II Fixed Equipment Weight: Proposed Aircraft

Component	Methods: Class I	Cessna Method	USAF method	Torenbeek Method	Use as Class II Estimate
Flight Control System	180	56	171	49	92
Electrical System		87	N.A.	N.A.	89
Instrumentation, avionics, and electronics	80	N.A.	N.A.	132	106
Oxygen	25	N.A.	N.A.	22	24
Furnishings	140	106	N.A.	107	118
Fixed Equipment Weight	425	249	171	310	429

(All weights are in 'lbs')

15.4) SUMMARY:

The class II empty weight of the proposed aircraft is 2375 lbs. This compares with 2515 lbs for the class I weight estimate. This represents a difference of 140 lbs. The difference is less than 5 percent. It therefore appears quite possible to bring the overall take-off weight in at the original estimate of 3335 lbs.

CHAPTER 16

BATTERY: ENERGY DENSITY OPTIMIZATION

16.1) INTRODUCTION:

During the last years, the development of electric propulsion system is pushed strongly. The efficiency of battery system is limited by the chemical processes occurring during charging and discharging. As discussed in chapter 3, the focus is cast on the energy storage problem. In this chapter, the limitations and required technology developments are demonstrated by introducing new trade studies. Also, the take-off weight for different combinations of payload and range is shown using the practical energy density found for the chosen battery system (Aluminium air + Lithium Ion).

16.2) TRADE STUDIES:

The trade study has been done using the range equation presented in ref. [7]. The range equation is as follows:

$$Range = E^* * \eta_{total} * \frac{1}{g} * \frac{L}{D} * \frac{m_{battery}}{m}$$

16.2.1) Range vs Payload:

By simplifying above equation, the range vs payload trade study has been done using $L/D=10$ & weight ratio=4.2.

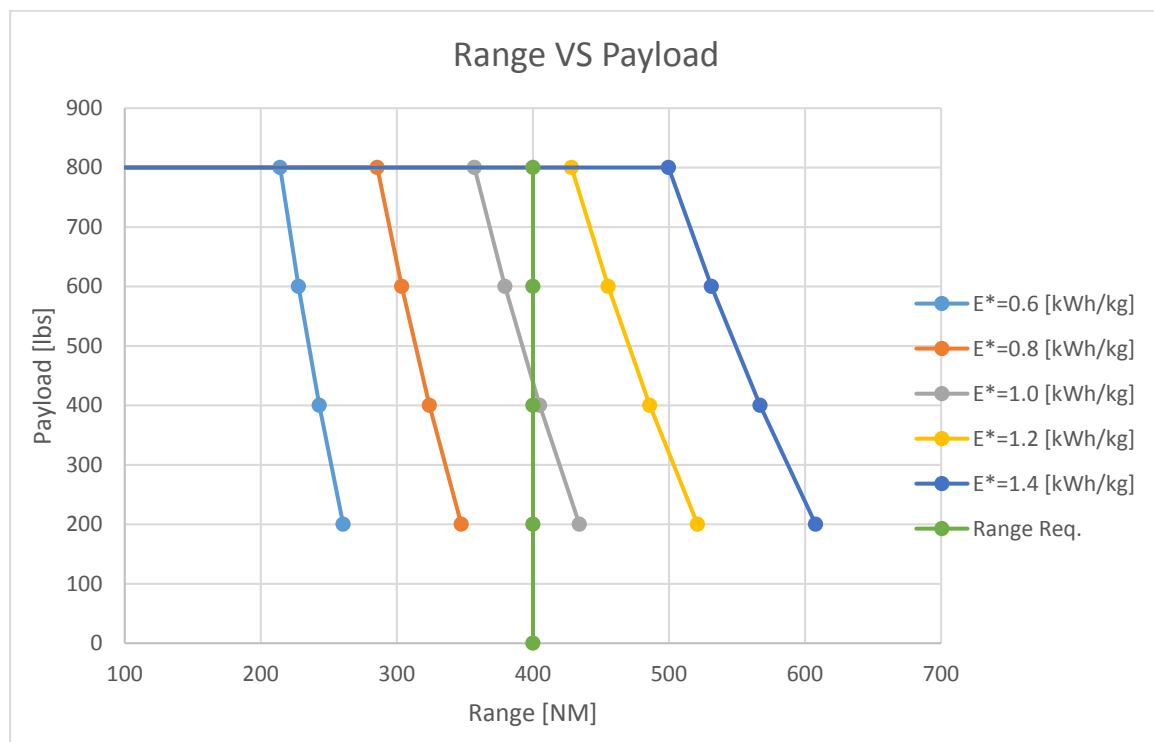


Figure 135 Range vs Payload: Proposed Aircraft

As we can see from above figure that the new required battery energy density for proposed range is reduced to 1.1 kWh/kg from 1.8 kWh/kg.

16.2.2) Range vs L/D:

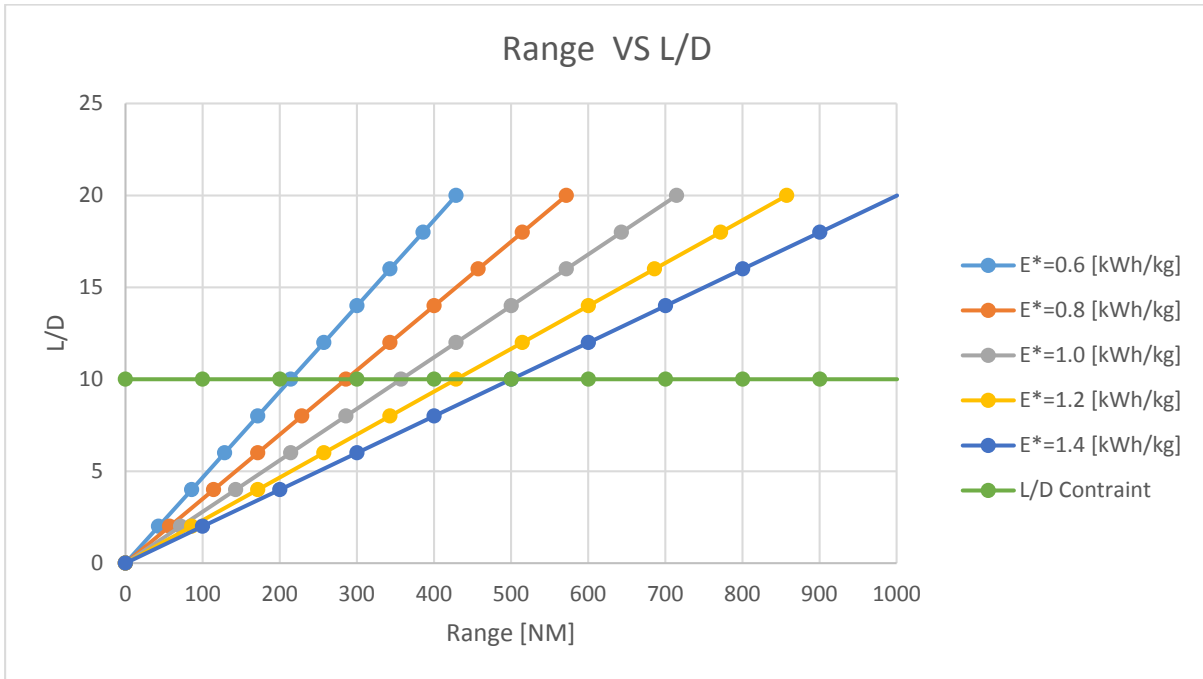


Figure 136 Range vs L/D: Proposed Aircraft

16.2.3) Range vs Take-off Weight:

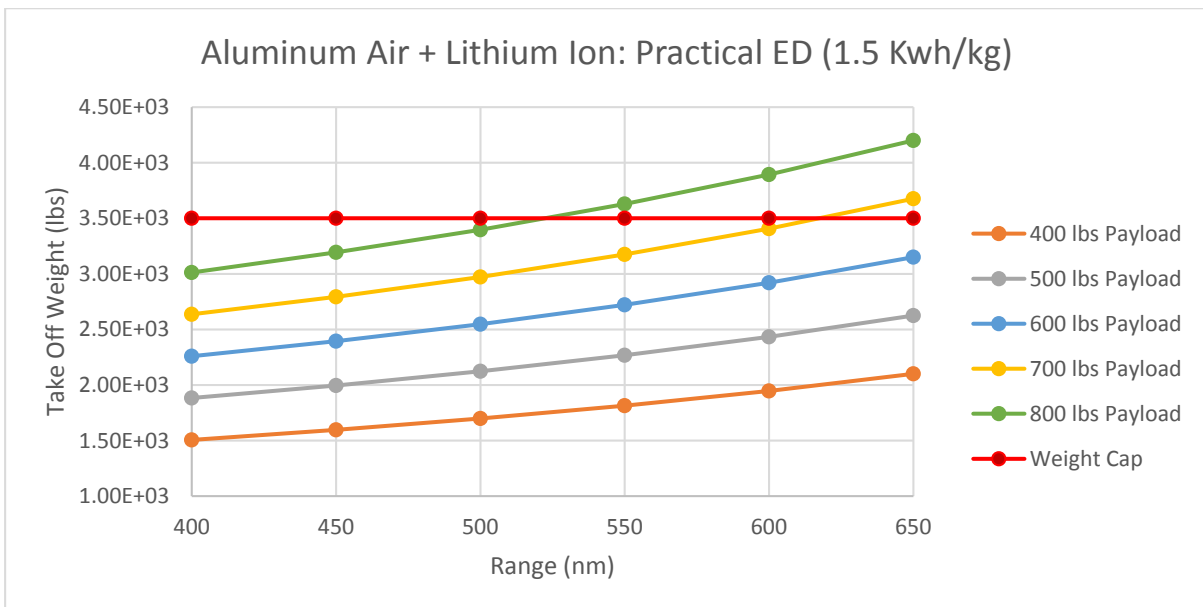


Figure 137 Range vs Take-off Weight (Practical E=1.5 kWh/kg): Proposed Aircraft*

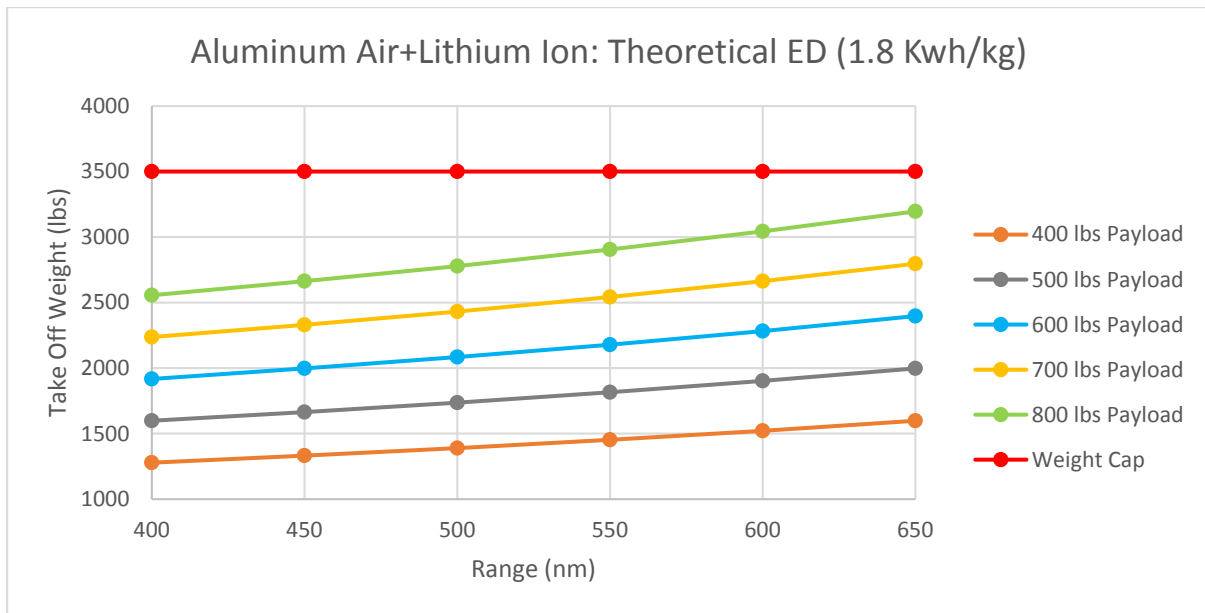


Figure 138 Range vs Take-off Weight (Theoretical $E^=1.8$ kWh/kg): Proposed Aircraft*

References

- [1] Transportation and climate change, United States Environmental Protection Agency, Retrieved from: <https://www.epa.gov/air-pollution-transportation/carbon-pollution-transportation>
- [2] Transportation and climate change, United States Environmental Protection Agency, Retrieved from: <https://www.epa.gov/regulations-emissions-vehicles-and-engines/regulations-greenhouse-gas-emissions-aircraft>
- [3] G.L. Dillingham, Aviation and the Environment, United States Government Accountability Office, 2008. Viewed at <http://www.gao.gov/assets/120/119976.pdf>
- [4] Global Electric Aircraft Market Analysis, Market size, Application Analysis, Regional Outlook, Competitive Strategies and Forecasts, 2015 to 2022, Retrieved from: <http://www.grandviewresearch.com/industry-analysis/the-global-electric-aircraft-market>
- [5] Yang, Shaohua, and Harold Knickle. "Design and Analysis of Aluminum/air Battery System for Electric Vehicles." Design and Analysis of Aluminum/air Battery System for Electric Vehicles. Dept. of Chemical Engineering, Univ. of Rhode Island, 14 June 2002. Web. 10 Feb. 2015.
<<http://www.sciencedirect.com/science/article/pii/S0378775302003701>>
- [6] Ohashi, Masato. "Liquid Aluminum Air Battery Operated at High Temperature." The Electrochemical Society 58.12 (2014): 75-84. ECS. Web. 15 Feb. 2015.
<<http://ecst.ecsdl.org/content/58/12/75.abstract>>
- [7] Hepperle, M. (n.d.). DLR Aerospace. Retrieved from DLR: <http://elib.dlr.de/78726/1/MPAVT-209-09.pdf>
- [8] Roskam, Jan. *Airplane Design*. Ottawa, Kan.: Roskam Aviation and Engineering, 1989. Print
- [9] NASA ARMD Design CHallenge 2020 E-GA Scuba Stingray by University of California, Davis
- [10] Sadraey, Mohammed H., *Aircraft Design: A Systems Engineering Approach.*, John Wiley and Sons, 2013. Web.
<<http://onlinelibrary.wiley.com/book/10.1002/9781118352700?systemMessage=Wiley+Online+Library+will+be+disrupted+on+21st+March+from+10%3A30+GMT+%2806%3A30+EDT%29+for+up+to+six+hours+for+essential+maintenance.+Apologies+for+the+inconvenience>>
- [11] *Design of A 4-Seat, General Aviation, Electric Aircraft* by Arvindhakshan Rajagopalan , San Jose State University.
- [12] Cooper, J.F., R. V. Hornsy, and J. H. Landrum. Proceedings of the Fifteenth Intersociety Energy Conversion Engineering Conference. Energy to the 21st Century. N.p.: n.p., n.d. 1487-495. ADS Database. Web. 15 Feb. 2015. <http://adsabs.harvard.edu/abs/1980iece.conf.1487C>
- [13] Zhang, Zhao, Chuncheng Zuo, Zihui Liu, Ying Yu, and Yuxin Zuo. "All-solid-state Al–air Batteries with Polymer Alkaline Gel Electrolyte." *Journal of Power Sources* 251 (2014): 470-75. Science Direct. Web. 14 Feb. 2015.
<<http://www.sciencedirect.com/science/article/pii/S0378775313018466>>.

- [14] Ingram, Antony. "How Hard Is Lithium-Air Battery Research? Pretty Tough, Actually." *Green Car Reports*. N.p., 8 May 2014. Web. 20 Apr. 2015. <http://www.greencarreports.com/news/1091967_how-hard-is-lithium-air-battery-researchpretty-tough-actually>.
- [15] Chen, Allen. "Energy Technologies Area." *Sulfur-graphene Oxide Material for Lithium-sulfur Battery Cathodes*. N.p., n.d. Web. 20 Apr. 2015. <<http://eetd.lbl.gov/news/article/56320/sulfurgraphene-oxide-material-for-lithium-sulfur-battery-cathodes>>.
- [16] "Tesla Gigafactory." *Tesla Gigafactory*. N.p., n.d. Web. 15 Feb. 2015.
- [17] Electric Vehicle Propulsion, Launch Point Technologies. <<http://www.launchpnt.com/portfolio/transportation/electric-vehicle-propulsion>>
- [18] Electric Aircraft Motors., < <https://www.experimentalaircraft.info/homebuilt-aircraft/electric-aircraft-engines.php>>
- [19] Aircraft Performance, Chapter 11., <https://www.faa.gov/regulations_policies/handbooks_manuals/aviation/phak/media/13_phak_ch11.pdf>
- [20] Fuel Cell and Battery Electric Vehicles Compared by C. E. Thomas, Ph. D., President. H2Gen Innovations, Inc., Virginia. <https://www1.eere.energy.gov/hydrogenandfuelcells/education/pdfs/thomas_fcev_vs_battery_evs.pdf>